

## Transient simulations of offshore substation installation by heavy lift vessel from a moored barge in OrcaFlex

**Auteur :** Abu Sabbah, Jawdat

**Promoteur(s) :** Rigo, Philippe

**Faculté :** Faculté des Sciences appliquées

**Diplôme :** Master : ingénieur civil mécanicien, à finalité spécialisée en "Advanced Ship Design"

**Année académique :** 2023-2024

**URI/URL :** <http://hdl.handle.net/2268.2/22245>

---

### Avertissement à l'attention des usagers :

Tous les documents placés en accès ouvert sur le site le site MatheO sont protégés par le droit d'auteur. Conformément aux principes énoncés par la "Budapest Open Access Initiative"(BOAI, 2002), l'utilisateur du site peut lire, télécharger, copier, transmettre, imprimer, chercher ou faire un lien vers le texte intégral de ces documents, les disséquer pour les indexer, s'en servir de données pour un logiciel, ou s'en servir à toute autre fin légale (ou prévue par la réglementation relative au droit d'auteur). Toute utilisation du document à des fins commerciales est strictement interdite.

Par ailleurs, l'utilisateur s'engage à respecter les droits moraux de l'auteur, principalement le droit à l'intégrité de l'oeuvre et le droit de paternité et ce dans toute utilisation que l'utilisateur entreprend. Ainsi, à titre d'exemple, lorsqu'il reproduira un document par extrait ou dans son intégralité, l'utilisateur citera de manière complète les sources telles que mentionnées ci-dessus. Toute utilisation non explicitement autorisée ci-avant (telle que par exemple, la modification du document ou son résumé) nécessite l'autorisation préalable et expresse des auteurs ou de leurs ayants droit.

---



POLITÉCNICA



Universität  
Rostock



Traditio et Innovatio



SOLENT  
UNIVERSITY  
SOUTHAMPTON



Zachodniopomorski  
Uniwersytet  
Techniczny  
w Szczecinie



With the support of the  
Erasmus+ Programme  
of the European Union



Jan De Nul  
GROUP

# Transient Simulations of Offshore Substation Installation by Heavy Lift Vessel from a Moored Barge in OrcaFlex

Submitted on 30<sup>th</sup> August 2024

By

**ABU SABBAH Jawdat**

Rue des horticulteurs 107 | 1020 Bruxelles | Belgium

[jawdat.abusabbah@alumnos.upm.es](mailto:jawdat.abusabbah@alumnos.upm.es)

Student ID No.: S223055

## First Reviewer:

Prof. Sascha Kosleck  
University of Rostock  
Universitätsplatz 1  
18055 Rostock  
Germany

## Second Reviewer:

Eng. Gustavo Fabian Acosta  
Polytechnic University of Madrid  
Avenida de la Memoria, 4  
28040 Madrid  
Spain



[This page is intentionally left blank]

---

# CONTENTS

Contents .....	i
List of Figures .....	iv
List of Tables.....	vii
NOMENCLATURE .....	ix
DECLARATION OF AUTHORSHIP .....	xii
ACKNOWLEDGEMENT .....	xiv
ABSTRACT .....	xvi
<b>1. INTRODUCTION .....</b>	<b>1</b>
1.1. Background.....	1
1.2. Motivation .....	2
1.3. Objective.....	4
1.3.1. The Simulation of Installation Dynamics .....	4
1.3.2. Assessing the Effects of Environment:.....	4
1.3.3. Assessment of System Reactions: .....	4
1.3.4. Optimizing Installation Processes: .....	5
1.3.5. Verifying Simulation Outcomes: .....	5
<b>2. LITERATURE REVIEW .....</b>	<b>6</b>
2.1. Offshore Windfarm .....	6
2.2. Overview of Power Generation .....	6
2.2.1. Turbine Components .....	7
2.2.2. Foundations, Array Cables, and Offshore Substation .....	8
2.2.3. Export Cable and Onshore Connection .....	8
2.3. Offshore Substation (OSS) .....	9
2.4. Grid Technology .....	10
2.4.1. Alternating Current (AC) Grid Connection .....	10
2.4.2. Direct Current (DC) Grid Connection.....	11
2.5. Installation Methods of Offshore Substation.....	11
2.5.1. Self-Installing Structures .....	12
2.5.2. Float-Over .....	12
2.5.3. Heavy Lifting .....	13
<b>3. THEORY OF ORCAFLEX.....</b>	<b>15</b>
3.1. Type of Analysis.....	15
3.1.1. Static Analysis.....	15
3.1.2. Dynamic Analysis .....	15
3.1.3. Explicit Integration Scheme.....	16
3.1.4. Implicit Integration Scheme.....	16
3.2. Environment .....	17
3.3. Coordinate Systems.....	17
3.4. Objects.....	18
3.4.1. Vessels .....	18
3.4.2. 6D Buoys .....	18
3.4.3. Lines .....	19
3.4.4. Links .....	19
3.4.5. Winches .....	19
3.4.6. Shapes.....	19
3.4.7. Constraints .....	19
<b>4. MODEL SET-UP .....</b>	<b>20</b>
4.1. Orcaflex Modelling Procedure .....	20
4.1.1. Les Alizes .....	20
4.1.2. Crane Model.....	21

4.1.3.	Main Hoist Block .....	23
4.1.4.	Slings and Crane Wires .....	25
4.1.5.	Rigging system.....	28
4.1.6.	OSS Model.....	29
4.1.7.	Tugger Lines .....	32
<b>5.</b>	<b>SIMULATION SETTINGS AND PARAMETERS.....</b>	<b>37</b>
5.1.	Crane Tip Stiffness.....	37
5.2.	Rope Stiffness .....	38
5.3.	Environmental Conditions.....	39
5.3.1.	JONSWAP Spectrum .....	39
5.3.2.	Kinematic Stretching Method .....	40
5.3.3.	Wave Conditions .....	41
5.4.	Key Factors for Wave Condition Decision .....	41
5.4.1.	Operational Safety.....	41
5.4.2.	DP System Performance .....	41
<b>6.</b>	<b>NUMERICAL SIMULATIONS.....</b>	<b>42</b>
6.1.	Static Analysis .....	42
6.2.	Dynamic Analysis .....	43
6.2.1.	Implicit Time Domain Simulation .....	43
6.2.2.	Explicit Time Domain Simulation .....	44
6.3.	Simulation Process.....	44
<b>7.</b>	<b>STATISTICAL CONSIDERATIONS .....</b>	<b>46</b>
7.1.	Most Probable Maximum (MPM) .....	46
7.1.1.	Continuous Probability Distribution .....	47
7.1.2.	Weibull Distribution.....	48
7.1.3.	Rayleigh Distribution .....	51
7.2.	MPM Amplitude .....	52
<b>8.</b>	<b>RESULTS AND DISCUSSION.....</b>	<b>54</b>
8.1.	Pick-Up Phase.....	54
8.1.1.	DAF Of Main Hoist.....	54
8.1.2.	Off Lead (OL) of Crane Wires.....	57
8.1.3.	Side Lead (SL) of Crane Wires.....	58
8.1.4.	Load Tugger Power.....	59
8.1.4.1	Load tugger 1 .....	60
8.1.4.2	Load tugger 2 .....	61
8.1.5.	Trolley Tugger Power.....	61
8.1.5.1	Trolley tugger 1 .....	62
8.1.5.2	Trolley tugger 2 .....	63
8.2.	Slew and Transfer Phase 214° .....	63
8.2.1.	DAF of Main Hoist.....	64
8.2.2.	Off Lead (OL) of Crane Wires.....	65
8.2.3.	Side Lead (SL) of Crane Wires.....	66
8.2.4.	Load Tugger Power.....	67
8.2.4.1	Load tugger 1 .....	67
8.2.4.2	Load tugger 2 .....	68
8.2.5.	Trolley Tugger Power.....	69
8.2.5.1	Trolley tugger 1 .....	69
8.2.5.2	Trolley tugger 2 .....	70
8.2.6.	Offshore Substation Motion Study.....	71
8.2.6.1	OSS movement in global X and Y .....	71
8.2.6.2	OSS velocity in global X and Y .....	72
8.3.	Slew and Transfer Phase 224° .....	75

---

8.3.1.	DAF of Main Hoist.....	75
8.3.2.	Off Lead (OL) of Crane Wires.....	76
8.3.3.	Side Lead (SL) of Crane Wires.....	77
8.3.4.	Load Tugger Power.....	78
8.3.4.1	Load tugger 1 .....	78
8.3.4.2	Load tugger 2 .....	79
8.3.5.	Trolley tugger power.....	79
8.3.5.1	Trolley tugger 1 .....	79
8.3.5.2	Trolley tugger 2 .....	80
8.3.6.	Offshore Substation Motion Study.....	81
8.3.6.1	OSS movement in global X and Y .....	81
8.3.6.2	OSS velocity in global X and Y .....	83
8.4.	Workability.....	85
8.4.1.	Pick-Up Phase Workability .....	86
8.4.2.	Slew and Transfer Phase Workability .....	86
<b>9.</b>	<b>IMPOSED MOTION ANALYSIS (ADDITIONAL PART) .....</b>	<b>91</b>
<b>10.</b>	<b>CONCLUSION .....</b>	<b>89</b>
10.1.	Thesis Sum Up.....	89
10.2.	Future Work.....	90
<b>REFERENCES .....</b>		<b>92</b>
<b>APPENDICES .....</b>		<b>96</b>

---

## List of Figures

1. Greenhouse gas emissions by sector in the world (Climate Watch, 2023).....	1
2. (CO <sub>2</sub> eq) share of (GHG) by sector (Climate Watch, 2023) .....	2
3. 2023: Record falls in EU coal and gas electricity generation (Ember, 2024).....	3
4. Share of EU electricity generation, by source (%) (Ember, 2024).....	3
5. North Falls Offshore Wind Farm (North Falls, 2024) .....	6
6. Power generation components (NYSERDA, 2024) .....	7
7. Main parts in offshore wind turbine (NYSERDA, 2024) .....	7
8. Power transfer from OWT to OSS via inter-array cables (NYSERDA, 2024).....	8
9. Power transmission from offshore to onshore substations via export cables (NYSERDA, 2024).....	9
10. Triton Knoll offshore wind farm substation (Buljan, 2020) .....	10
11. Typical Offshore HVAC radial link (DNV, 2022).....	11
12. Typical Offshore HVDC radial link (DNV, 2022).....	11
13. Alstom's GIS substation (Froese, 2016).....	12
14. HVDC Sylwin alpha (OVERDICK GmbH, 2012).....	13
15. Current thesis OSS installation by Les alizes (Jan de Nul, 2023) .....	14
16. Global and local coordinate system according to OrcaFlex.....	18
17. Les Alizes naked model sided with a barge .....	20
18. Les Alizes equipped with TMC (JDN, 2021).....	21
19. TMC integrated with Les Alizes model on OrcaFlex .....	23
20. Hook interface .....	24
21. Crane wire length explanatory example.....	27
22. Side views of rigging arrangement .....	28
23. Top view of rigging arrangement .....	29
24. OSS side view.....	29
25. OSS front view .....	30
26. OSS top view .....	30
27. Reference shape for rectangular cube (Cameron et al) .....	31
28. OrcaFlex model for OSS .....	31
29. Forward view of the OrcaFlex model .....	33
30. Side view of the model.....	34
31. Top view of the model .....	35
32. Graphic isometric view of the model.....	36
33. Crane stiffness representation.....	38
34. Implicit time domain simulation duration.....	45

---

35. Kernel density estimation result showing a smooth distribution (the gray bell curve), (M. W. Toews, sd) .....	47
36. A continuous probability distribution showing SAT scores, (Turney, 2022) .....	48
37. Shape parameter influence on Weibull distributions, (Frost, Statistics By Jim, sd) ....	50
38. Scale parameter implication on Weibull distribution, (Frost, Statistics By Jim, sd)....	50
39. Threshold parameter influence on Weibull distribution, (Frost, Statistics By Jim, sd)	51
40. Rayleigh distributions with different shape parameters, (statistics How To, sd).....	52
41. Crane wire DAF, $H_s = 1.5\text{m}$ .....	55
42. Crane wire DAF, $H_s = 2.5\text{m}$ .....	55
43. Modal analysis for the modelled system .....	56
44. Off lead illustration, (Huisman).....	57
45. Crane wire mean off lead angle, $H_s = 1.5\text{m}$ .....	57
46. Crane wire mean off lead angle, $H_s = 2.5\text{m}$ .....	58
47. Side lead illustration, (Huisman) .....	58
48. Crane wire mean side lead angle, $H_s = 1.5\text{m}$ .....	59
49. Crane wire mean side lead angle, $H_s = 2.5\text{m}$ .....	59
50. Load tugger 1 power limit, $H_s = 1.5\text{ m}$ and $H_s = 2.5\text{ m}$ above and below respectively .....	60
51. Load tugger 2 power limit, $H_s = 1.5\text{ m}$ and $H_s = 2.5\text{ m}$ above and below respectively .....	61
52. Trolley tugger 1 power limit, $H_s = 1.5\text{ m}$ and $H_s = 2.5\text{ m}$ above and below respectively .....	62
53. Trolley tugger 2 power limit, $H_s = 1.5\text{ m}$ and $H_s = 2.5\text{ m}$ above and below respectively .....	63
54. Crane wire DAF, $H_s = 1.5\text{m}$ .....	64
55. Crane wire DAF, $H_s = 2.5\text{m}$ .....	64
56. Crane wire mean off lead angle, $H_s = 1.5\text{m}$ .....	65
57. Crane wire mean off lead angle, $H_s = 2.5\text{m}$ .....	65
58. Crane wire mean side lead angle, $H_s = 1.5\text{m}$ .....	66
59. Crane wire mean side lead angle, $H_s = 2.5\text{m}$ .....	66
60. Load tugger 1 power limit, $H_s = 1.5\text{ m}$ and $H_s = 2.5\text{ m}$ above and below respectively .....	67
61. Load tugger 2 power limit, $H_s = 1.5\text{ m}$ and $H_s = 2.5\text{ m}$ above and below respectively .....	68
62. Trolley tugger 1 power limit, $H_s = 1.5\text{ m}$ and $H_s = 2.5\text{ m}$ above and below respectively .....	69
63. Trolley tugger 2 power limit, $H_s = 1.5\text{ m}$ and $H_s = 2.5\text{ m}$ above and below respectively .....	70
64. OSS movement in global X for $H_s = 1.5\text{ m}$ , $2.5\text{ m}$ , above and below respectively .....	71

---



---

65. OSS movement in global Y for Hs = 1.5 m, 2.5 m, above and below respectively .....	72
66. OSS velocity in global X for Hs = 1.5 m, 2.5 m, above and below respectively .....	73
67. OSS velocity in global Y for Hs = 1.5 m, 2.5 m, above and below respectively .....	74
68. Crane wire DAF, Hs = 1.5m.....	75
69. Crane wire DAF, Hs = 2.5m.....	75
70. Crane wire mean off lead angle, Hs = 1.5m.....	76
71. Crane wire mean off lead angle, Hs = 2.5m.....	76
72. Crane wire mean side lead angle, Hs = 1.5m .....	77
73. Crane wire mean side lead angle, Hs = 2.5m .....	77
74. Load tugger 1 power limit, Hs = 1.5 m and Hs = 2.5 m above and below respectively .....	78
75. Load tugger 2 power limit, Hs = 1.5 m and Hs = 2.5 m above and below respectively .....	79
76. Trolley tugger 1 power limit, Hs = 1.5 m and Hs = 2.5 m above and below respectively .....	80
77. Trolley tugger 2 power limit, Hs = 1.5 m and Hs = 2.5 m above and below respectively .....	81
78. OSS movement in global X for Hs = 1.5 m, 2.5 m, above and below respectively .....	82
79. OSS movement in global Y for Hs = 1.5 m, 2.5 m, above and below respectively .....	83
80. OSS velocity in global X for Hs = 1.5 m, 2.5 m, above and below respectively .....	84
81. OSS velocity in global X for Hs = 1.5 m, 2.5 m, above and below respectively .....	84

---

## List of Tables

1. Crane components physical properties .....	22
2. 6D Buoy inertia portal on OrcaFlex.....	22
3. Crane wire and sling line type properties.....	24
4. Physical and geometrical properties of the slings.....	25
5. Slings geometrical and physical properties.....	26
6. Sample calculation of crane wire stiffness (Pick-up case).....	28
7. Properties of OSS model in OrcaFlex.....	31
8. Control mode of load and trolley tuggers in the upper and lower tables respectively .	32
9. Wave conditions for the analysis.....	41
10. Workability table of pick-up phase.....	86
11. Workability table of slew and transfer phase of $214^{\circ}$ .....	87
12. Workability table of slew and transfer phase of $224^{\circ}$ .....	88
13. Workability table of IMA.....	92

[This page is intentionally left blank]

## **NOMENCLATURE**

AC Alternating Current

CFD Computational Fluid Dynamics

CO<sub>2</sub>eq Carbon Dioxide Equivalent

CoG Center of Gravity

DAF Dynamic Amplification Factor

DC Direct Current

DOF Degree of Freedom

GHG Greenhouse Gas

GPD Generalized Pareto Distributions

HLVs Heavy Lift Vessels

HVAC High Voltage Alternating Current

HVDC High Voltage Direct Current

IC Internal Confidential

IMA Imposed Motion Analysis

ISSC International Ship Security Certificates

JDN Jan De Nul

JONSWAP Joint North Sea Wave Project

KDE Kernel Density Estimation

MBL Maximum Breaking Load

MPM Most Probable Maxima

MEG 1 Germany's offshore wind farms

MV Medium Voltage

MSF Modular Support Frame

OL Off Lead

OSP Offshore Substation Platforms

OSS Offshore Substation

---

OWT Offshore Wind Turbine

PM Pierson-Moskowitz

PDF Probability Density Function

RAOs Response Amplitude Operators

SL Side Lead

SWL Safe Working Load

TMC Tub Mounted Crane

WLL Working Load Limit

[This page is intentionally left blank]

## DECLARATION OF AUTHORSHIP

I, **Jawdat Abu Sabbah** declare that this thesis and the work presented in it are my own and have been generated by me as the result of my own original research.

Where I have consulted the published work of others, this is always clearly attributed.

Where I have quoted from the work of others, the source is always given. With the exception of such quotations, this thesis is entirely my own work.


I have acknowledged all main sources of help.

Where the thesis is based on work done by myself jointly with others, I have made clear exactly what was done by others and what I have contributed myself.

This thesis contains no material that has been submitted previously, in whole or in part, for the award of any other academic degree or diploma.

I cede copyright of the thesis in favour of the Polytechnic University of Madrid (UPM) University of Liege (ULiege).

**Date:** 29 August 2023

**Signature:** 

[This page is intentionally left blank]



## ACKNOWLEDGEMENT

First and foremost, I want to sincerely thank University of Liege and University Polytechnic of Madrid for granting me the priceless chance to pursue my education and for their steadfast support over my whole academic career. This thesis has been completed in large part thanks to the excellent faculty's resources, advice, and encouragement.

I have the utmost gratitude to Jan de Nul for providing me with the space to do my research. The success of this work has been largely attributed to the practical experience, insights, and mentorship I acquired while working at the organization. I want to thank Geert Weymeis for his seamless efforts in integrating me with the offshore renewables team and always checking on my performance. Thanks to Thales Machado for his constructive critics and his follow up on my thesis progress through the whole internship. Nonetheless, I want to thank Kyaw Swa for providing and scheduling detailed explanation sessions for theoretical and practical knowledge serving the analysis.

I am also motivated by the eternal lessons imparted by notable historical people who have highlighted the value of morality and knowledge:

Prophet Muhammad (PBUH) said, "The acquisition of knowledge is a duty incumbent on every human being" This insightful remark has inspired me to pursue knowledge assiduously and relentlessly.

Jesus (PBUH) taught us, "Seek and you will find; knock and the door will be opened to you." This guiding concept has strengthened my resolve to pursue and preserve the truth in all of my research activities.

Imam Ali bin Abi Talib (AS) eloquently stated, "Knowledge enlivens the soul." This quotation serves as a continual reminder of the knowledge's transforming potential and capacity to uplift the human spirit.

To my family and friends, and EMship family your unwavering support and encouragement have been my pillars of strength. Your belief in me has been my greatest motivation.

Lastly, to all those who contributed directly or indirectly to this thesis, your support and assistance are greatly appreciated. Thank you all for being part of this journey.

[This page is intentionally left blank]

# ABSTRACT

Offshore wind energy is growing, and with it the need for safe and effective ways to deploy vital infrastructure, such as offshore windfarm substations. With an emphasis on the use of heavy lift vessels (HLVs) from moored barges, this thesis conducts a thorough investigation of the optimization possibilities in offshore substation installation. Using precise parameters transient simulations run in OrcaFlex, this study attempts to clarify the complex dynamics regulating these installations in order to improve operating efficiency and reduce related expenses and hazards.

The basis of the study is the creation of a strict numerical model that includes the complex interactions between the offshore substation structure, the moored barge, and the HLV. Environmental conditions including waves are taken into consideration in this model as they have a big impact on installation procedures. By carefully adjusting and verifying its predictions against real-world data and industry norms, the model guarantees a high level of accuracy.

Principal goals comprise an extensive investigation, starting with the study of vessel dynamics in various environmental conditions. Through an examination of variables including wave-induced movements and dynamic positions. The study aims to pinpoint crucial operating boundaries and possible obstructions. After that, optimization techniques are developed and assessed, with an emphasis on minimizing the total project duration and cost and optimizing installation procedures while maintaining safety requirements.

The study technique comprises a methodical investigation of several installation situations for three main stages: 1- Pick-up of OSS 2- Transfer to installation radius 3- Setting down on MSF, while taking into account substation characteristics, water depth, and sea state. The study examines the effects of operational factors on important performance measures, such as installation time, cost, and safety margins, using sensitivity analysis and iterative simulations.

The ultimate goal of this project is to offer practical advice and best practices for installing offshore substations using HLV from moored barges to it, this is achieved by analyzing the behavior of the system while being exposed to different sea-states while operating.

[This page is intentionally left blank]

## 1. INTRODUCTION

This thesis addresses the installation of offshore substation (OSS) by heavy lift vessel from a moored barge. The analysis is carried out by OrcaFlex with the aid of BricsCAD for reading/measuring dimensions. Excel and Python are used for pre and post-processing procedures. In this chapter, the background, motivation and objective of the thesis will be presented.

### 1.1. Background

The world's greenhouse gas (GHG) emissions are rising while they ought to be decreasing quickly. Knowing where emissions originate from and which industries contribute the most can help lower emissions efficiently (Ritchie et al, 2020). Figure 1-1 illustrates greenhouse gas emissions measured in tons of carbon dioxide-equivalents over the period from 1990 to 2020. It is worth noticing that the electricity and heat sector is the most producing of (GHG) for almost the past 30 years, with a share of approximately 15 billion tons (CO<sub>2</sub>eq) for the year 2020.

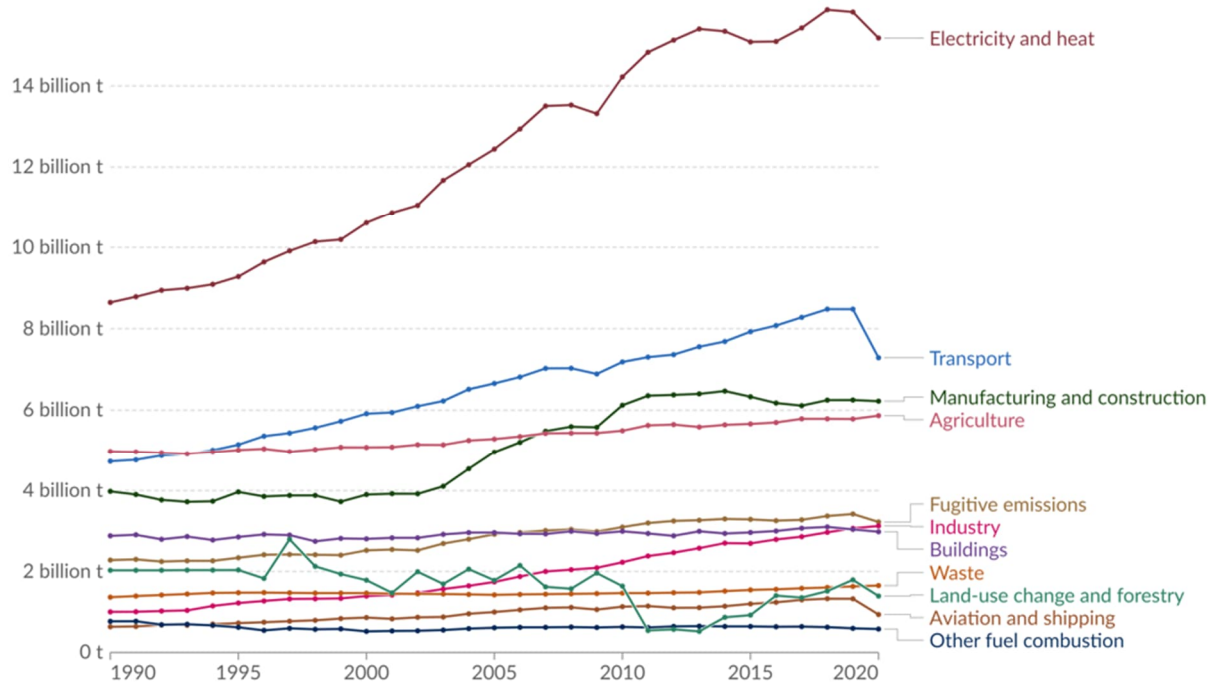


Figure 1-1: Greenhouse gas emissions by sector in the world (Climate Watch, 2023)

Based on the collected data from (Climate Watch), the most emitting sectors for (GHG) were listed and monitored based (CO<sub>2</sub>eq) key indicator for the past 30 years, noting from the collected results in Figure 1-2 that electricity and heat sector is the topmost emitting of (GHG) with a value of 15.18 billion tons of (CO<sub>2</sub>eq).

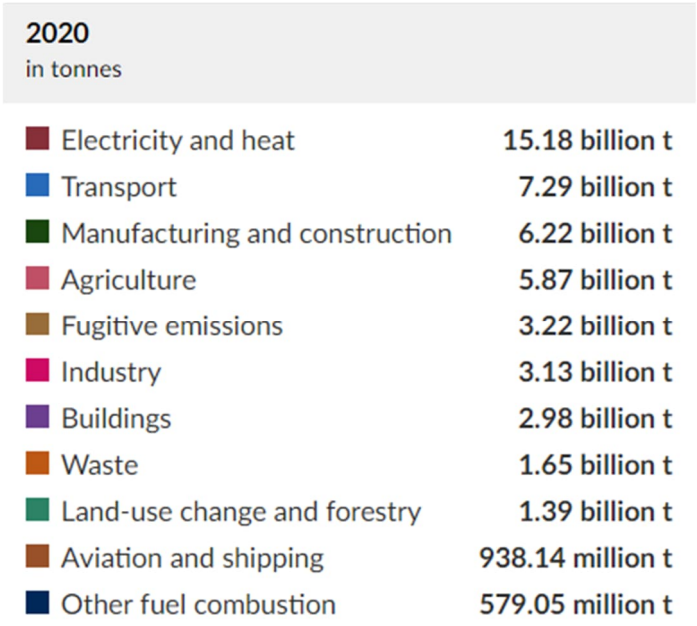


Figure 1-2: (CO2eq) share of (GHG) by sector (**Climate Watch, 2023**)

1.2. Motivation

Based on the European commission on the renewable energy targets, the EU's mandatory renewable energy objective for 2030 is increased to a minimum of 42.5% under the updated Renewable Energy Directive, which was approved in 2023. Thus, boosting the proportion of renewable energy in all economic sectors is essential to achieving the targets of cutting net greenhouse gas emissions by at least 55% by 2030 and turning the continent into a climate-neutral region by 2050 (European Commission, 2023).

With record-low coal, gas, and emission levels in 2023, the EU expedited its transition away from fossil fuels. Figure 1-3 illustrates how the amount of power generated in the EU by fossil fuels fell to a historic low level of less than one third of its electricity generation, a record 19% decline. For the first time, renewables surpassed 40% to reach a record 44% share. Figure 1-4 shows how wind and solar power remained the main forces behind the expansion of renewable energy, accounting for a record above 27% of EU electricity production in 2023 and recording their largest-ever annual capacity increases. In addition, wind power achieved a significant milestone by overtaking gas for the first time (Brown et Johns, 2024).

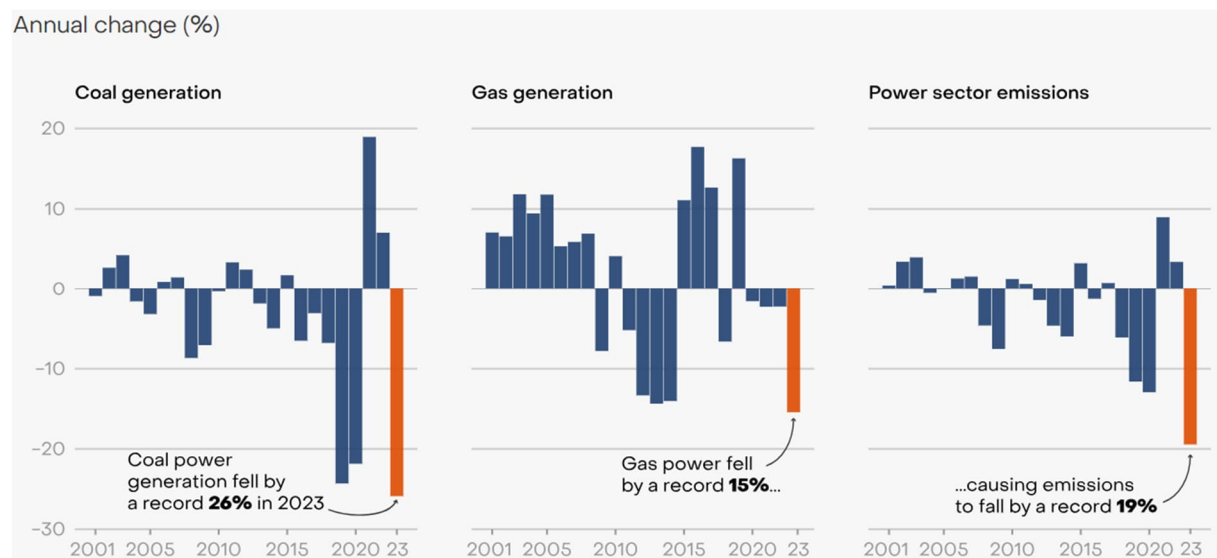


Figure 1-3: 2023: Record falls in EU coal and gas electricity generation (Ember, 2024)

For the first time, wind and solar power generated 27% of the electricity in the EU in 2023, up from 23% in 2022. As a result, renewable power reached a record high of 44% and crossed the 40% threshold for the first time in the history of the EU. The record of yearly generation rise to 55 TWh (+13%) in wind power in 2023. As a consequence, wind energy generation finally surpassed gas. Compared to 452 TWh from gas, 475 TWh of electricity - equivalent to France's entire power demand - was generated by wind energy (Brown et Johns, 2024).

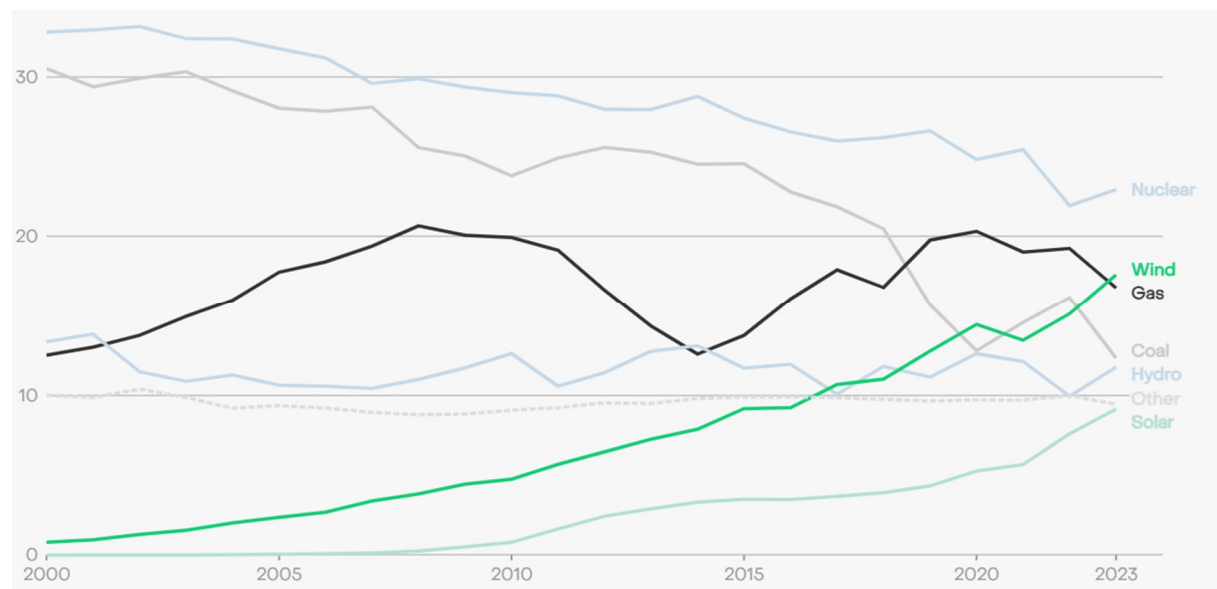


Figure 1-4: Share of EU electricity generation, by source (%) (Ember, 2024)

### 1.3. Objective

Using a heavy lift vessel from a moored barge, this thesis uses the advanced simulation program OrcaFlex to perform transient simulations of the offshore substation installation process. This includes a number of specific sub-goals:

#### *1.3.1. The Simulation of Installation Dynamics*

- Detailed Modelling: To build precise models in OrcaFlex for the moored barge, the offshore substation, and the heavy lift vessel. Determining each component's physical characteristics, geometry, and interaction dynamics falls under this category.
- Transient Stages: To replicate different stages of the installation procedure, such as hoisting the substation off the barge, guiding it into place, and lowering it onto the assigned offshore location. Transient (time-dependent) analysis will be used in each phase to record dynamic responses.

#### *1.3.2. Assessing the Effects of Environment:*

- Realistic environmental factors: such as wave height and duration should be incorporated into the simulations. The installation process's stability and safety may be greatly impacted by these variables.
- Scenario Analysis: To conduct scenario studies in a variety of weather situations, including severe, moderate, and tranquil ones. This will make it easier to comprehend how different circumstances affect the installation process.

#### *1.3.3. Assessment of System Reactions:*

- Stability Analysis: To assess the heavy lift vessel's and the moored barge's stability during the lifting and installation processes. Studying the impacts of dynamic loads, and ship movements are all part of this.
- Load Transfer: To investigate how loads are moved during raising and lowering between the substation, the moored barge, and the heavy lift vessel. It is essential to comprehend these load paths in order to guarantee operational safety and structural integrity.
- Operational Limits: To determine the important parameters, such as the maximum permitted wave height or wind speed, that might jeopardize the installation procedure.



***1.3.4. Optimizing Installation Processes:***

- Procedure Development: To create installation protocols that are as safe and effective as possible. This entails figuring out the optimal time, order of events, and coordination between the barge and vessel.
- Risk Mitigation: To guarantee a safe and effective installation, it is necessary to identify possible hazards and suggest mitigation techniques, such as changing lift speeds or slewing speed which will be presented in the imposed motion analysis.

***1.3.5. Verifying Simulation Outcomes:***

- Benchmarking: To compare the outcomes with accepted engineering guidelines and procedures for offshore installation. This will support method validation and guarantee that it satisfies industry standards.

## 2. LITERATURE REVIEW

This section provides a bibliographical overview for things related to the thesis. The section starts with addressing Offshore windfarm components. Since the focus oriented towards installation of Offshore Substation (OSS), a preview on power generation, offshore substations and types of grid connection will be presented. Installation methods of offshore substation will be reviewed as well.

### 2.1. Offshore Windfarm

A wind farm typically consists of export cables, onshore infrastructure, offshore wind turbines on foundations, and array cables connecting the turbines to the offshore substation. Figure 2-1 shows the proposed North Falls offshore wind farm schematic for graphical clarification, which assumes an onshore grid link. It displays the essential elements from offshore to onshore, including above and below the sea level.

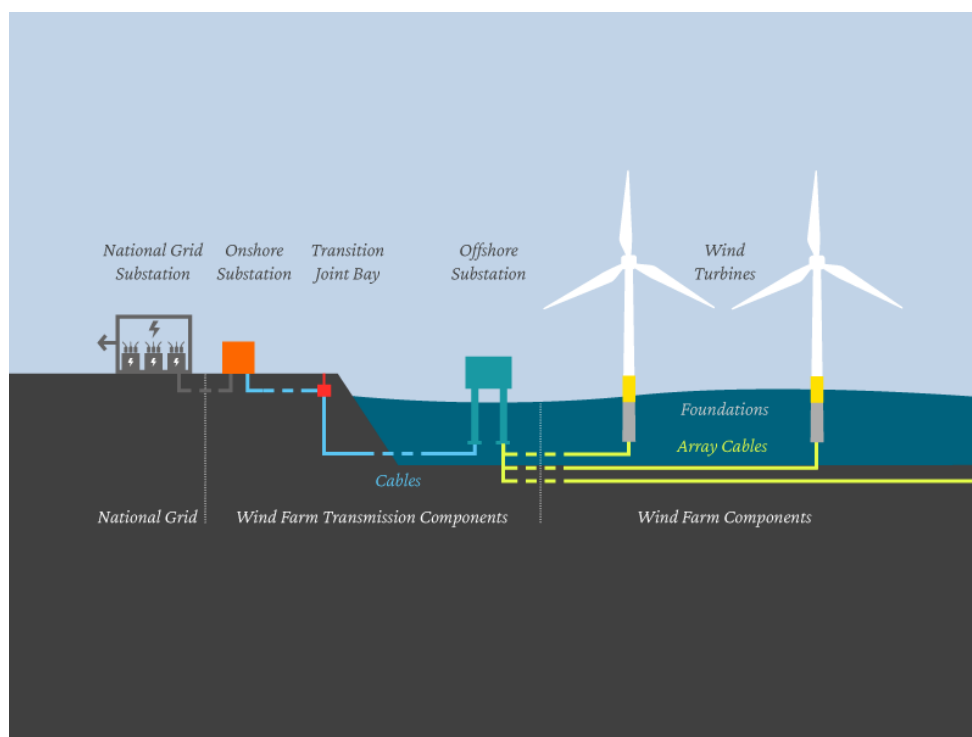


Figure 2-1: North Falls Offshore Wind Farm (North Falls, 2024)

### 2.2. Overview of Power Generation

Figure 2-2 illustrates the onshore and offshore environments in relation to the production and transmission of offshore wind energy. There are two offshore wind turbines seen. Undersea cables carry the electricity from the turbines to an offshore substation. After that, a subterranean

cable carries the electricity to the onshore substation, where it is connected to the current transmission network.

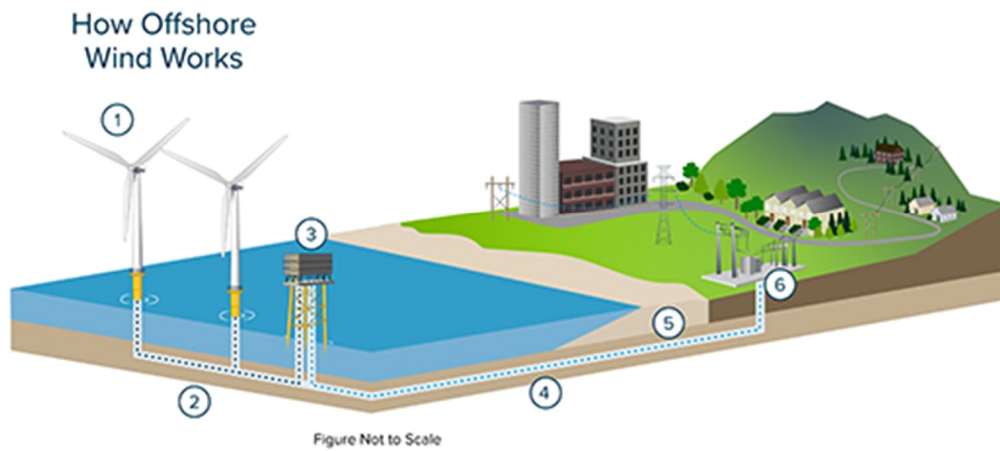


Figure 2-2: Power generation components (NYSERDA, 2024)

### 2.2.1. Turbine Components

Figure 2-3 displaying the essential parts of an offshore wind turbine. The pitch system, which optimizes blade angle and rotating speed, is housed in the hub and supports the blades. The wind's energy is captured by the blades and transformed into mechanical energy. The parts that transform mechanical energy into electrical energy are housed in the nacelle. The hub, blades, and nacelle mass are all supported by the tower.

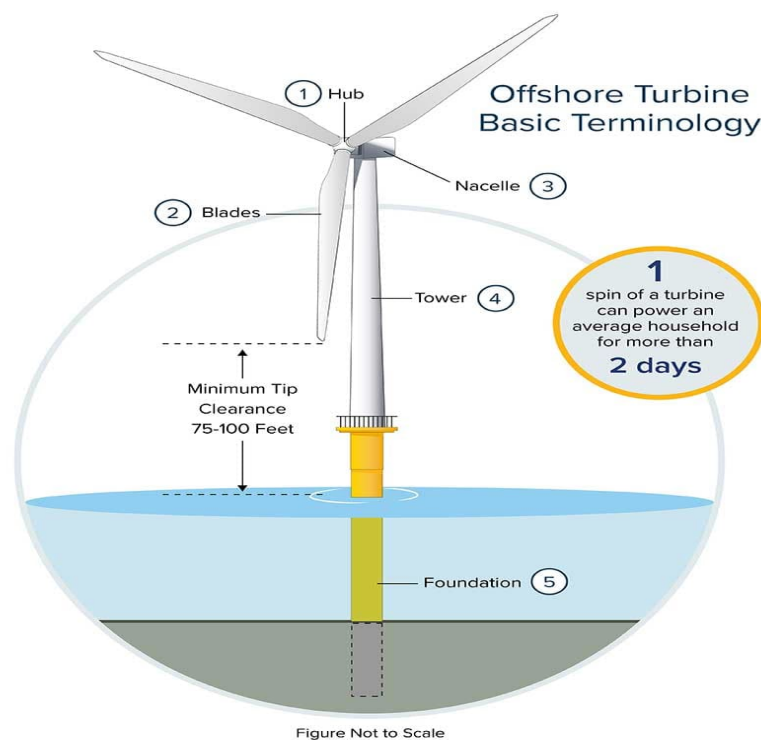


Figure 2-3: Main parts in offshore wind turbine (NYSERDA, 2024)

### 2.2.2. Foundations, Array Cables, and Offshore Substation

Figure 2-4 presents the transfer of power from an offshore wind farm to the offshore substation. The tower and above-water turbine components are fastened to the seabed by the monopile foundation. The offshore substation receives electricity from the wind turbines via array cables that connect them. The power is gathered and prepared for transmission to the coast by the offshore substation.

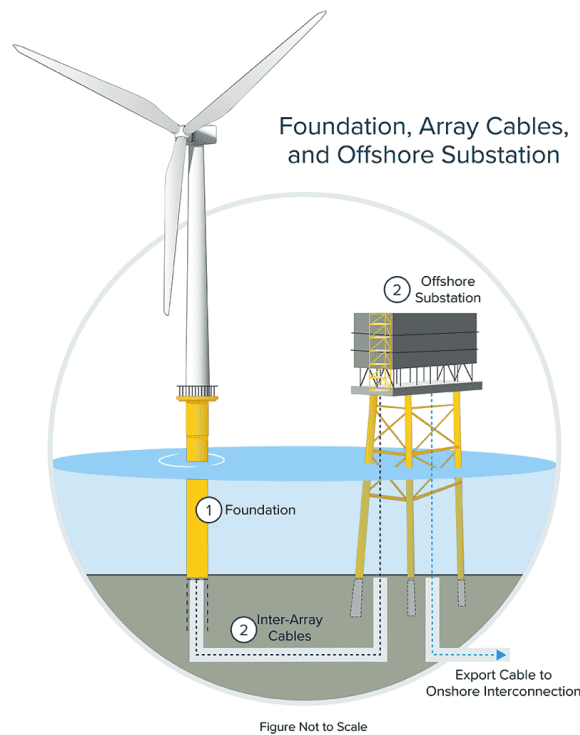


Figure 2-4: Power transfer from OWT to OSS via inter-array cables (NYSERDA, 2024)

### 2.2.3. Export Cable and Onshore Connection

Figure 2-5 illustrates the transfer of electricity from the offshore to the onshore substation. Power is transferred from the offshore substation to the onshore substation via the buried export cable. The export cable transfers electricity from the offshore substation to the onshore substation, and it is buried deep enough to prevent disturbing marine life and consumers.

After then, electricity is moved to the current transmission infrastructure. The most environmentally friendly way to land export transmission cables from offshore wind farms is by horizontal direction drilling, which also reduces disturbance to beaches and the coastline (New York State Official Website, 2024).

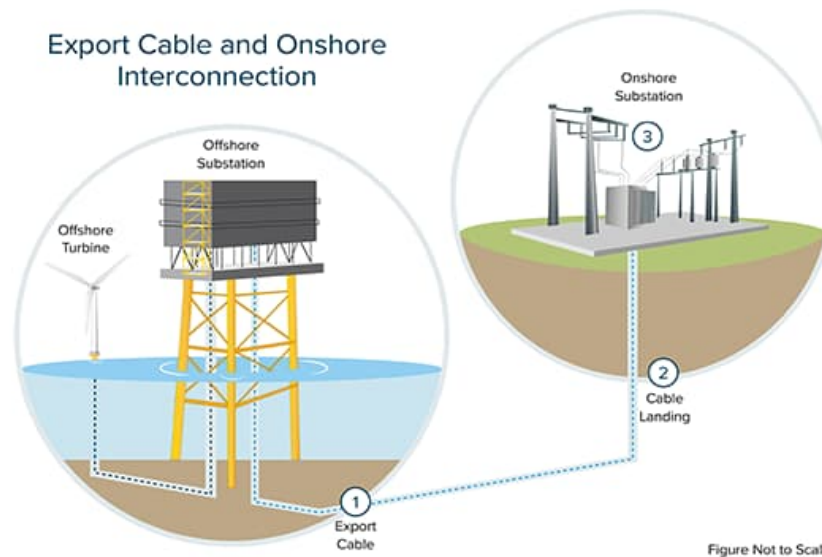


Figure 2-5: Power transmission from offshore to onshore substations via export cables (NYSERDA, 2024)

### 2.3. Offshore Substation (OSS)

A building that transfers energy from onshore power sources to offshore generation facilities is known as an offshore substation. These substations are connected to onshore power networks and are often situated close to an electrical transmission line. Offshore substations are built to withstand the harsh marine environment and are installed using a process known as subsea installation because they are situated in maritime environments that are subject to extreme weather conditions, such as strong winds and waves, and must remain operational for many years. They can be employed in many different fields, including as aquaculture, oil and gas extraction, and offshore wind farms (Bouwer, 2023). Figure 2-6 shows an installed offshore substation for Triton Knoll offshore wind farm.



Figure 2-6: Triton Knoll offshore wind farm substation (Buljan, 2020)

The substation itself consists of a jacket foundation, monopile, or transition component sitting atop a topside. Substations come in a variety of sizes, however they typically have four floors: An offshore cable deck used for pull-in export cable installation. For the high voltage transformer, a main deck supporting medium and high voltage equipment. A roof deck housing the primary lifting crane and day crew quarters are among the amenities found on the utility deck (Thomsen, 2023).

## 2.4. Grid Technology

An export cable connects offshore wind farms to the transmission grid because of their maritime setting. The export cable frequently acts as a bottleneck or single point of failure and is usually a major cost factor. There are several cable transmission methods available. The merits and cons of each option are explained in this section along with the different possibilities for alternating current (AC) and direct current (DC) technologies. In bottom-fixed offshore wind transmission connections, both AC and DC cables are now in use, and this trend is probably going to continue with floating offshore wind transmission (DNV, 2022).

### 2.4.1. Alternating Current (AC) Grid Connection

Wind energy from individual turbines is collected by the AC array cables and sent to the OSP, which is home to the AC switchgear and high voltage step up transformer. The array voltage is converted from medium voltage (MV) to high voltage alternating current (HVAC) by the step-up transformer, which is more suited for power transfer. The electricity is then sent to an onshore substation (SS) via the HVAC undersea export cable, where the voltage is converted to grid voltage. A schematic of a typical HVAC grid connection is shown in Figure 2-7 (DNV, 2022).

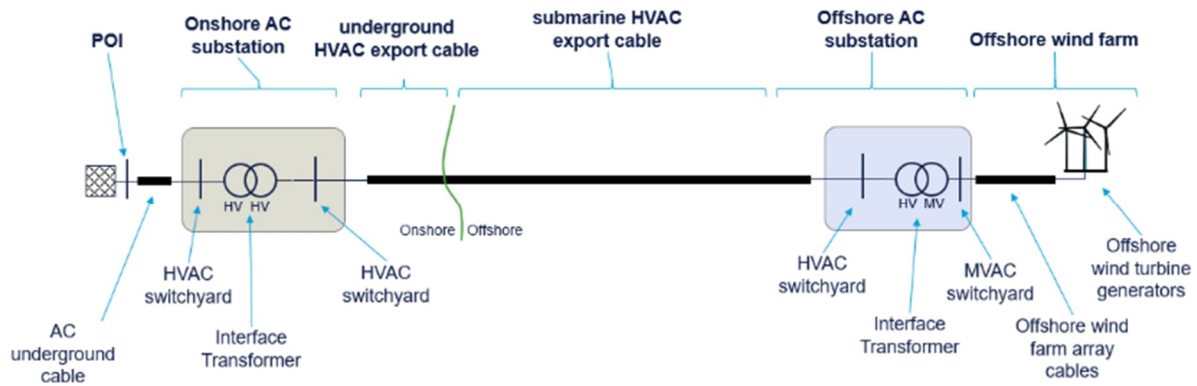


Figure 2-7: Typical Offshore HVAC radial link (DNV, 2022)

#### 2.4.2. Direct Current (DC) Grid Connection

MV array cables are used to gather electricity from individual turbines and send it to the offshore platform, much like the AC method is used for DC grid connections. The OSP has a converter station in the HVDC solution, which raises the array medium voltage to a high voltage before converting it to high voltage DC. The electricity is transported to the onshore converter station via the HVDC undersea export cable, where it is once more converted to grid voltage. Similar to HVAC, there are several HVDC transmission connection topologies with various characteristics that might influence footprints and costs. A typical HVDC grid connection solution for offshore applications is shown schematically in Figure 2-8 (DNV, 2022).

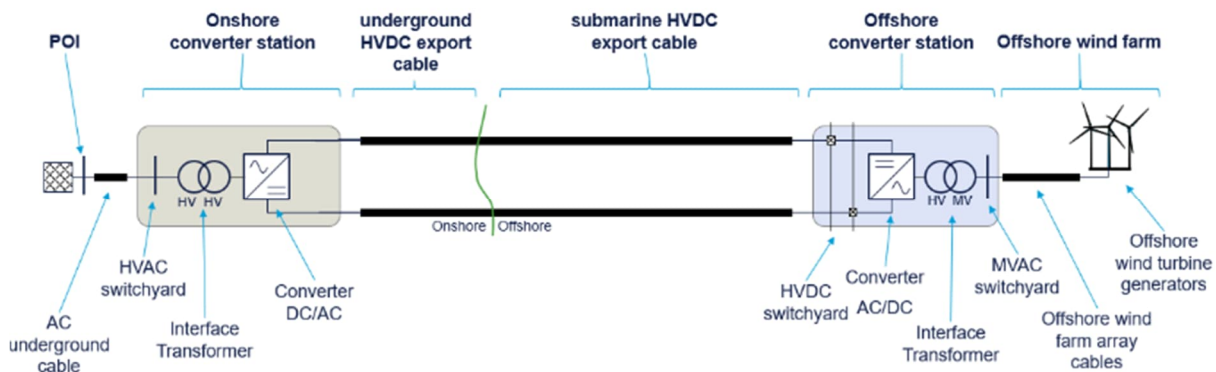


Figure 2-8: Typical Offshore HVDC radial link (DNV, 2022)

### 2.5. Installation Methods of Offshore Substation

As the joint component between the offshore wind farms and the onshore grid, offshore substations gather and transfer the power produced by the wind turbines. These substations are installed using a variety of techniques, each selected in accordance with the particular site characteristics, substation design and logistical factors. The following are the main techniques for setting up offshore substations:



### ***2.5.1. Self-Installing Structures***

ABB and Alstom Grid both use self-installing platforms as a solution to the size and expense issues associated with substation installation. The German high-voltage direct current system was connected to the 400-MW MEG 1 offshore wind farm through its self-installing, floating HVDC offshore substation.

Alstom claims that the platform is completely self-contained to safeguard electrical equipment and that the foundations are set to the seabed bottom using a "suction can" technique. When compared to traditional solutions, the process is thought to be less expensive, produces less noise pollution, and be safer for the environment (Froese, 2016). Figure 2-9 shows Alstom's closed substation when installation done in MEG 1 offshore wind farm.



Figure 2-9: Alstom's GIS substation (Froese, 2016)

### ***2.5.2. Float-Over***

An alternative way for installing an OSS's topside on its foundation is called a float-over; in this method, a jacket has been taken into consideration for the foundation. Owing to a rising trend in the offshore wind farms' capacity, depth, and distance from shore, OSS is experimenting with raising their weight, which lowers the availability of heavy lift vessels and raises their cost.

The float-over technique needs a barge that is used for topside transit and installation. Once at the location, the barge is pushed between the jacket's legs and lowered by ballasting to facilitate the connection of the topside and jacket (Seiji et al, 2007). Figure 2-10 illustrates the installation



of HVDC Sylwin alpha. There is no offshore crane that can lift SylWin Alpha's record-breaking weight from the topsides. Consequently, the design team decided to combine self-installation ideas with a float-over installation for the platform (OVERDICK, 2014).



Figure 2-10: HVDC Sylwin alpha (OVERDICK GmbH, 2012)

### 2.5.3. Heavy Lifting

Installing an offshore substation involves significant lifting (more than 2,000 tonnes), hence ships need to have enough crane capability. Most ships having the required lift capability don't have enough deck room for a substation platform. As a result, the substation is transported by barge from the substation manufacturing factory to the wind farm location. Installing the substation foundation, which comes before the topside construction, can be done as part of the turbine foundation installation package (The Crown Estate, 2019). It can be a jacket or a monopile as in Figure 2-11.



Figure 2-11: Current thesis OSS installation by Les alizes (**Jan de Nul, 2023**)

### 3. THEORY OF ORCAFLEX

This section outlines the theory used in OrcaFlex software based on User Manual, Orcina Ltd. 1987-2024. An overview about analysis used, environmental conditions, coordinate systems and elements utilized will be presented in this section.

#### 3.1. Type of Analysis

OrcaFlex is a well-known time domain finite element program in the offshore sector. The software program, created by Orcina, is used to analyze maritime risers, mooring systems, installations, and towing systems both statically and dynamically.

##### 3.1.1. Static Analysis

Finding the locations and orientations of each model piece such that all forces and moments are in equilibrium is the final objective of OrcaFlex's statics computation. This might be done as a means to an end in and of itself, or it could be done to provide a dynamic simulation of a starting configuration. The goal of the static analysis is to assure the system's equilibrium position, which is then utilized in the dynamic analysis.

##### 3.1.2. Dynamic Analysis

There are two steps in the dynamic analysis. It comprises of the build-up phase, during which the system's motion and waves are permitted to progress from a motionless state to a fully formed one. Reducing the transients that arise during the transition from the static stage to the fully formed dynamic motion is the purpose of this. The build-up stage, denoted by the number 0, should last for at least one wave cycle. This is to guarantee that the system's motion is completely established. The dynamic equation of motion is examined in the simulation portion, which makes up the second half of the dynamic analysis.

Explicit or implicit integration can be used to calculate the dynamic equation. Both integration techniques solve the system's new geometry at each time step by applying the start conditions that were calculated during the static analysis. This gives OrcaFlex control over all geometric nonlinearities, including the wave loads' spatial fluctuation, the local equation (1) of motion for every item in the system, may be determined by computing the forces and moments acting on each free body and node.

$$\mathbf{M}(\mathbf{p}, \mathbf{a}) + \mathbf{C}(\mathbf{p}, \mathbf{v}) + \mathbf{K}(\mathbf{p}) = \mathbf{F}(\mathbf{p}, \mathbf{v}, t) \quad (1)$$

Where  $M(p, a)$  is the system inertia load,  $C(p, v)$  is the system damping load,  $K(p)$  is the system stiffness load,  $F(p, v, t)$  is the external load.  $p$ ,  $v$  and  $a$  are the position, velocity and acceleration vectors respectively,  $t$  is the simulation time.

### 3.1.3. Explicit Integration Scheme

The explicit scheme is semi-implicit Euler with a constant time step. The static analysis provides the starting locations and orientations of every item in the model, including every node in every line, at the beginning of the time simulation. Next, each free body and node's forces and moments are computed. Considered moments and forces include:

- weight
- buoyancy
- hydrodynamic and aerodynamic drag
- hydrodynamic added mass effects, calculated using the usual extended form of Morison's equation with user-defined coefficients
- tension and shear
- bending and torque
- seabed reaction and friction
- contact forces with other objects
- forces applied by links and winches.

After that, Newton's law, the equation of motion, is created for every free body and every line node.

$$M(p)a = F(p, v, t) - C(p, v) - K(p) \quad (2)$$

Semi-implicit Euler integration is used to integrate the local equation of motion after it has been solved for the acceleration vector, each free body and each line node at the start of each time step. The location, velocity, and acceleration at time step  $t$  may be represented as follows:

$$v_{t+dt} = v_t + dt a_t \quad (3)$$

$$p_{t+dt} = p_t + dt(v_t + dt a_t) \quad (4)$$

Every time step ends with the locations and orientations of every node and free body known once more, at which point the process is resumed.

### 3.1.4. Implicit Integration Scheme

The same formulas that apply to the explicit scheme are used to determine the forces, moments, damping, mass, etc. At the end of the time step, the system equation of motion is then solved.

An iterative solution approach is needed since at the end of the time step,  $p$ ,  $v$  and  $a$  are unknown. As a result, compared to explicit time steps, each implicit time step requires a substantial amount of calculation time. On the other hand, the implicit scheme is usually quicker since it is stable for considerably longer time steps than the explicit system.

### 3.2. Environment

In OrcaFlex, wave trains can be defined by a time history, as random waves, or as regular waves. A sequence of sine waves with a constant amplitude and pseudo-random phase are combined to produce the random waves. A random number generator is used to allocate phases to the phases. This implies that the wave train will always come from the same seed.

The wave kinematics are only defined by linear wave theory up to the mean sea level. Three methods of stretching the wave kinematics are available in OrcaFlex to anticipate the wave kinematics above the mean water level: Vertical stretching, wheeler stretching, and extrapolation stretching. Vertical stretching substitutes the values at the mean water level  $z = 0$  for the values for  $z > 0$ . The extrapolation technique linearly extrapolates the tangent at the mean water level, whereas Wheeler stretching compresses or stretches the water column into a height equal to the mean water depth.

### 3.3. Coordinate Systems

OrcaFlex represents several coordinate systems using a variety of frames of reference, each of which consists of a reference origin and a set of axis directions. First, we designate GXYZ as our single global frame of reference. The global axis directions are GX, GY, and GZ, and the reference origin is the global origin. Next, there are many local coordinate systems, usually one for each model item, indicated by the notation Lxyz, with axis directions pointing in the directions of Lx, Ly, and Lz. Figure 3-1 shows the difference between global and local coordinate systems representation in OrcaFlex.

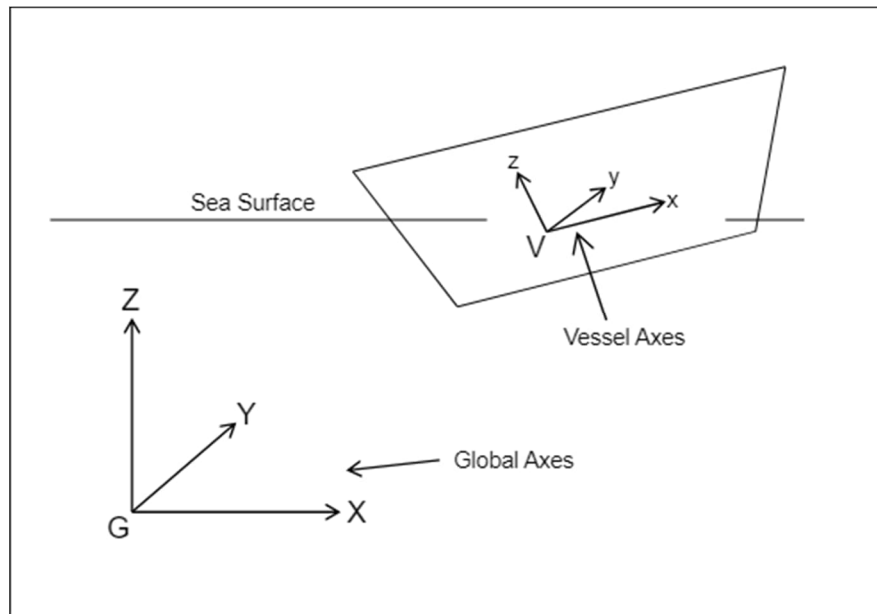


Figure 3-1: Global and local coordinate system according to OrcaFlex

### 3.4. Objects

In order to evaluate a system using OrcaFlex, you must first create a mathematical model of the actual system by use the several modelling tools that OrcaFlex offers. The model is made up of the maritime environment that the system operates in, as well as an arbitrary number of user-selected model objects that are positioned inside the environment and linked together as needed. The environment controls the current, wave excitation, and other factors that the objects are exposed to, while the objects themselves represent the structures under analysis.

#### 3.4.1. Vessels

Vessels are employed to represent floating platforms, barges, ships, and other objects. These are rigid bodies that move in ways that the user specifies. There are several methods to specify the motion of the vessel the usual approach is giving response amplitude operators (RAOs) for each of the six degrees of freedom (surge, sway, heave, roll, pitch, and yaw).

#### 3.4.2. 6D Buoys

6D buoys are rigid entities possessing all six degrees of freedom. OrcaFlex is utilized to compute their rotational and translational motions. There are several types of 6D buoys available for simulating various kinds of sea objects. The mostly used types are lumped and spar buoys, where physical properties are specified properties such as: Mass, mass moment of inertia and center of gravity in local coordinate system, as well as buoyant forces through introducing a certain volume for the 6D-buoy.

### **3.4.3. Lines**

Catenary components, such as pipes, cables, mooring lines, and flexible hoses, are represented by lines. Line characteristics can change as it goes, allowing you to depict a segment that is buoyant, for example. During a simulation, line ends can be disconnected. They can also be fixed, free, or attached to other objects like buoys or boats. In lifting operations like the one performed in the thesis, lines are usually used to represent crane wires and slings.

### **3.4.4. Links**

Links in a model are massless connections that join two other objects. There are two types available. Simple linear elastic links that can withstand tension but not compression are called tethers. Spring/damper component can be nonlinear, and it can withstand both compression and tension.

### **3.4.5. Winches**

Winches serve as massless objects connecting two or more model objects. A winch drive installed on the first item feeds and controls the winch wire used to make the connection. The winch drive has two operating modes: tension-controlled mode, which applies a user-specified tension to the winch wire, or length-controlled mode, which pays out or hauls in the winch wire at a user-specified pace. They can represent tuggers in lifting operations.

### **3.4.6. Shapes**

There are three different kinds of geometric shapes. Since elastic solids are formed of an elastic substance, any item that penetrates them will experience a response force. This means that elastic solids may be utilized as physical barriers to limit the movement of other objects in the system. Parts of the sea that are protected from the waves, such moonpools, can be modelled using trapped water forms. Drawing shapes has no impact on or interaction with the rest of the model; it is just done for visualization purposes. Mainly they were used as objects that represent pulleys.

### **3.4.7. Constraints**

Constraints are massless objects intended to provide general-purpose connections between objects. Two independently rotating and translating frames of reference make up constraint objects. It is possible for one frame to be attached to a parent object and for another frame to be connected to one or more child objects. Degrees of freedom can be added, fixed, or have movements forced upon them by constraint objects. Constraint used to govern the slewing angle of the crane.

## 4. MODEL SET-UP

This section illustrates the steps taken to perform the analysis of the heavy lift operation for the offshore substation. The section starts with a preview on OrcaFlex modelling procedure. Since the focus oriented towards installation of Offshore Substation (OSS), a sequence of modelling the installation scenarios will be presented.

### 4.1. Orcaflex Modelling Procedure

The OrcaFlex model that will be used for the analysis is made up of several objects assembled together to give the final model. Some of these objects are composed of a subsystem that later will be added to the other subsystems to form the final version of OrcaFlex model used for analysis.

#### 4.1.1. *Les Alizes*

Les Alizes is modelled as a vessel object as shown in Figure 4-1.

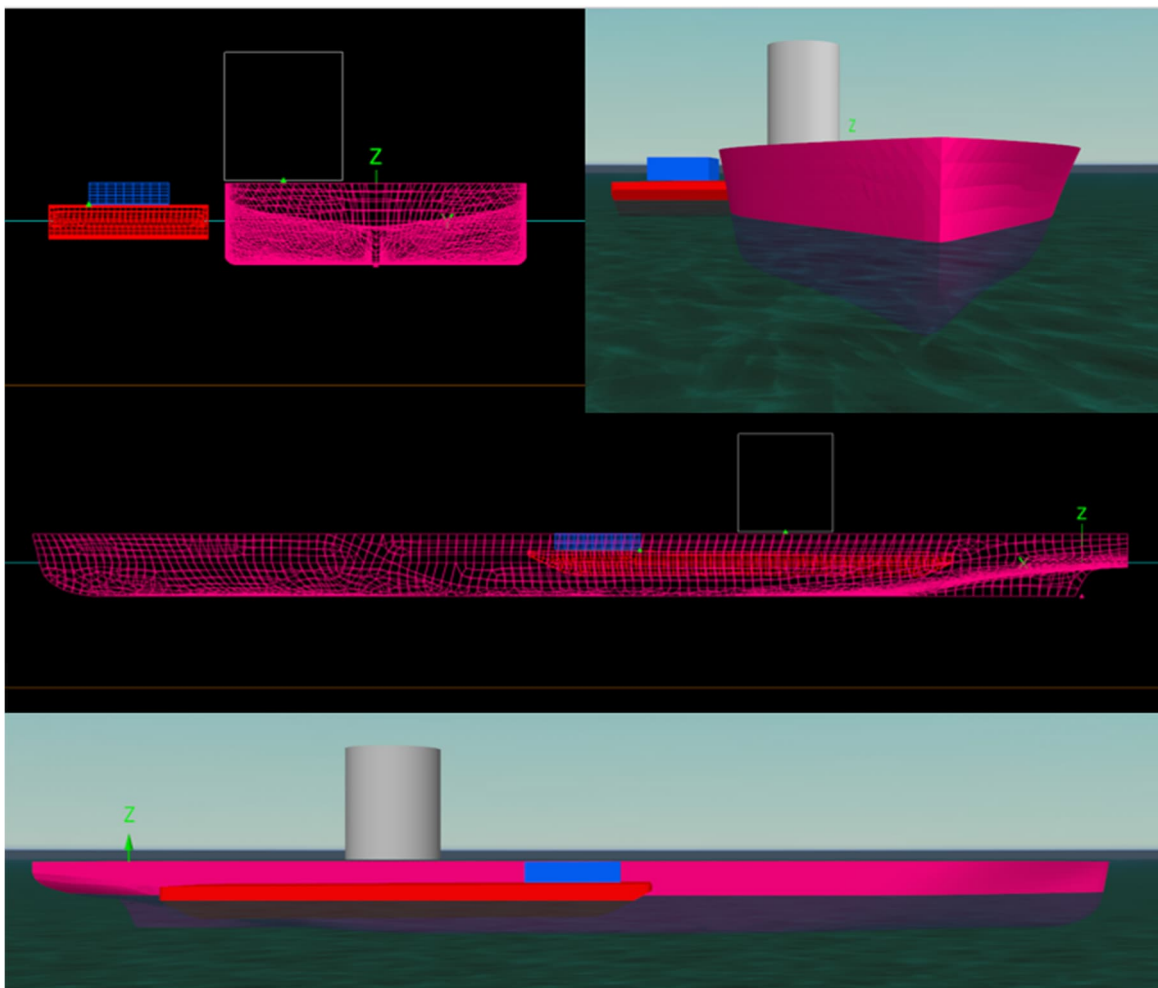


Figure 4-1: Les Alizes naked model sided with a barge



In order to implement the characteristics of the Les Alizes, JDN marine design department have done several hydrodynamic simulations using AnsysAQWA to specify the motion of the vessel for different peak periods and a wave headings range from  $0^\circ$  to  $345^\circ$  with  $15^\circ$  wave heading increment to get the response amplitude operators (RAOs) for each of the six degrees of freedom (surge, sway, heave, roll, pitch, and yaw). This procedure will result in the hydrodynamic data set that is provided to the vessel object that resembles Les Alizes.

#### 4.1.2. Crane Model

The analysis starts when the model that represents the real-life lifting operation is ready. For this operation, Les Alizes is equipped with TMC (Tub mounted crane) to perform all the steps of lifting operation. Figure 4-2 shows Les Alizes with the TMC in its rest position.



Figure 4-2: Les Alizes equipped with TMC (JDN, 2021)

The crane main components are modelled using 6D buoy element. With this element, several physical properties can be defined to represent well the parts of the crane. Mainly, the mass in tons, COG (Center of gravity), mass moment of inertia with respect to the 3 local axis (x,y and z). As well, the visual shape can be approximated to match the real-life appearance through specifying some points then connecting them in a certain manner with lines.

The TMC consists of several components that can be modelled separately, the physical properties of these components are provided by the manufacturer (Huisman, 2019). In addition, the decided configuration to be used in the operation indicates what components should be taken into consideration when modelling. Table 4-1 shows the components with their physical properties needed to be introduced in OrcaFlex.

Table 4-1: Crane components physical properties

Huisman Inertia analysis		Mass	Dimensions			CoG			Moment of Inertia		
		M kg	Lx m	Ly m	Lz m	x m	y m	z m	Jx k .m2	Jy k .m2	Jz k .m2
		Crane cabinet objects									
Crane house		IC	20	20	4.8	0	0	22.3	IC	IC	IC
Slew bearing	Cylinder	IC	20.8	20.8	0.6	0	0	19.6	IC	IC	IC
Winch room	Rectangle	IC	7.4	18	13.7	-14.7	0	21.5	IC	IC	IC
Luffing frame back leg	Rectangle	IC	4.3	15	40.1	-10.5	0	46.3	IC	IC	IC
Luffing frame head	Rectangle	IC	4.5	7.2	4.8	-12.7	0	68.2	IC	IC	IC
Luffing frame front leg	Rectangle	IC	19.6	13.6	36.6	-2.5	0	49.4	IC	IC	IC
		Boom objects									
Boom	Rectangle	IC	112.8	11.7	7.4	71.3	0	32.8	IC	IC	IC
Boom hoist wire	Rectangle	IC	125.4	11.7	33.7	51.4	0	53.2	IC	IC	IC
		Fly and stay objects									
Main hoist block	Point	IC	0	0	0	114.1	0	24.2	IC	IC	IC
Aux hoist block	Point	IC	0	0	0	153.1	0	21.7	IC	IC	IC
Fly Jib	Rectangle	IC	36.6	7.2	5.8	138.4	0	31.6	IC	IC	IC
Stay Beam	Rectangle	IC	3.2	7.2	13.5	117.4	0	44	IC	IC	IC
Lower stay	Rectangle	IC	54.4	7.2	14.8	89.8	0	43.3	IC	IC	IC
Upper Stay	Rectangle	IC	33.7	7.2	19.1	136.2	0	40.9	IC	IC	IC

Table 4-2 illustrates how the physical properties (Mainly inertia properties are needed) of the part can be introduced using 6D Buoy element.

Table 4-2: 6D Buoy inertia portal on OrcaFlex

Inertia:						
Mass (te)	Mass moments of inertia (te.m <sup>2</sup> )			Centre of mass (m)		
	x	y	z	x	y	z
30.0	100.0	100.0	100.0	0.0	0.0	0.0

The standard geometry for the 6D Buoy defined as a cube with 6 m each side, the necessary modifications on dimensions were made so we could attain similar shapes of the crane elements. Some objects were implemented just for visual purposes, for instance; Pedestal, pulleys and links are represented just by shapes and links without any effective physical properties.

In order to represent the slew bearing component and crane tip stiffness a constraint object was utilized. Using constraint object allows the control over the DOFs as well as represent the stiffness of the crane tip. Figure 4-3 shows the TMC with the vessel in rest position model.

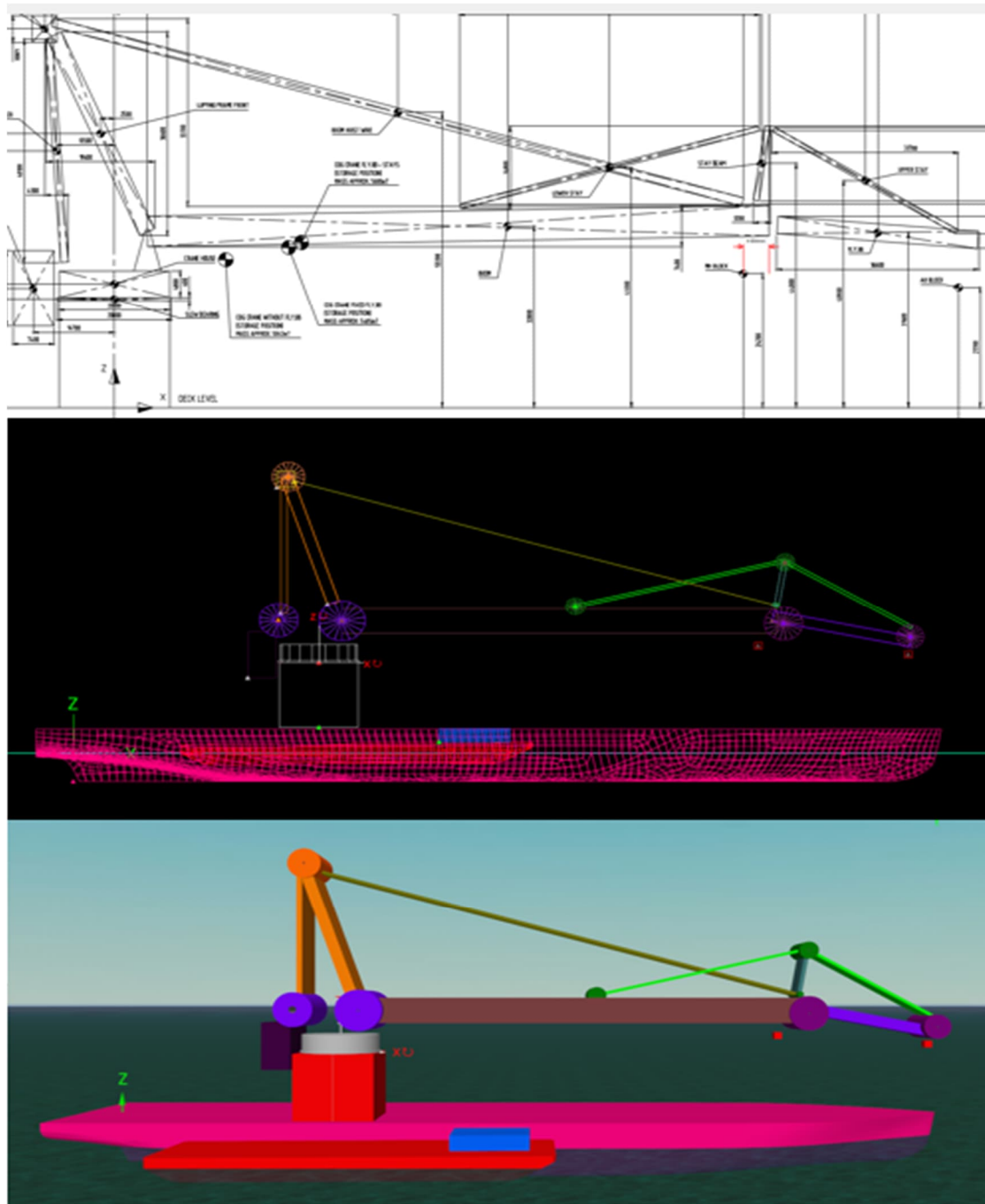


Figure 4-3: TMC integrated with Les Alizes model on OrcaFlex

#### 4.1.3. Main Hoist Block

The next step after modelling the crane and integrating it with the Les Alizes is to define a detailed model for main hoist of the crane, since the rigging system will be implemented to replace the simple model the main hoist of the crane used in the rest position earlier.

The 4 slings and the two crane wires were modelled using line element. Line discretization for smaller segments was used for all the lines. Defining separate type of lines for crane and sling wires each with different physical properties, such as: mass per length and axial stiffness. Table 4-3 shows the physical properties of crane wire and slings line types for pick-up case only.

Table 4-3: Crane wire and sling line type properties

Name		Diameters		Centre of mass		Bulk modulus (kPa)	Mass per unit length (te/m)	Expansion table
		Outer (m)	Inner (m)	x (m)	y (m)			
1	Crane wiresLT	0.24942	0.0	0.0	0.0	Infinity	0.38354	None
2	SlingsLT	0.16	0.0	0.0	0.0	Infinity	0.06639	None

Name		Bending stiffness (kN.m <sup>2</sup> )		Axial stiffness (kN)	Poisson ratio	Torsional stiffness (kN.m <sup>2</sup> )	Tension / torque coupling (kN.m)	Additional bending stiffness (kN.m <sup>2</sup> )
		x	y					
1	Crane wiresLT	120.0	~	2.175e6	0.5	80.0	0.0	0.0
2	SlingsLT	120.0	~	968.9e3	0.5	80.0	0.0	0.0

The main block was divided into main components to resemble its properties. The components of the main hoist block are spreader (Where the sheeves of the crane wires are available), pin connector/Adapter (Connects between the spreader and the hooks by the means of triangular plate) and hooks (Where slings are connected). Figure 4-4 give an idea for one of the main components available of the main hoist block.

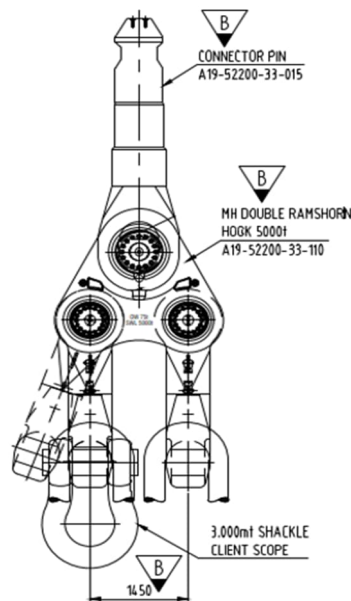


Figure 4-4: Hook interface

Each of these components has its own technical drawing that introduces geometrical and physical properties.

#### 4.1.4. Slings and Crane Wires

A sling, sometimes referred to as a lifting sling, is a piece of chain, webbing, or rope that is used to fasten a load to an independent lifting device like a hoist or crane. They facilitate the safe lifting and handling of bulky, awkwardly shaped, or heavy objects. The slings can be employed in a variety of ways to expand their capacity and improve the manner they sustain the weight. Depending on the climate and application, lifting slings are available in a variety of forms, materials, and load capacities.

There are a working load limit and a safe working load limit for all lifting equipment: The working load of a piece of lifting equipment is its tested limit. That is the most weight it can support, anymore and it will shatter. The safe working load is the maximum that the manufacturer has specified. The load at which you have to stay within to make sure lifting equipment is safe and long-lasting (RS Supplier, n.d.).

Table 4-4: Physical and geometrical properties of the slings

Position	Description	Quantity	WLL/MBL	Length	Diameter	Weight/pc
1	Ultraline dyneema 3-strand	1	MBL = 2622t	39.6m	160mm	1261kg
2	Ultraline dyneema 3-strand	1	MBL = 2622t	39.6m	160mm	1261kg
3	Ultraline dyneema 3-strand	1	MBL = 2622t	40.1m	160mm	1275kg
4	Ultraline dyneema 3-strand	1	MBL = 2622t	40.1m	160mm	1275kg
Total:						4638kg

In order to model the slings and integrate them with main hoist detailed model, properties in Table 4-4 is utilized.

To calculate the axial stiffness of the slings, we could use MBL values provided by the manufacturer using the following series of equations. Stress from the given MBL could be obtained using equation (5):

$$\sigma = \frac{MBL \cdot g}{A} \quad (5)$$

Where:

- $\sigma$ : Stress at MBL in (GPa)
- $MBL$ : Minimum breaking load in (Tons)
- $g$ : Gravitational acceleration of a value 9.81 in (m/s<sup>2</sup>)

- $A$ : Area of the sling in (mm<sup>2</sup>)

Based on the recommendation of the manufacturer, a safety factor of 3.38 should be taken into consideration then the WLL becomes:

$$WLL = \frac{\sigma}{3.38} \quad (6)$$

Where:

- WLL: Working load limit in (GPa)

To get elastic modulus  $E$ , elongation of 1% is considered:

$$E = \frac{WLL}{0.01} \quad (7)$$

Lastly, the axial stiffness will be implemented in OracFlex in kN so the conversion equation states:

$$Axial\ Stiffness = E \cdot A \quad (8)$$

Table 4-5: Slings geometrical and physical properties

Slings								
Diameter m	Area m <sup>2</sup>	E kPa	Axial stiffness kN	Weight t/m	MBL t	WLL	Elongation	E kPa
0.16	0.03	37849064.33	968936.05	0.07	2622	775.74	0.01	37849064.33

After applying unit conversions, the properties needed to model the slings in OrcaFlex are listed in **Table 4-5**.

Crane wires modelling is based on the crane manufacturer technical documentation. The manufacturer proposed an analytical method to obtain crane wire stiffness depending on the considered wire lengths in between elements shown in Figure 4-5.

Below we can see various components of the crane considered to calculate the total length of the crane wire. The following abbreviations are necessary to introduce in order to proceed with our analysis:

$L_{block-tip}$ : Vertical length between the main block bottom and crane tip at the end of the boom.

$z_{tip}$  and  $z_{pivot}$ : Vertical length between crane tip at the boom higher end and the length from the bottom of the boom (Pivot) to the pedestal respectively.

$z_{hook\ below\ pivot}$ : Vertical length between the bottom of the main block and the pivot.



$$\text{Hoist stiffness} = \frac{falls_{hoist} \cdot E_{rope} \cdot fill\ factor \cdot \frac{1}{4} \cdot \pi \cdot d_{rope}^2}{L_{total} / falls_{hoist}} \quad (13)$$

To get each crane wire stiffness, the number of falls in between crane tip and the spreader should be combined in 2 crane wires, each having a common diameter representing the falls used in the operation. The hoist stiffness value should be multiplied by the crane wire length to be complying with OrcaFlex input portal, since the allowed value to be used as input for axial stiffness will be of kN unit, and hoist stiffness is calculated in kN/m.

Table 4-6: Sample calculation of crane wire stiffness (Pick-up case)

E rope MPa	F fill	d rope mm	L block tip mm	falls/wire	L tip crane house mm	falls tip crane house	L return mm	falls return	L total mm	K 1rope in spreader hoist kN/m	Axial stiffness kN
100000	0.67	72	104226	12	99542	2	140300	2	1730396	22701.09	2175445.23

#### 4.1.5. Rigging system

Figure 4-6 and Figure 4-7 gives an overview about the configuration for the rigging arrangement utilized for the lifting operation of OSS.

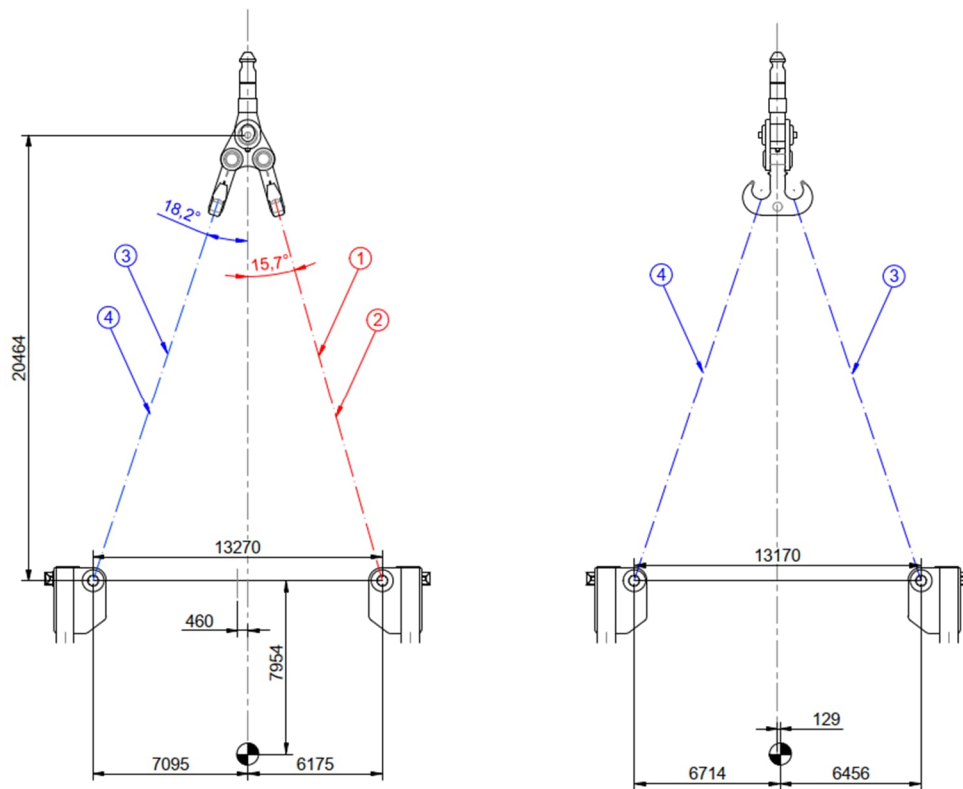


Figure 4-6: Side views of rigging arrangement



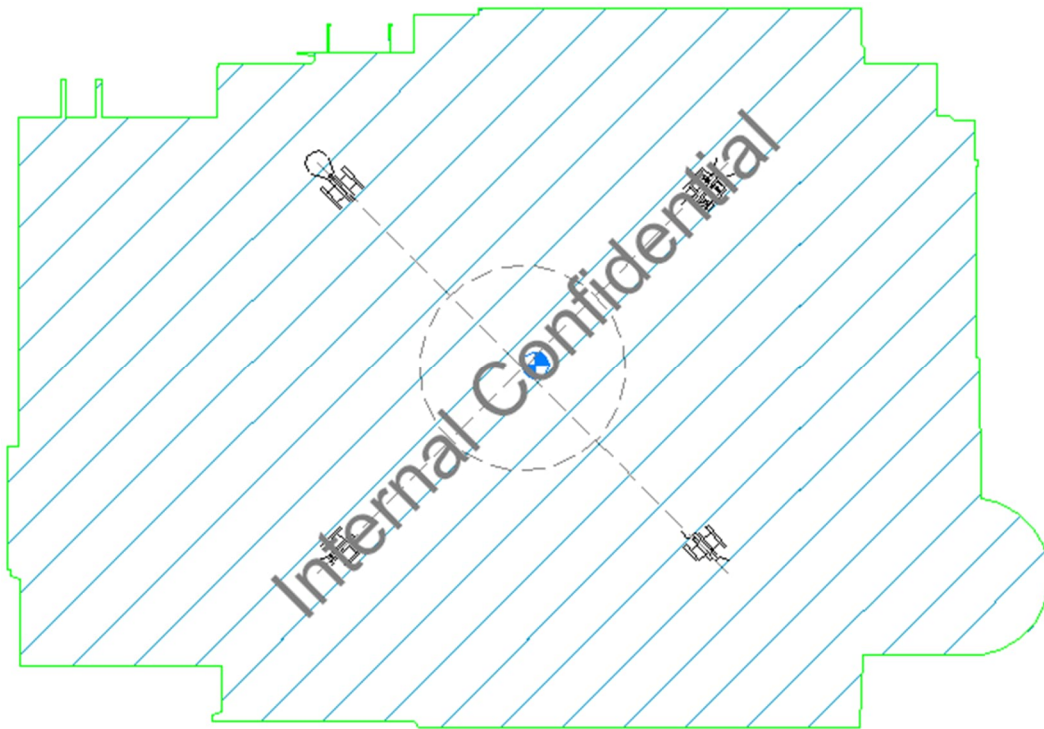


Figure 4-7: Top view of rigging arrangement

#### 4.1.6. OSS Model

The offshore substation this study conducted for is associated for the offshore wind farms Gode Wind 3 (253 MW) and Borkum Riffgrund 3 (913 MW) in the German North Sea, developed by the Danish leader in offshore renewables Ørsted (Jan de Nul, 2023).

The different views of the real-life offshore substation design are shown in from Figure 4-8 to Figure 4-10.

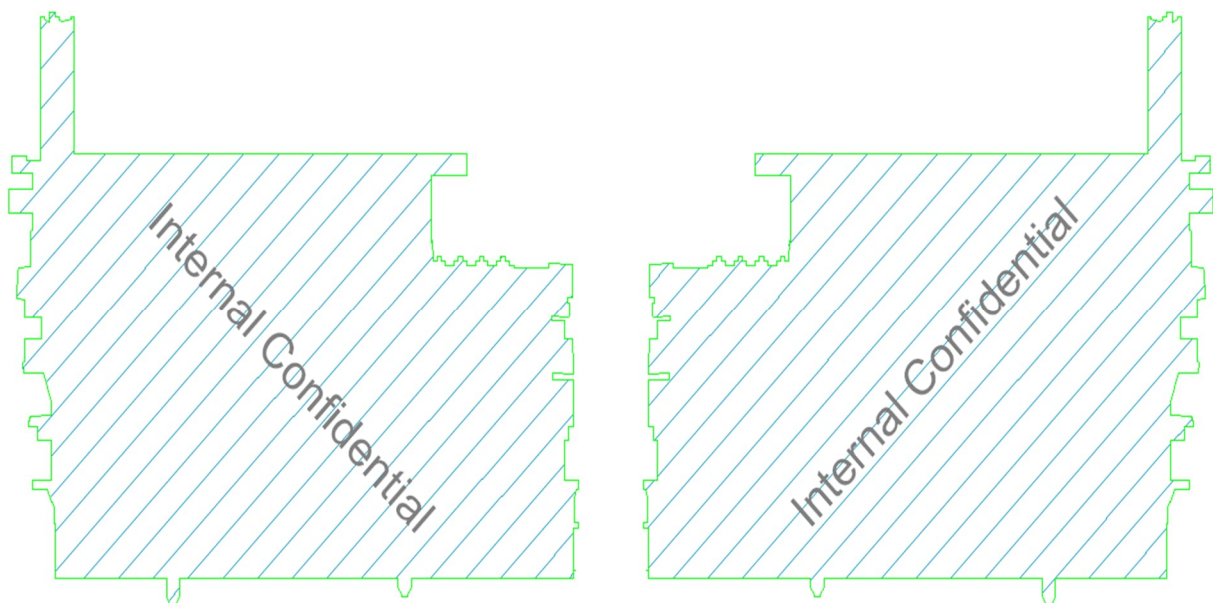


Figure 4-8: OSS side view

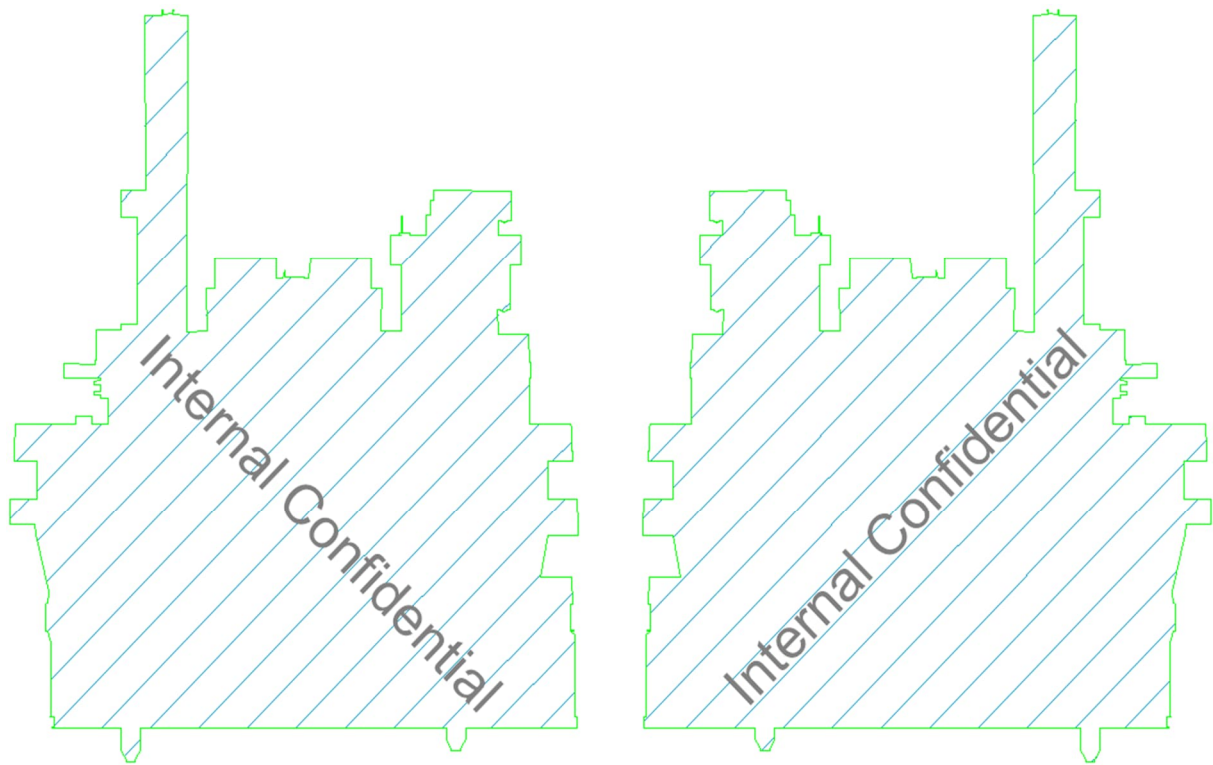


Figure 4-9: OSS front view

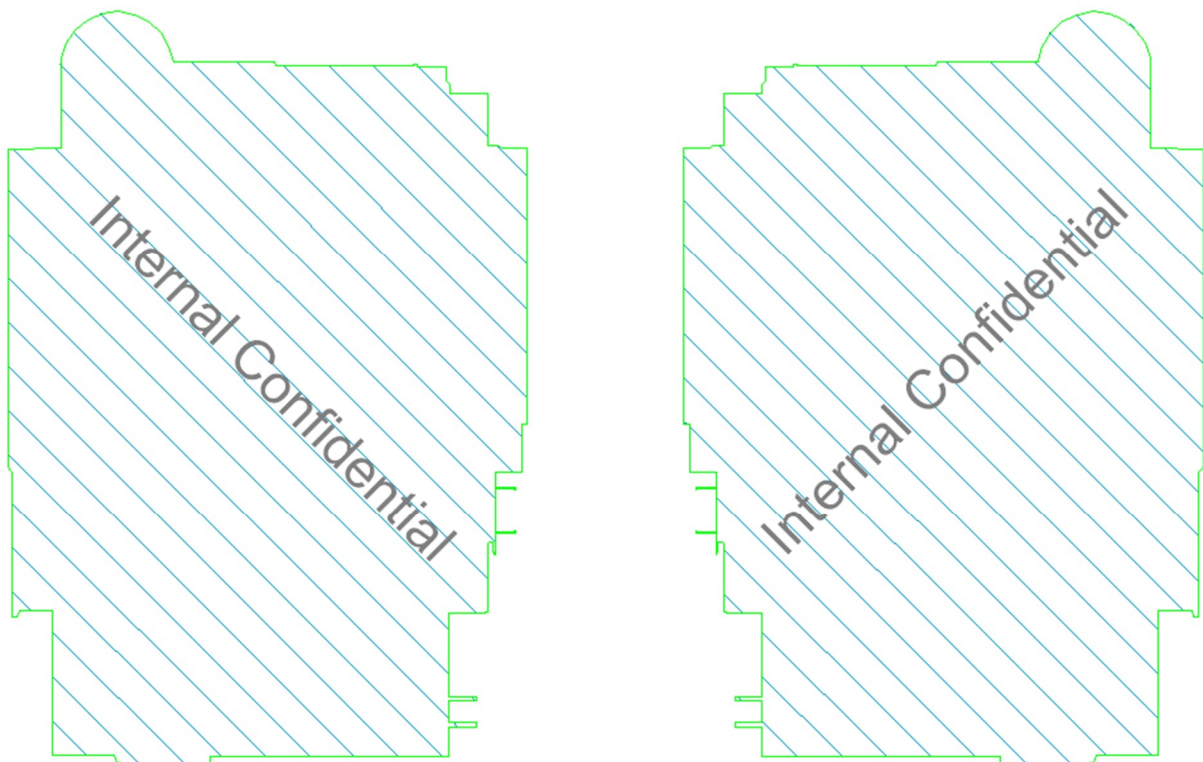


Figure 4-10: OSS top view

In order to calculate the inertia characteristics of the OSS the following equations and Figure 4-11 are used as a reference. (Cameron et al).

$$= \begin{pmatrix} I_{xx} = \frac{1}{12} m (h^2 + d^2) & 0 & 0 \\ 0 & I_{yy} = \frac{1}{12} m (w^2 + d^2) & 0 \\ 0 & 0 & I_{zz} = \frac{1}{12} m (h^2 + w^2) \end{pmatrix} \quad (14)$$

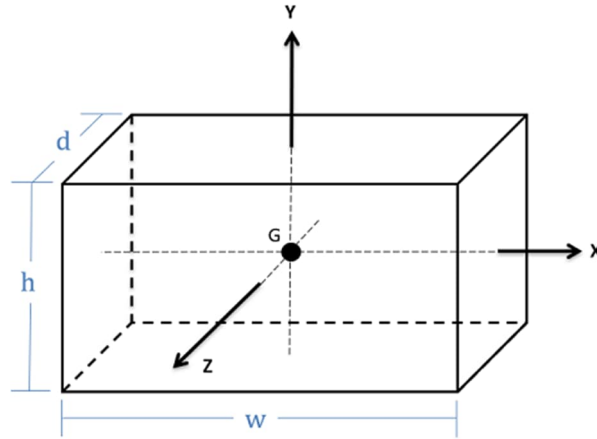


Figure 4-11: Reference shape for rectangular cube (Cameron et al)

Our simplified model for the OSS is represented as rectangular cube shown in Figure 4-12, the main dimensions and physical properties are summarized in Table 4-7;

Table 4-7: Properties of OSS model in OrcaFlex

Mass (t)	Mass moment of inertia (t.m <sup>2</sup> )			Dimensions (m)		
	x	y	z	x	y	z
1904.9	2.05E+05	1.21E+05	2.37E+05	2.20E+01	31.8	16.77

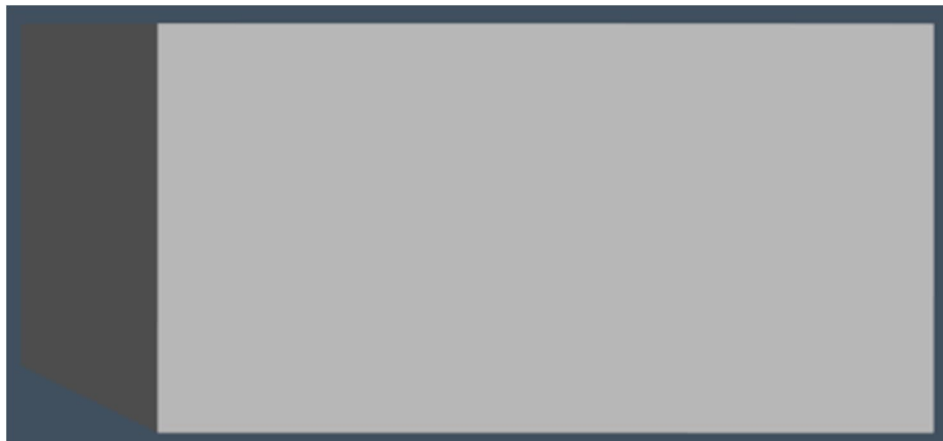


Figure 4-12: OrcaFlex model for OSS

#### 4.1.7. Tugger Lines

Since the operation is very critical, motions of the OSS and the spreader should be minimized to the lowest possible. For this reason, a tug line is implemented. This system consists of two types of tuggers, each serve a specific purpose. Two trolley tuggers used to prevent high main hoist movements through constraining the spreader, while load tuggers trying to prevent OSS deviations from its stable position. Tuggers are modelled as winch objects in OrcaFlex due to their ability to absorb the energy while hauling in and paying out with response to the movements.

There are various modes to control the tuggers behaviour in each stage of the simulation. As it can be seen from Table 4-8 the tuggers utilized are controlled by specified tension in all the simulation stages.

Table 4-8: Control mode of load and trolley tuggers in the upper and lower tables respectively

Stage	Stage duration (s)	Simulation time (s)		Mode		Value
		Stage start	Stage end			
Statics				Specified tension	▼	100.0
0	300.0	-300.0	0.0	Specified tension	▼	100.0
1	10.8e3	0.0	10.8e3	Specified tension	▼	100.0
Stage	Stage duration (s)	Simulation time (s)		Mode		Value
		Stage start	Stage end			
Statics				Specified tension	▼	50.0
0	300.0	-300.0	0.0	Specified tension	▼	50.0
1	10.8e3	0.0	10.8e3	Specified tension	▼	50.0

This tension is based on each type of tuggers limitations provided by the manufacturer. The technical documentation was used to obtain properties concerning tugger lines.

Figure 4-13 to Figure 4-16 illustrate how the complete model will look like before inputting simulation settings. Also, the tug line system is shown how it is integrated with the whole model of the crane made in the previous steps. The tuggers are fixed within the boom of the crane from one end, meanwhile the other end is connected to the object that tries to stabilize during the operation. The shown configuration is only for pick-up phase, other phases of the lifting operation have different model designs.

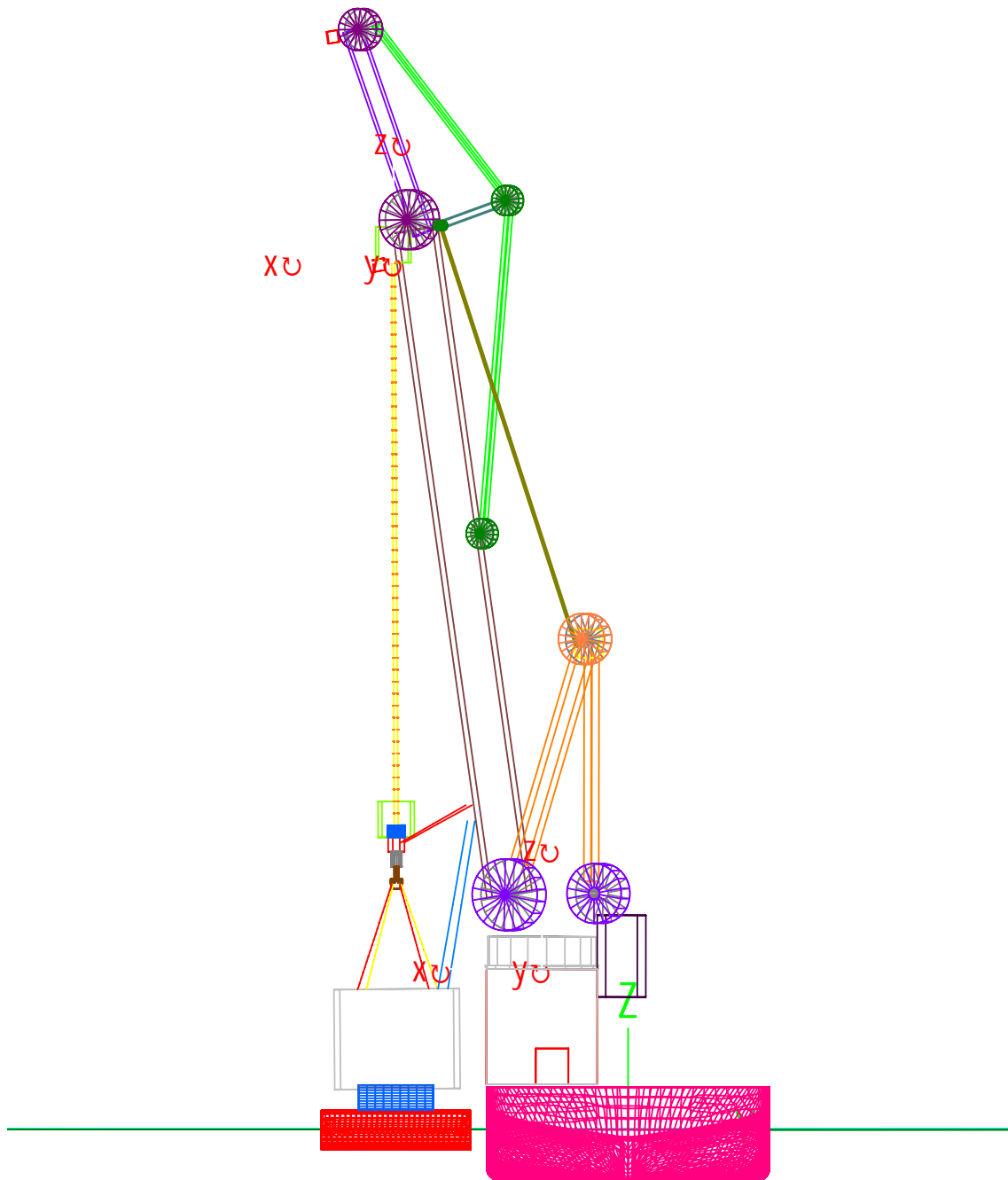


Figure 4-13: Forward view of the OrcaFlex model

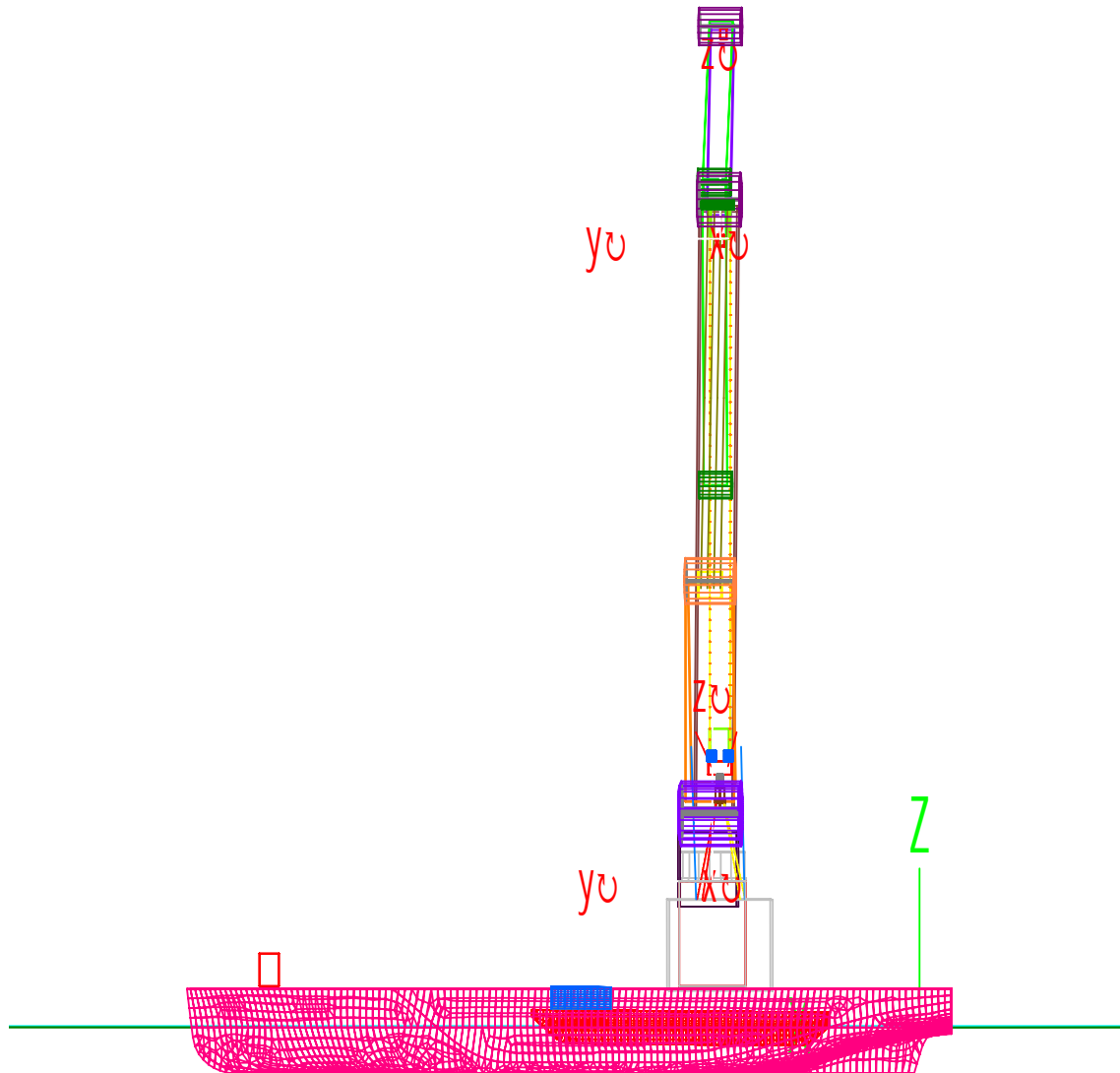


Figure 4-14: Side view of the model

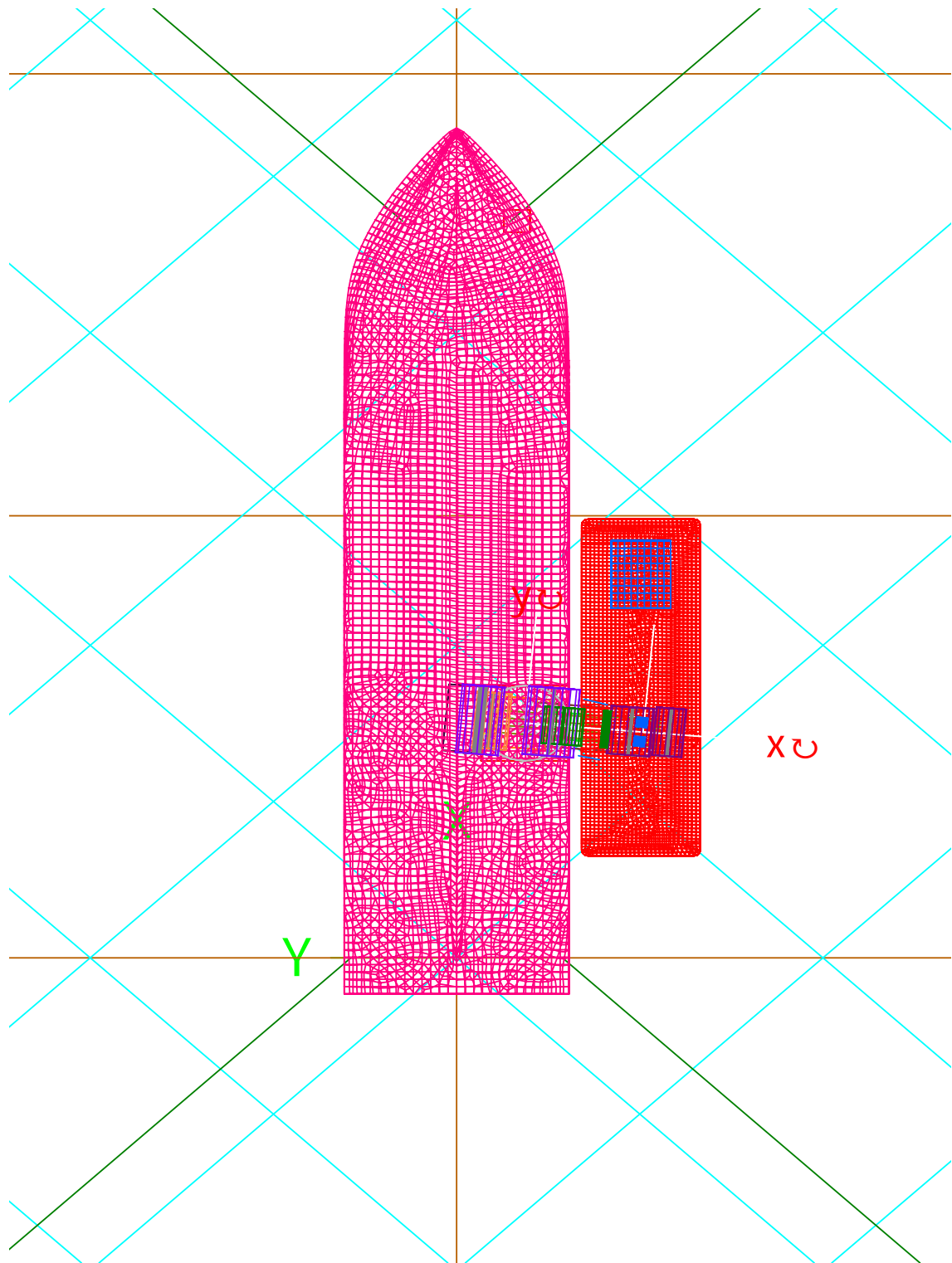


Figure 4-15: Top view of the model



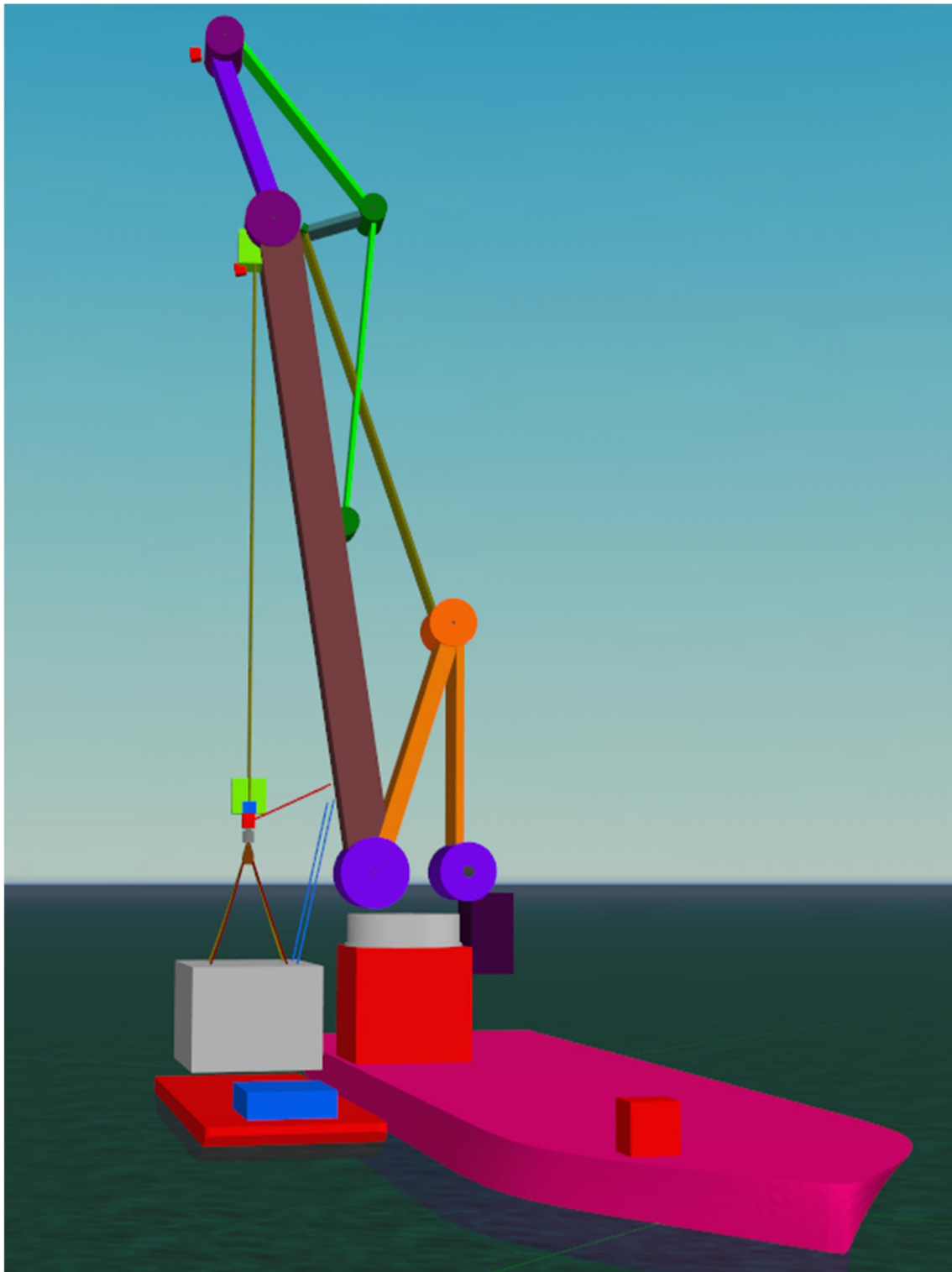


Figure 4-16: Graphic isometric view of the model



## 5. SIMULATION SETTINGS AND PARAMETERS

After building the model and implementing the corresponding physical and geometrical properties that approximate the model to the real-life operation objects, some conditions will be adapted and additional parameters will be adjusted before starting the simulation process.

### 5.1. Crane Tip Stiffness

The crane stiffness for the main hoist and aux hoist is also supplied in order to more precisely compute the dynamic impacts on the crane, load, and/or vessel during a designed lift. The force (in [N/mm] or [kN/m]) required to produce a unit deflection at the hook is the definition of crane stiffness.

Since the wire ropes are significantly less stiff than the steel crane framework, the active hoist and boom hoist wire ropes have the biggest impact on the stiffness of the crane. But when the crane is loaded, its construction will also deform; that is, the luffing frame will bend and the boom length will decrease.

The crane tip stiffness is calculated as follows:

$$k_{crane\ tip} = \frac{k_{crane\ house} \cdot k_{boom} \cdot k_{boom\ hoist}}{k_{crane\ house} \cdot k_{boom} + k_{crane\ house} \cdot k_{boom\ hoist} + k_{boom} \cdot k_{boom\ hoist}} \quad (15)$$

**Figure 5-1** represents the crane system stiffness. The system provides the stiffness of each essential component as a spring element.

Based on the crane manufacturer, it is listed the necessary elements stiffnesses that can help calculate the crane tip stiffness. Different crane radii with different configurations of the main hoist falls were tested in a finite element model that led to getting all necessary elements stiffnesses. The lifting operation will be carried out by the crane with a suitable configuration for this lift.

The main elements are of our interest for the crane tip stiffness calculation for the concerned lifting operation are: Boom, Boom hoist and winch room.

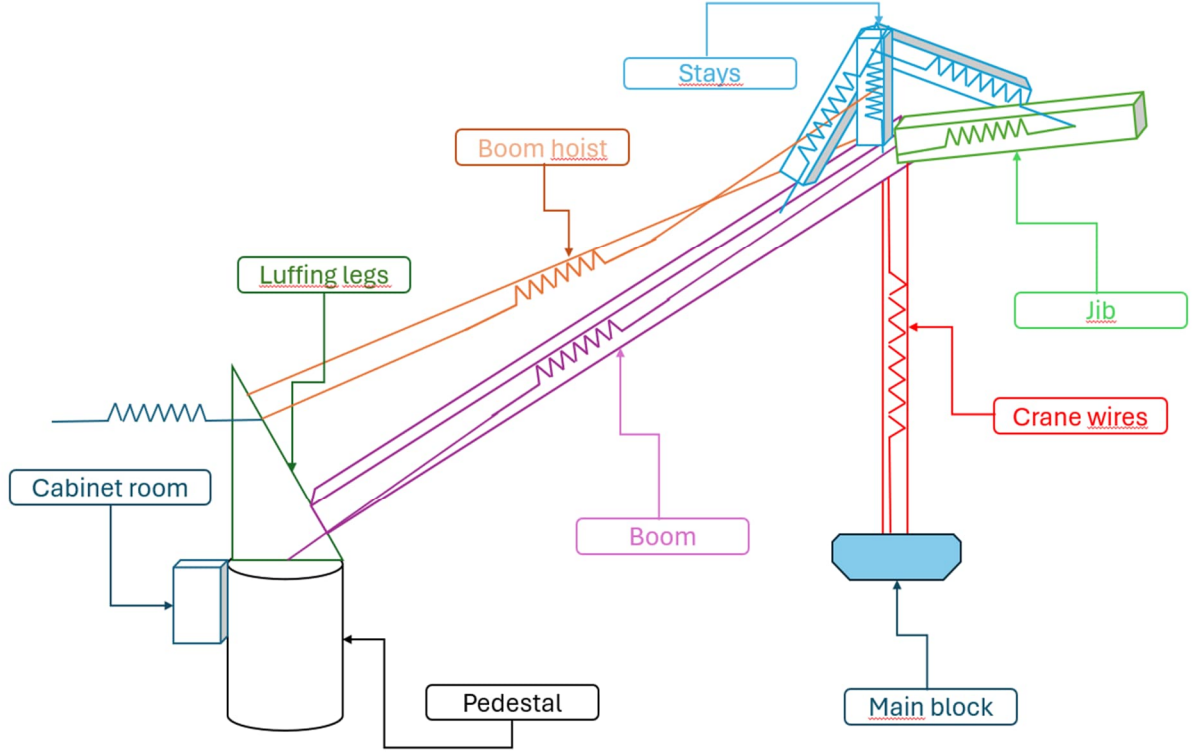


Figure 5-1: Crane stiffness representation

Based on equation (15) and Figure 5-1 above, the crane tip stiffness for the pick-up and transfer and set down phase of operation have been calculated.

## 5.2. Rope Stiffness

The rope stiffness  $k_{rope}$  of a wire rope with length  $L_{rope}$  is calculated as follows:

$$k_{rope} = \frac{E \cdot f_{fill} \cdot \pi \cdot d_{rope}^2}{4 \cdot L_{rope}} \quad (16)$$

where  $E$ ,  $f_{fill}$  and  $d_{rope}$  are the rope's elasticity, fill factor and diameter respectively.

The fill factor of all wire ropes is indicated based on the manufacture's specification. The wire rope length depends on the radius, for the boom hoist wire rope this is the length between the winch via the luffing frame head and the boom head. For the active hoist this is the length between the winch through the crane via the boom tip (last sheave) and the assumed hook position of the indicated distance above or below the boom pivot or the length of the tackle below the hoist upper block sheave shaft. The number of boom and hoist tackle falls, as well as the stays is also taken into account.

### 5.3. Environmental Conditions

Since this OSS associated topside is meant to be installed for the offshore wind farms Gode Wind 3 (253 MW) and Borkum Riffgrund 3 (913 MW) in the German North Sea, the environmental data is therefore based on the wave characteristics of the North Sea.

#### 5.3.1. JONSWAP Spectrum

The offshore sector makes considerable use of the JONSWAP spectrum (17), which was created by the Joint North Sea Wave Project for the restricted fetch North Sea. This spectrum is important since it was designed with wave growth over a finite fetch and shallow water wave attenuation in mind. The spectral formulation was obtained by applying the least squares method to over 2000 observed spectra, under the assumption of near-uniform winds. (Tchetai, 2005).

The JONSWAP spectrum is utilized, which is a standard spectrum derived from data gathered during the Joint North Sea Wave Observation Project. A peak enhancement factor  $\gamma$  is applied to this spectrum, which is a modification of a Pierson-Moskowitz (PM) spectrum. Here is the definition of the JONSWAP spectrum:

$$S(f) = \frac{\alpha g^2}{16\pi^4} f^{-5} e^{(-\frac{5}{4}(\frac{f}{f_m})^{-4})} \gamma^b \quad (17)$$

With:

$$b = e^{(-\frac{1}{2\sigma^2}(\frac{f}{f_m}-1)^2)} \quad (18)$$

As well:

$$\sigma = \begin{cases} \sigma_1 & \text{for } f \leq f_m \\ \sigma_2 & \text{for } f > f_m \end{cases} \quad (19)$$

The various spectral parameters are as follows:  $H_s$ ,  $T_z$ ,  $f_m$ ,  $T_p$ .

$H_s$  is the significant wave height.  $T_z$  is the zero-crossing period.  $T_p$  and  $f_m$  ( $=1/T_p$ ) are the spectral peak period and peak frequency, i.e. those with largest spectral energy.

For the ISSC spectrum,  $T_z$ ,  $T_p$ , and  $f_m$  are interdependent: setting the value of any one of them sets the other two to match.

For the JONSWAP spectrum,

- Automatic parameters mean that you set  $H_s$  and  $T_z$ , and OrcaFlex calculates  $T_p$  and  $f_m$ .
- Partially specified parameters,  $T_z$ ,  $T_p$ , and  $f_m$  are interdependent, so setting any one of them sets the other two accordingly. You must also set the (independent) value of  $H_s$ .

- Fully specified parameters require that you set one of the interdependent values  $T_p$  and  $f_m$ , from which OrcaFlex calculates  $H_s$  and  $T_z$ .

### 5.3.2. *Kinematic Stretching Method*

Based on User Manual, Orcina Ltd, the method of extending linear Airy wave theory to forecast fluid velocity and acceleration (kinematics) at locations above the mean water level is known as kinematic stretching. It is only applicable to Airy waves and random waves (which are composed of many Airy waves).

The notion of linear waves is limited to relatively small waves in theory. Since they are not in the fluid, points above the mean water level are not predicted by it; instead, the theory must be "stretched" to account for them. Three different stretching methods are available in OrcaFlex: vertical, wheeler, and extrapolation approaches.

the horizontal particle velocity  $u$ . In Airy wave theory the formula for  $u$  at position  $(x, z)$  and time  $t$  is:

$$u = E(z) \cdot a \cdot \omega \cdot \cos(\omega t - \phi - k \cdot x) \quad (20)$$

where  $a$ ,  $\omega$ ,  $\phi$  and  $k$  are the wave amplitude, angular frequency, phase lag and wave number, respectively,  $x$  is the distance downstream from the wave origin and  $z$  is measured positive upwards from the mean water level.

The term  $E(z)$  is a scaling factor, given for Airy waves by:

$$E = \frac{\cosh(k(d + z))}{\sinh(k \cdot d)} \quad (21)$$

Where  $d$  is the mean water depth. It is an exponential decay term that models the fact that the fluid velocity reduces with increasing depth.

The followed kinematic stretching method for our operations is the Wheeler stretcher, since this method stretches (or compresses) the water column linearly into a height equivalent to the mean water depth. This is done by replacing  $E(z)$  with  $E(z')$ , where:

$$z' = d \frac{d + z}{d + \zeta} - d \quad (22)$$

and  $\zeta$  is the  $z$ -value at the instantaneous water surface. This formula for  $z'$  essentially shifts  $z$  linearly to be in the range  $-d$  to  $0$ .

### 5.3.3. Wave Conditions

Based on the engineering investigation to determine the limits for the operation done, it is recommended to perform the analysis on certain wave conditions considering the capabilities of Les Alizes DP2 as listed in Table 5-1.

Table 5-1: Wave conditions for the analysis

Tp [s]	Significant Wave height (Hs) [m]						
	135°	150°	165°	180°	195°	210°	225°
4	1.5; 2.5	1.5; 2.5	1.5; 2.5	1.5; 2.5	1.5; 2.5	1.5; 2.5	1.5; 2.5
5	1.5; 2.5	1.5; 2.5	1.5; 2.5	1.5; 2.5	1.5; 2.5	1.5; 2.5	1.5; 2.5
6	1.5; 2.5	1.5; 2.5	1.5; 2.5	1.5; 2.5	1.5; 2.5	1.5; 2.5	1.5; 2.5
7	1.5; 2.5	1.5; 2.5	1.5; 2.5	1.5; 2.5	1.5; 2.5	1.5; 2.5	1.5; 2.5
8	1.5; 2.5	1.5; 2.5	1.5; 2.5	1.5; 2.5	1.5; 2.5	1.5; 2.5	1.5; 2.5
9	1.5; 2.5	1.5; 2.5	1.5; 2.5	1.5; 2.5	1.5; 2.5	1.5; 2.5	1.5; 2.5
10	1.5; 2.5	1.5; 2.5	1.5; 2.5	1.5; 2.5	1.5; 2.5	1.5; 2.5	1.5; 2.5
11	1.5; 2.5	1.5; 2.5	1.5; 2.5	1.5; 2.5	1.5; 2.5	1.5; 2.5	1.5; 2.5
12	1.5; 2.5	1.5; 2.5	1.5; 2.5	1.5; 2.5	1.5; 2.5	1.5; 2.5	1.5; 2.5

## 5.4. Key Factors for Wave Condition Decision

There are several key factors to choose wave headings from 135° to 225° for the concerned operation, the listed factors are the most crucial concerning offshore heavy lifting operations.

### 5.4.1. Operational Safety

Quartering seas are generally represented by headings between 135° and 225°. These are essential for evaluating the stability and station-keeping ability of the ship since waves coming from these directions can produce large roll and yaw moments that are difficult for DP systems to correct.

Precise control over vessel position and orientation is necessary for HLV operations, such as lifting and installing offshore substations or other heavy structures. It is ensured that the vessel can retain even keel position under the most severe conditions by analyzing these wave headings. It is necessary to start the operation with initial heel and trim of 0°.

### 5.4.2. DP System Performance

Dynamic positioning systems undergo tests to see how well they can resist forces from the wind, waves, and current. Wave heads between 135° and 225° present unique challenges because of the vessel's interaction with both rotational and lateral forces. A soft mooring system was implemented to resemble the DP system of the HLV.

## **6. NUMERICAL SIMULATIONS**

The numerical simulations were carried out using OrcaFlex software. This chapter will be focused on how the full simulation is performed, the different stages involved to accomplish the simulations, since the software starts with static simulation and then when it is finished it starts the dynamic phase which could take different approaches to perform it and what limits we are concerned about. Most of the information in this chapter will be based on User Manual, Orcina Ltd. unless it is mentioned.

### **6.1. Static Analysis**

Finding the locations and orientations of each model piece so that all forces and moments are in equilibrium is the final objective of OrcaFlex's statics analysis. This could be done as a means just if the analysis required needs statics results, or it could be done to provide a dynamic simulation which could be an implicit, explicit time domain or even frequency domain a starting configuration. If the system were linear, the equilibrium configuration could be found simply using a single matrix solve; however, because OrcaFlex models are almost always nonlinear, determining statics necessitates an iterative process that makes use of Newton's method in its multidimensional form.

The first step in line statics calculation, only the line object statics are computed. Every other item has fixed degrees of freedom. Establishing an initial configuration for the system's overall statics is the aim of line statics determination. Many techniques are available for the first phase. The catenary approach is used for the falls, which are the model's line objects. The object's weight, buoyancy, and drag are all permitted by the analytic catenary technique, but bending stiffness and form interaction are not. After the catenary technique is completed, the full statics approach is used, which utilizes the equilibrium position found by the catenary method's position to account for bending stiffness and form interaction.

Usually, after establishing the model and providing the proper relations and connections between the objects, it comes setting a correct orientation and segmentation of the sling ropes as line elements. As the segmentation is so fine it might lead to over defined line and static could not be converged. As well as if the followed segmentation is course, the line statics might not or might converge providing not realistic effective tension and line configuration.

One of the crucial variables should be checked before running dynamics is the equilibrium of HLV. The statics should be solved resulting in the correct vessel trim/heel before launching the dynamic simulation, as it will have negative influence on the limits concerning crane wires.

Following the computation of the line statics, the system statics is determined. Now that each object's position and orientation have been established, the model is ready to carry out the dynamic simulation.

## 6.2. Dynamic Analysis

Either the frequency domain or the time domain is used to carry out the dynamic simulation. The dynamic response is solved at discrete frequencies in the frequency domain. In general, simulations in the frequency domain operate more quickly than those in the time domain. Nonetheless, since the analysis is linear, the model's nonlinearities will be linearized. This suggests that sizable nonlinearities have a detrimental effect on the simulation's accuracy and outcomes.

Nonlinearities are implied by multi-body interaction, such as that which occurs between the OSS and the vessel. Time-domain simulations are therefore required.

The equation of motion based on Newton's second law is solved in the time domain as follows:

$$\mathbf{M}(\mathbf{x}, \ddot{\mathbf{x}}) + \mathbf{C}(\mathbf{x}, \dot{\mathbf{x}}) + \mathbf{K}(\mathbf{x}) = \mathbf{F}_E(\mathbf{x}, \dot{\mathbf{x}}, \ddot{\mathbf{x}}, t) \quad (23)$$

with the following:  $F_E(\mathbf{x}, \dot{\mathbf{x}}, \ddot{\mathbf{x}})$  the external load;  $\mathbf{x}, \dot{\mathbf{x}}, \ddot{\mathbf{x}}, t$  the position, velocity, acceleration, and simulation time;  $\mathbf{C}(\mathbf{x}, \dot{\mathbf{x}})$  the system damping load;  $\mathbf{K}(\mathbf{x})$  the system stiffness load. In Section 6.2.1, implicit methods and Section 6.2.2, explicit methods are the two categories of numerical integration techniques used to solve this differential equation in time domain will be explained. Different strategies exist for both implicit and explicit methods; however, OrcaFlex provides one strategy for the former and one for the latter. The ensuing sections address these integration schemes.

### 6.2.1. Implicit Time Domain Simulation

The equation of motion must be solved at the conclusion of each time step in implicit time-domain integration techniques. The Backward Euler technique and the Trapezoidal method are two instances of implicit methods (C. Vuik et al., 2016). The Backward Euler method's significant degree of high frequency damping is one of its issues. With the use of the generalized- $\alpha$  approaches, damping can be adjusted by varying the parameter  $\alpha$ . As a result,

there is less dampening and increased accuracy. It also suggests a less steady outcome, though. The generalized- $\alpha$  integration scheme of Chung and Hulbert is the only one that OrcaFlex provides (J. Chung et al., 1993). In comparison to the explicit integration scheme, this way of solving problems iteratively suggests a longer computing time. On the other hand, in contrast to the explicit method, it provides a more stable way solving the problem.

### 6.2.2. *Explicit Time Domain Simulation*

There are other explicit time-domain techniques, including the Runge Kutta 4 and Forward Euler techniques (C. Vuik et al., 2016). Only the semi-implicit Euler method is available with OrcaFlex. For the acceleration vector, the equation of motion is first solved only locally at the start of the time step. Semi-implicit Euler integration is then used to integrate it. While the Forward Euler technique employs the current derivative, this method uses the derivative at the end of the time step to derive the state of the system. At the conclusion of the continuous time step ( $t + dt$ ), the values of the position  $p$ , velocity  $v$ , and acceleration  $a$  are provided by:

$$v_{t+dt} = v_t + dtat \quad (24)$$

$$p_{t+dt} = p_t + dtv_{t+dt} \quad (25)$$

Each free object and line node's positions and orientations are known at the conclusion of the time step, at which point the procedure is repeated. A reliable approach is the semi-implicit Euler technique. However, the time steps can be quite short due to stability constraints, leading to lengthy calculation times.

The generalized- $\alpha$  approach with a constant time step is utilized for the implicit integration scheme numerical simulations in the time domain of this thesis. The computation time of the implicit integration scheme is longer. Nevertheless, it is more stable than the explicit integration technique, which owing to stability constraints likely requires smaller time steps.

## 6.3. **Simulation Process**

The lifting operation of the OSS mainly consist of three steps:

- 1- Pick-up the OSS.
- 2- Slew and transfer to the position of installation.
- 3- Set up on the MSF.

For our analysis the following scenarios will be considered:

- 1- Pick-up of the OSS.



2- Slew and transfer which will have 2 slew angle options.

The followed method for the dynamic part of the simulation is the implicit time domain analysis. The simulation's duration of 10800 seconds was chosen since it was determined to be a good representation of the 3-hours sea state reference period. As seen in Figure 6-1, in addition to the 10800 seconds of actual simulation time, a 300 second build-up period is used. Sea conditions are gradually built up throughout the build-up phase to prevent transients when the simulation begins, during which wave and vessel motions are smoothly ramped up from zero to their full size.

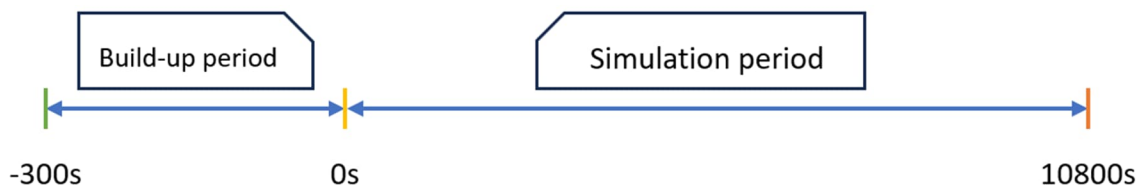


Figure 6-1: Implicit time domain simulation duration

## 7. STATISTICAL CONSIDERATIONS

Upon completion of the necessary simulations for the assumed motion scenarios for the OSS lifting operation, the data related to operation limitations will be extracted. Some parameters are calculated to ensure the feasibility of the operation.

### 7.1. Most Probable Maximum (MPM)

In the field of naval and maritime engineering, it is frequently necessary to forecast the greatest value (extreme value) of a variety of random occurrences that are likely to occur within a specific time frame. For instance, designing ships and other marine structures requires the ability to forecast the biggest motions and wave-induced forces, among other things.

In naval and maritime engineering, random phenomena are often stationary Gaussian (normal) processes that are described as having narrow-band spectra. In contrast to a narrow-band random process, which has a single peak and trough, the spectra of many random phenomena observed in practice span a particular range of frequencies and frequently include many maxima and minima throughout a single cycle as determined from zero crossings. (Michel K. Ochi, 1988).

Depending on which distribution of extreme value statistics is selected, OrcaFlex's results are calculated:

- The Rayleigh distribution method uses a direct calculation, based on the spectral moments of all the data.
- The Weibull and generalized Pareto distributions (GPD) are fitted to selected extremes of the data, those extremes being selected using the peaks-over-threshold method with declustering to reduce dependence between the selected extremes.

To further understand the approach followed to calculate MPM values from the time domain dynamic integration simulations, it is important to differentiate between the types of distributions. A small explanation about different types of statistical distributions that are linked to our analysis will be illustrated in the following part.

### 7.1.1. Continuous Probability Distribution

The range of values in a continuous distribution is unlimited. This indicates that there are an infinite number of different outcomes, as is frequently the case with variables like temperature or time.

For this reason, a continuous distribution is sometimes called a smooth distribution as it likewise follows a smooth curve. For instance, instead of separate dots on a graph, the temperature would follow a curve if you were examining the temperatures of every city in the world throughout time.

A continuous probability distribution is referred to as a "smooth distribution" in statistics. Smoothing, a method of replacing a noisy distribution to filter or attenuate noise, can also result in a smooth distribution. For example, in kernel density estimation (KDE) shown in Figure 7-1, an expanded probability distribution known as a kernel is used in place of discrete points in a sample. (Statistics How To, sd)

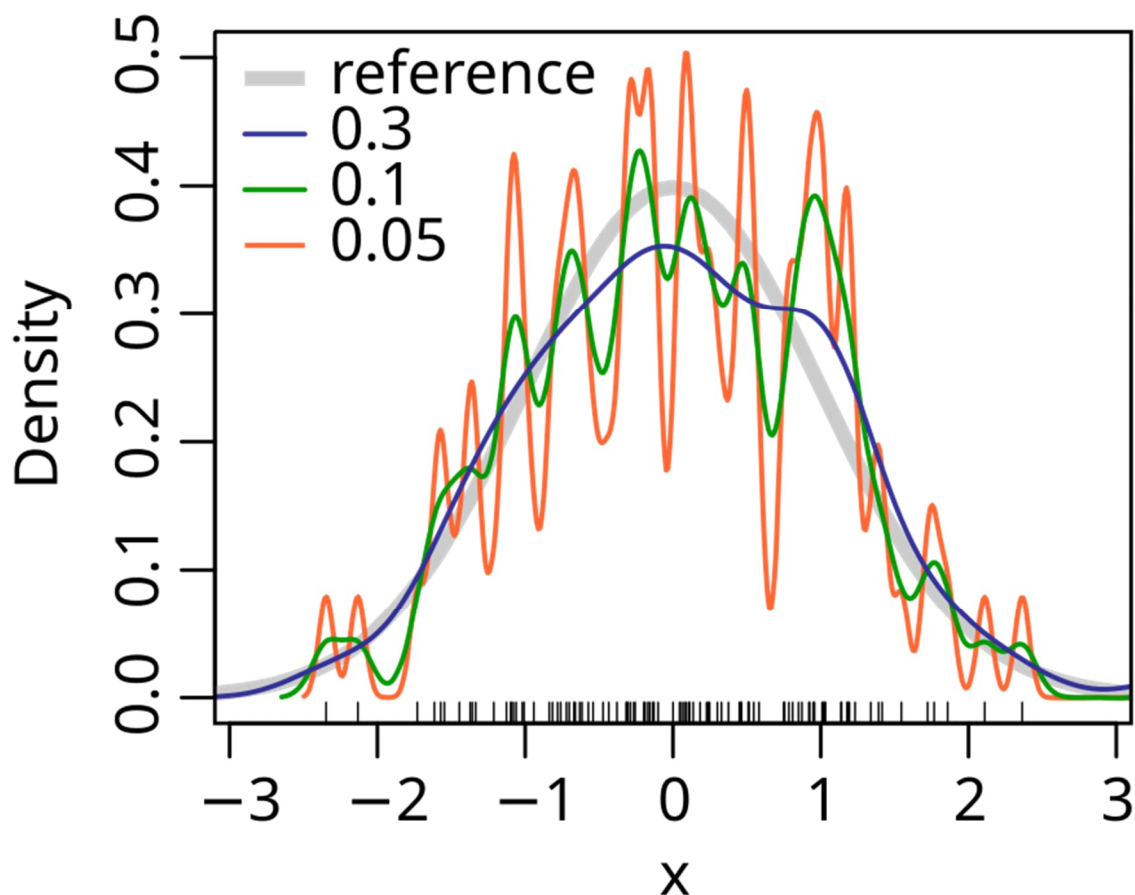


Figure 7-1: Kernel density estimation result showing a smooth distribution (the gray bell curve), (M. W. Toews, sd)

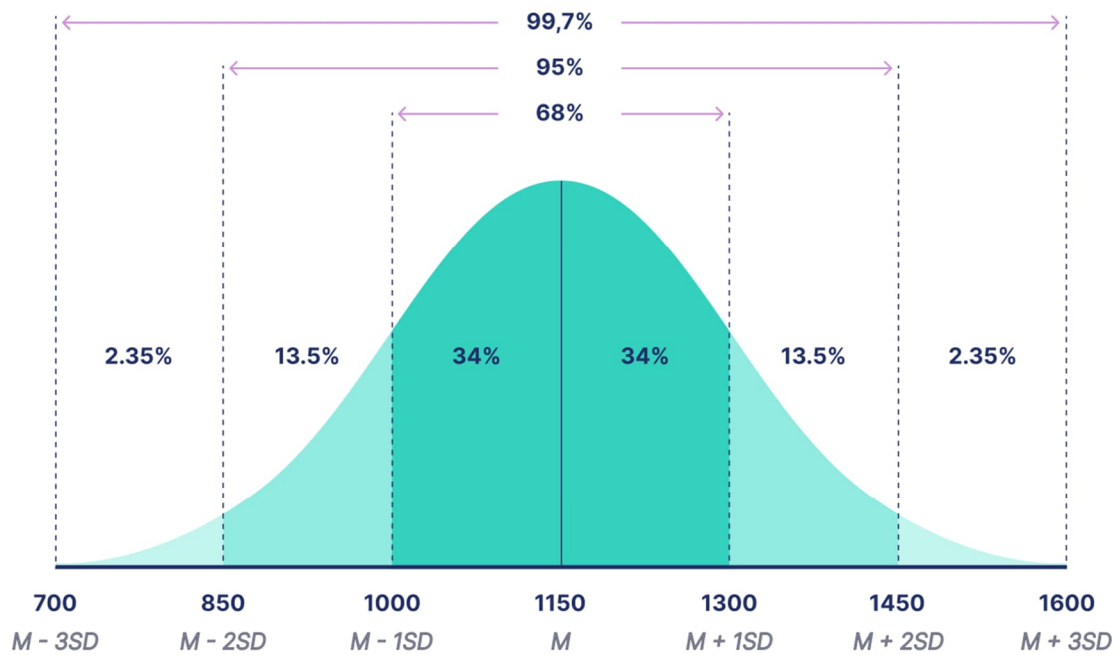


Figure 7-2: A continuous probability distribution showing SAT scores, (Turney, 2022)

**Figure 7-2** presents the SAT results of students enrolled in a new test-prep course. With a mean score ( $M$ ) of 1150 and a standard deviation ( $SD$ ) of 150, the data has a normal distribution. Between 1,000 and 1,300, or one standard deviation above and below the mean, are where 68% of scores fall. Between 850 and 1,450, or two standard deviations above and below the mean, are where about 95% of scores fall. Between 700 and 1,600, or three standard deviations above and below the mean, are where 99.7% of scores fall.

A probability density function (PDF) can be defined for several continuous random variables in order to determine the likelihood that the variable will fall within two ranges,  $a$  and  $b$ .  $P(a < X < b)$  represents this probability, which is more formally expressed as:

$$P(a \leq X \leq b) = \int_a^b f(x) dx \quad (26)$$

By integrating the PDF of the random variable  $X$ , one can determine the probability that  $X$  is on the closed interval  $[a, b]$ . (Statistics How To, sd).

### 7.1.2. Weibull Distribution

The Weibull distribution is a continuous probability distribution named after Swedish mathematician Waloddi Weibull, (Statistics How To, sd). The Weibull distribution is unimodal and explains probabilities associated with continuous data, just like the normal distribution. It can, however, also represent skewed data, in contrast to the normal distribution. In reality, it

can model both left- and right-skewed data because to its tremendous flexibility. Given its flexibility to accommodate a wide range of geometries, this distribution is an exceptionally flexible probability density function. Even the normal distribution and other distributions can be approximated by it. The formula for the probability density function of the three-parameter general Weibull distribution is as follows:

$$f(x) = \frac{\gamma}{\alpha} \frac{(x - \mu)^{(\gamma-1)}}{\alpha} e^{-(\frac{x-\mu}{\alpha})^\gamma} \quad (27)$$

With:

$$x \geq \mu; \gamma, \alpha > 0 \quad (28)$$

Where the shape parameter, or Weibull slope, is denoted by  $\gamma$ . The characteristic life parameter, or scale parameter, is denoted by  $\alpha$ . The location parameter, denoted by  $\mu$ , is sometimes known as the waiting time parameter or, occasionally, the shift parameter. (Statistics How To, sd).

The distributional shape of data is described by the shape parameter. Because its value is equal to the slope of the line on a probability plot, statisticians also refer to it as the Weibull slope.

The Weibull distribution's four main shape value ranges are as follows. It is maintained the scale and threshold settings constant, 4 and 0 respectively in these probability distribution graphs shown in Figure 7-3 to emphasize the effect of varying the shape.

The upper left graph previews the case where  $\gamma < 1$ ; Steadily decreasing values, The Weibull distribution is equal to a two-parameter exponential distribution when the shape parameter is equal to 1.

The upper right graph shows the case where  $1 < \gamma < 2.6$ ; Right skewed, the Weibull distribution becomes a Rayleigh distribution when the shape parameter is equal to 2.

The lower left graph illustrates the case where  $\gamma = 3$ ; Approximates a normal distribution, also known as the Gaussian distribution.

The lower right graph clarifies the case where  $\gamma > 3.7$ ; Left-skewed. (Frost, Statistics By Jim, sd).

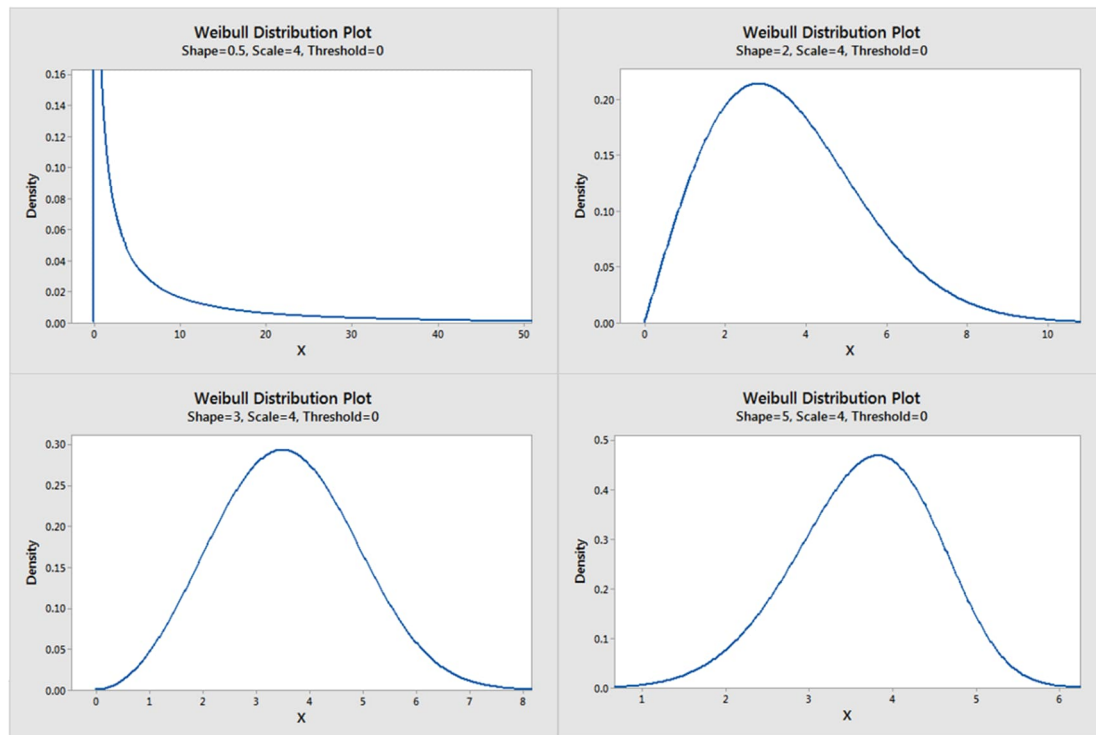


Figure 7-3: Shape parameter influence on Weibull distributions, (Frost, Statistics By Jim, sd)

The distribution's variability is represented by the scale parameter. The extent to which the probability distribution expands is dependent on the scale parameter. The distribution moves further to the right and the height gets shorter as you increase the scale. As can be seen in Figure 7-4, decreasing the scale causes the distribution to decrease to the left and raise its peak. (Frost, Statistics By Jim, sd).

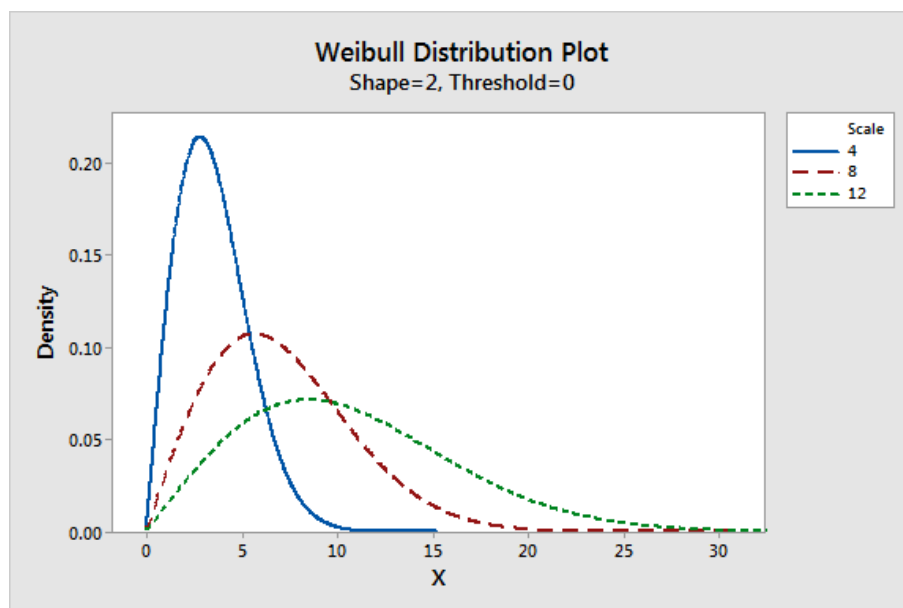


Figure 7-4: Scale parameter implication on Weibull distribution, (Frost, Statistics By Jim, sd)

The lowest value that can exist in a Weibull distribution is defined by the threshold parameter. This parameter is referred to as the location parameter by certain analysts. Every value needs to be higher than the threshold parameter. As a result, the distribution can accommodate both negative and positive values when the threshold values are negative. It can only have positive values when the value is zero. The threshold of a two-parameter Weibull distribution is simply set to zero. An illustrative example is shown in Figure 7-5, where both shape and scale parameters are set into constant values, 2 and 4 respectively, meanwhile the threshold parameter given several values. (Frost, Statistics By Jim, sd).

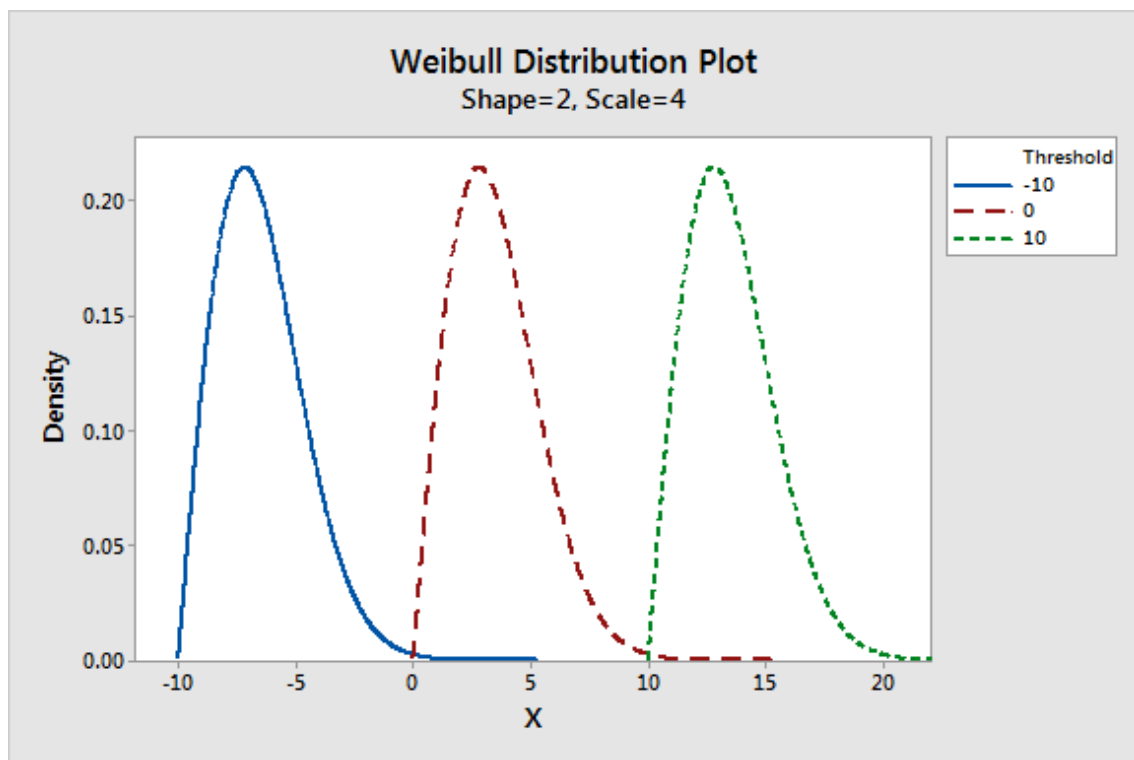


Figure 7-5: Threshold parameter influence on Weibull distribution, (Frost, Statistics By Jim, sd)

### 7.1.3. Rayleigh Distribution

A continuous probability distribution called the Rayleigh distribution bears the name of the Englishman lord Rayleigh. With a scale parameter of 2, it is a particular instance of the Weibull distribution.

As the shape parameter increases, the distribution gets wider and flatter. Figure 7-6 shows the probability density function of several Rayleigh distributions with different several different shape parameter ( $\sigma$ ). (statistics How To, sd)

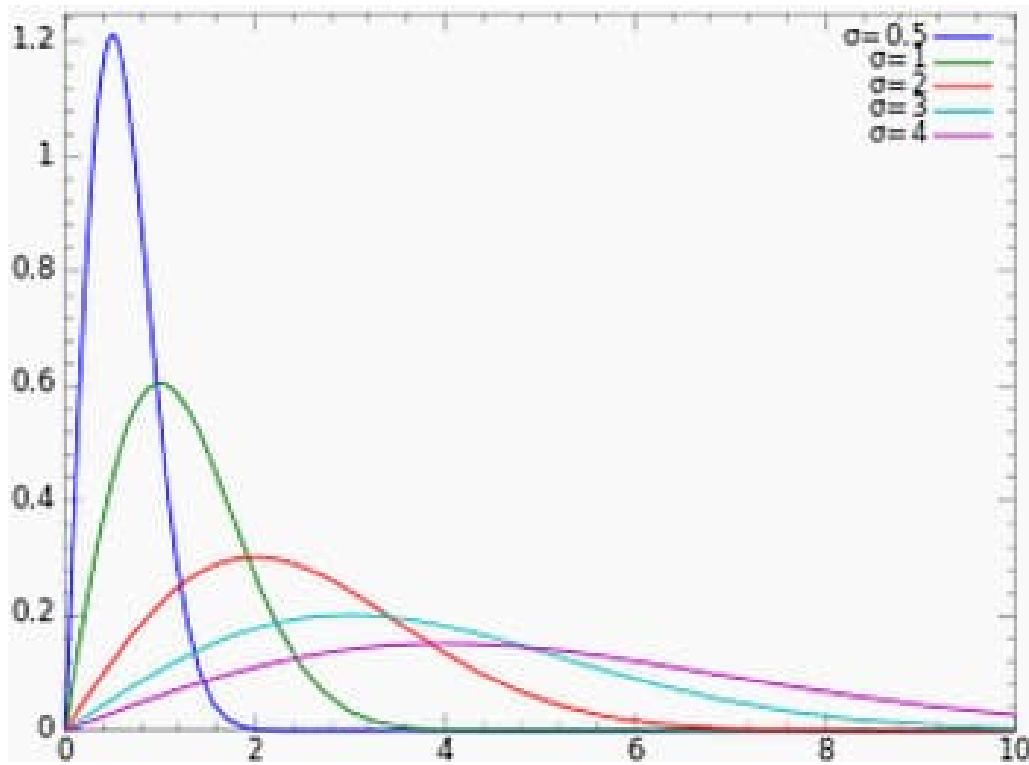


Figure 7-6: Rayleigh distributions with different shape parameters, (**statistics How To, sd**)

## 7.2. MPM Amplitude

To calculate the key indicators that judge the workability of the operation, MPM amplitude is needed to be evaluated. Requirements are imposed by classification societies according to extreme values that represent the distribution's mode. The most probable maximum (MPM) is the name given to this extreme number. Though it isn't the biggest maxima, it happens the most often. Additional criteria apply to maxima falling between the 85th and 95th percentile, (Det Norske Veritas, 2014). Compared to other maxima, this extreme value is often less frequently used. Yet, it is one of the highest values ever recorded.

The following equation gives the general value of the MPM amplitude, it could be used as a part of calculating a certain key parameter that limits lifting operation. The MPM or expected reaction amplitude, is the amount that will, on average, be exceeded once per 1000 wave encounters, or around every three hours. The MPM response, which is equivalent to a factor of 1.86 on the significant value, is widely recognized as the design value.

$$\text{MPM amplitude} = \text{MPM factor} \times \text{Standard deviation} \quad (29)$$

$$\text{MPM factor} = \sqrt{2 \ln \left( \frac{T}{T_z} \right)} \quad (30)$$



---

Where T is the estimated simulation period equals to 10800s and Tz is the mean up-crossing period of a value of 10.8s,

$$\mathbf{MPM\ amplitude = 2 \times 1.86 \times Standard\ devialtion} \quad (31)$$

For some parameters it is necessary to add the mean value to the MPM amplitude as it counts to calculate some limitation. For instance, the dynamic load (Effective tension in kN) in crane wire will be:

$$\mathbf{Crane\ wire\ dynamic\ load = crane\ wire\ mean\ load + MPM\ amplitude} \quad (32)$$

## 8. RESULTS AND DISCUSSION

The following section addresses the results extracted from OrcaFlex simulations and rises a discussion about them to come up with a conclusion. Indicating which practices and results will lead to violate the limitations set for the operation. The decision will be made depending on several key indicators that will help upon deciding the possibility of executing the operation. The analysis will be stated for the 3 steps carried out during the lifting operation. The concerning parameters that limit the operation will be presented such as: DAF, Off lead, Side lead, power for load as well for trolley tuggers, OSS motion and velocity.

### 8.1. Pick-Up Phase

The pick-up phase refers to the phase where the OSS is being lifted from the moored barge by the HLV after ensuring the rigging of the eye pads with the sling ropes and cutting off the sea fastening tools in between the barge and the OSS.

#### 8.1.1. DAF Of Main Hoist

In the world of offshore heavy lifting, dynamic amplification factor (DAF) is one of limitation criteria that assist the safety of the operation carried out. The application of dynamic loading is necessary to take into consideration the combined impacts of vessel motions, boom, wire and rigging stiffness, boom tip placement and motions, crane movements, and wind loading. Usually, this is stated as a DAF, or dynamic amplification factor. (DNV, 2023).

In simple terms, to evaluate DAF:

$$DAF = \frac{\text{Dynamic load}}{\text{Static load}} \quad (33)$$

Where *Dynamic load* consists of all the earlier mentioned impacts possible to happen.

The DAF for the crane wires is displayed in Figure 8-1 and Figure 8-2 refers to  $H_s = 1.5\text{m}$  and  $H_s = 2.5\text{m}$  respectively. Keep in mind that the total of the line loads in the two crane wires is summed and divided by their static load.

It is noticed that the DAF values for wave headings  $210^\circ$  and  $225^\circ$  are not following a certain or the expected trend. As the waves encounter the system have higher  $T_p$ , the system response would be more tense, higher  $T_p$  waves means that they traveled more distance above the sea surface without breaking, thus accumulating more energy prior to their encountering with the model. Since these two headings are not favorable specially to heavy lift vessels, having more

probability to excite DOFs (Roll and Pitch) motion and so the HLV might experience combined motion impacts of the past mentioned DOFs causing erratic motion. This can lead to random dynamics and inconsistent tension in the crane wires.

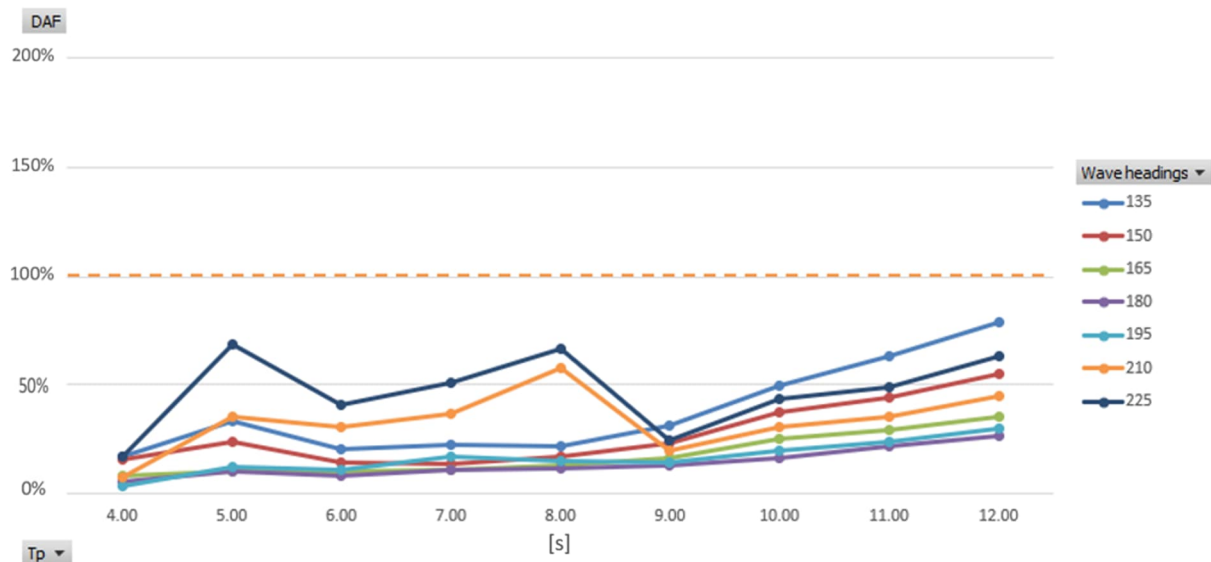


Figure 8-1: Crane wire DAF,  $H_s = 1.5\text{m}$

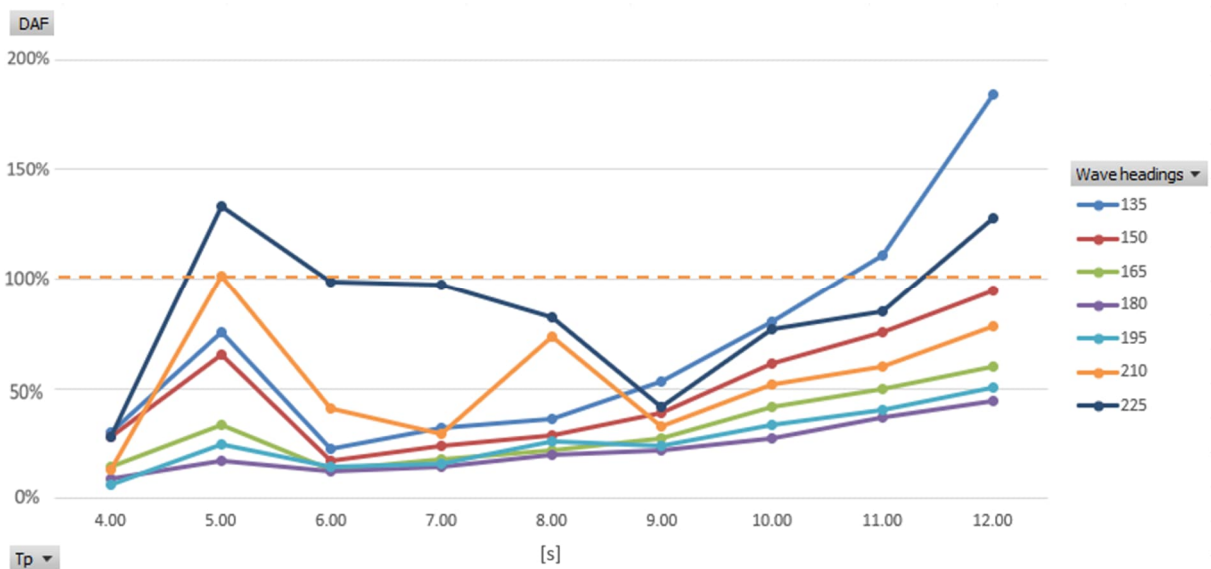


Figure 8-2: Crane wire DAF,  $H_s = 2.5\text{m}$

In addition, it is noticed for both graphs that the DAF values at  $T_p = 5\text{s}$  are experiencing a sudden rise for all the wave headings. As shown in Figure 8-3, a modal analysis of the modelled system is carried out, the first 20 mode shapes are carried out. It is noticed the mode shapes for periods close to 5s lead to high excitation of the system. The shown motion graphics in Figure 8-3 are amplified to give clearer idea on the system excitation.

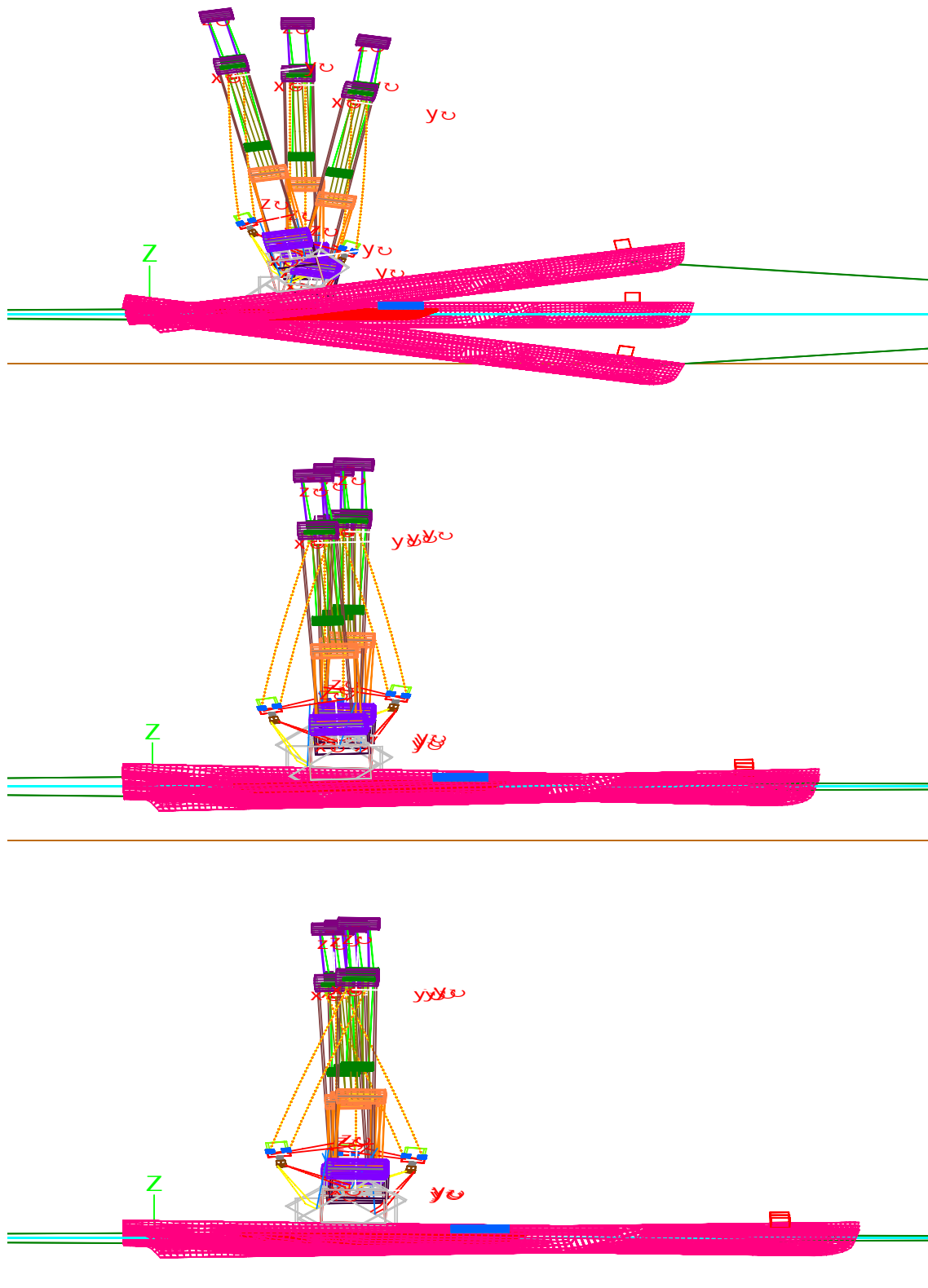


Figure 8-3: Modal analysis for the modelled system

It is noticed that from  $T_p = 6s$  until  $T_p = 12s$ , the DAF values for all wave headings, excluding the  $210^\circ$  and  $225^\circ$  wave headings for the above-mentioned reasons are following the expected trend, where DAF values are increasing with the increase of the  $T_p$  of the encountered wave.

### 8.1.2. Off Lead (OL) of Crane Wires

In the plane of the jib and boom, off lead is the angle formed by the hoist tackle and the boom's centerline (weight going sideways) as shown in Figure 8-4. (Huisman user manual).

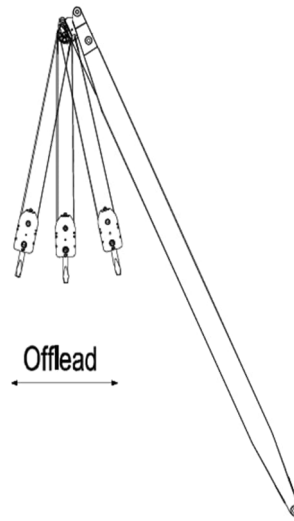


Figure 8-4: Off lead illustration, (Huisman)

Figure 8-5 and Figure 8-6 show the mean MPM OL angles for  $H_s = 1.5\text{m}$  and  $H_s = 2.5\text{m}$  respectively, the mean MPM OL angle is obtained by calculating the MPM OL angle for the right and left wire, then summing up their values and dividing by 2.

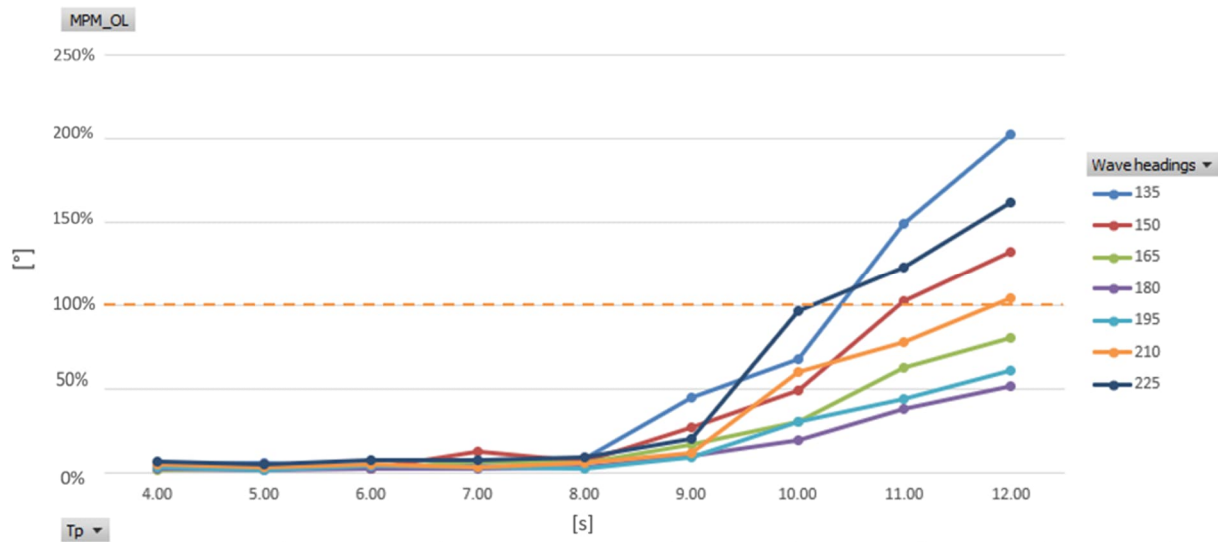


Figure 8-5: Crane wire mean off lead angle,  $H_s = 1.5\text{m}$

In the above graph, it is clear that the off-lead deviation rises in value with the rise of  $T_p$  value with all the considered wave headings, which is expected. At  $T_p = 11\text{s}$ , some exceedances for the MPM OL limit are noticed for wave headings  $135^\circ$  and  $225^\circ$ . Moreover, heading  $150^\circ$  exceeds the limit at  $T_p = 12\text{s}$  as well.

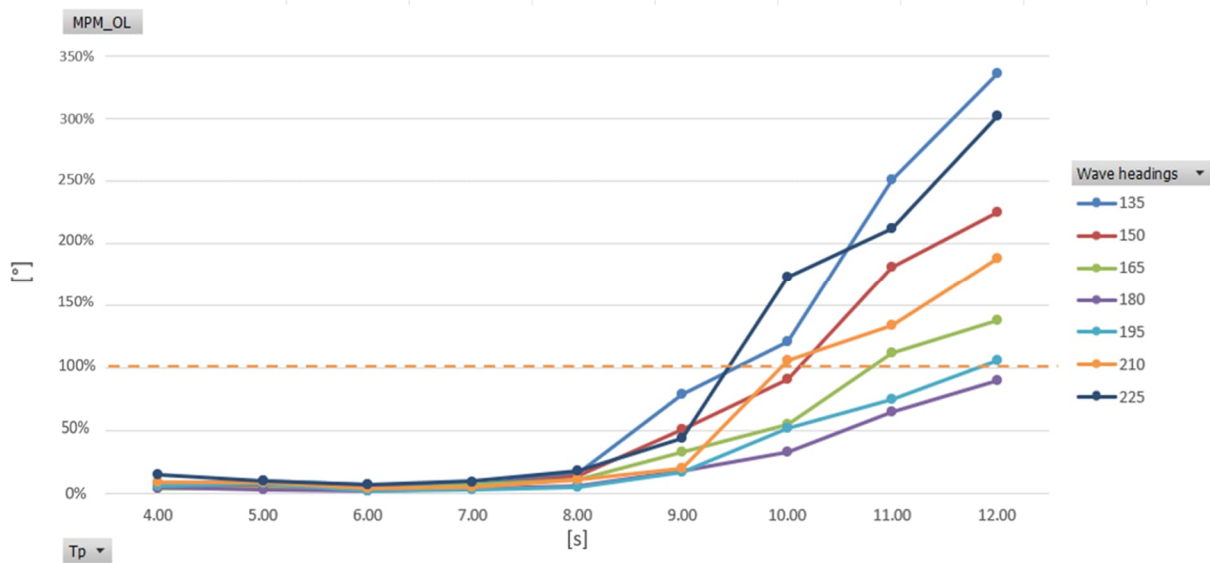


Figure 8-6: Crane wire mean off lead angle, Hs = 2.5m

It is evident from the above graph that, as would be predicted, the off-lead deviation increases in value as the Tp value ascends for all wave heads taken into consideration. At Tp = 10s, wave headings 135°, 210° and 225° exhibit some exceedances of the MPM OL limit. Furthermore, for Tp = 12s, all the headings surpass the limit as well expect for heading 180°.

### 8.1.3. Side Lead (SL) of Crane Wires

The angle formed by the hoist tackle and the boom's centerline when the weight moves sideways out of the plane of the jib and boom is known as the side lead. Shown in Figure 8-7. (Huisman user manual).

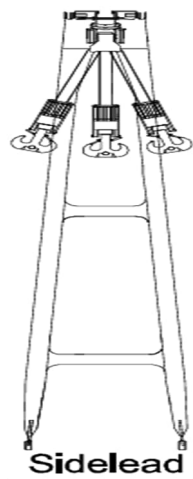


Figure 8-7: Side lead illustration, (Huisman)

The mean MPM SL angles for Hs = 1.5m and Hs = 2.5m, respectively, are displayed in Figure 8-8 and Figure 8-9.

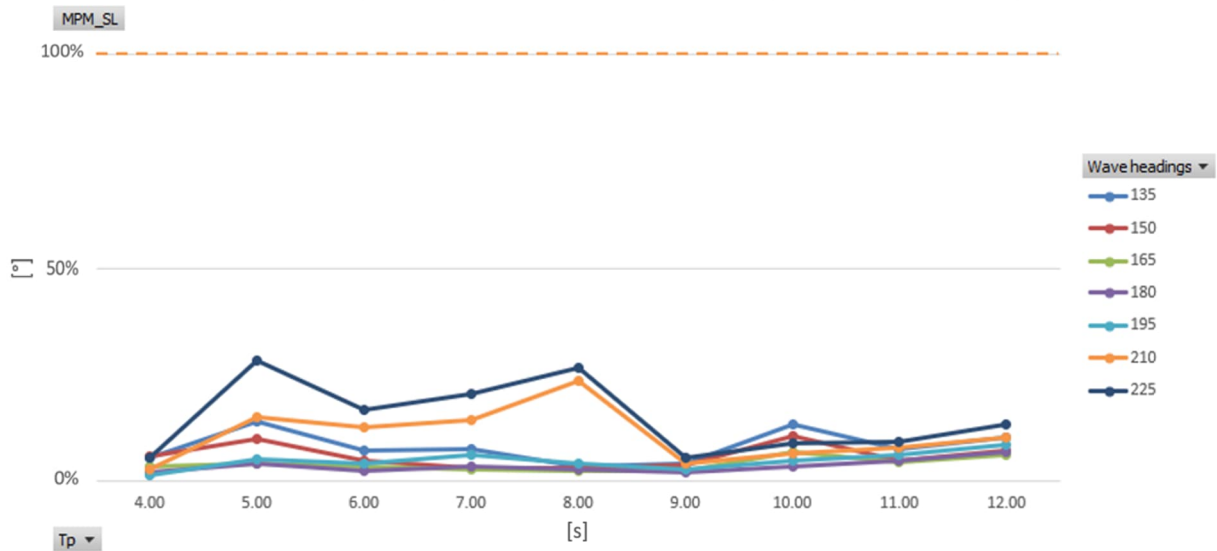


Figure 8-8: Crane wire mean side lead angle, Hs = 1.5m

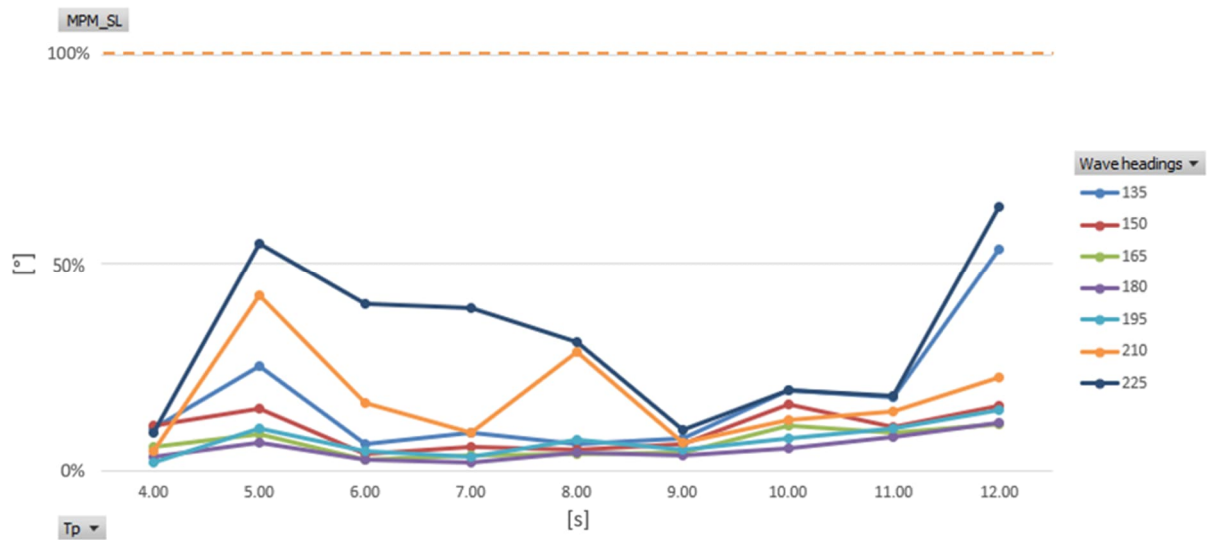


Figure 8-9: Crane wire mean side lead angle, Hs = 2.5m

Clearly no case in both graphs violates MPM SL limit, however it is worth mentioning that the followed trend in wave headings 210° and 225° is the same that they followed in the graphs of the DAF analysis.

#### 8.1.4. Load Tugger Power

In order to set a limit for the load tuggers in use, it is decided to bound their functionality by power limit. If this value of kW exceeded, then the tuggers will fail and eventually the operation will not be realized. The following equation used to specify the power limit of the load tugger.

$$P = T \cdot V \quad (34)$$

Where:

P: The power of load tugger in kW. Limit: 331 kW

T: The constant tension constraint of a load tugger: 100 kN

V: The payout/haul in speed of the load tugger in m/s

#### 8.1.4.1 Load tugger 1

In the following 2 graphs presented by Figure 8-10, the power limit is monitored throughout the whole simulation (10800s). The tension is fixed for load tugger as states at 100 kN, meanwhile the velocity that the tugger haul in or payout is changing with time.

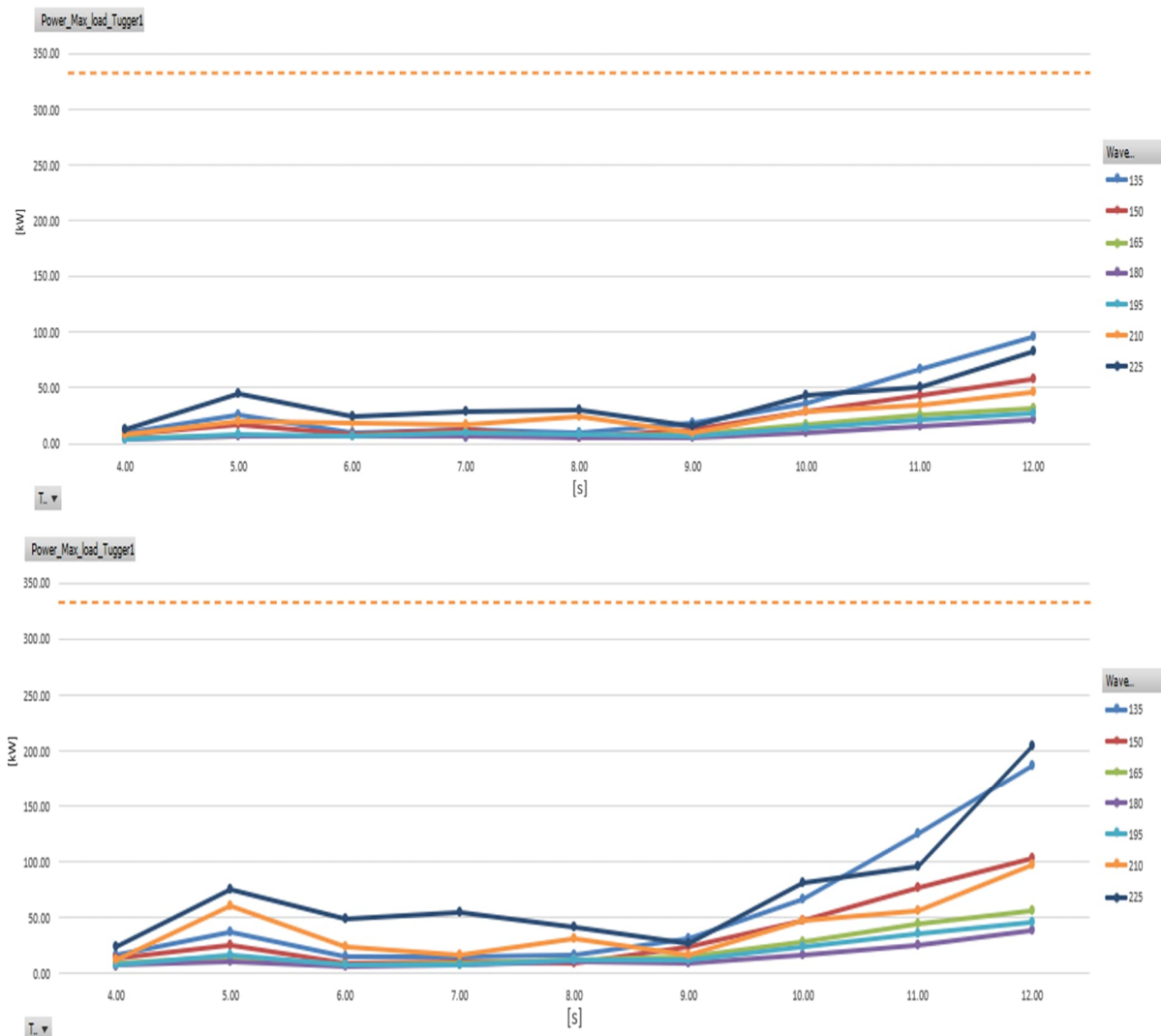


Figure 8-10: Load tugger 1 power limit, Hs = 1.5 m and Hs = 2.5 m above and below respectively

Following the results got from the simulations, it is noticed that no violation for the power limit witnessed in both the cases of Hs = 1.5m and that of 2.5m, however a little intense response is noticed at  $T_p = 5s$  for all wave headings due to the same phenomenon stated in section 8.1.1. Moreover, the response took on slightly more aggressive behavior for Hs = 2.5m.



### 8.1.4.2 Load tugger 2

Figure 8-11 displays 2 graphs that show the power limit being monitored for the duration of the analysis (10800s). Although the load tugger's tension is set at 100 kN, the tugger's payout or haul-in velocity varies with time.

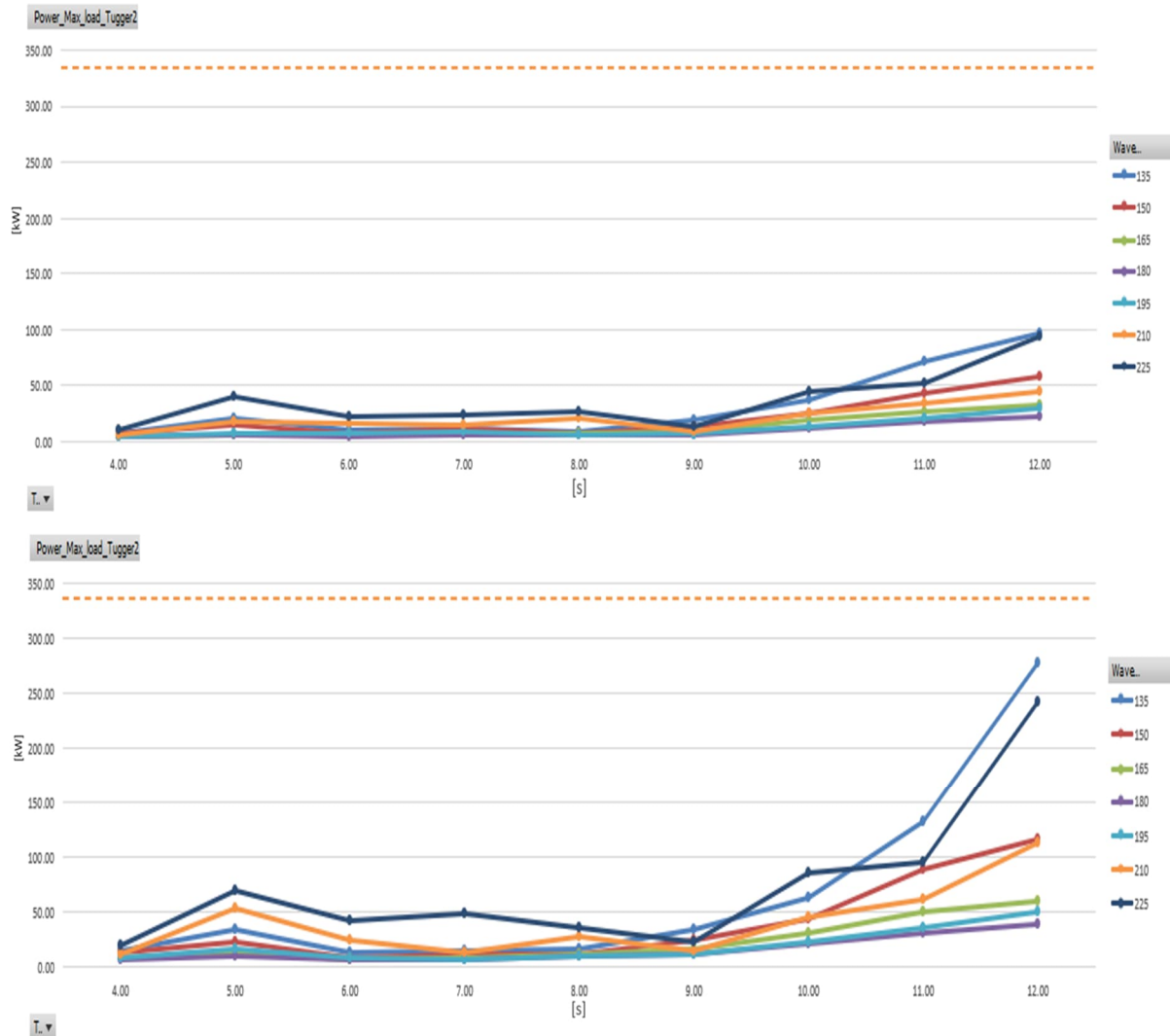


Figure 8-11: Load tugger 2 power limit,  $H_s = 1.5$  m and  $H_s = 2.5$  m above and below respectively

Based on the simulation findings, it is observed that there is no power limit violation as well in load tugger 2 in either of the two conditions ( $H_s = 1.5$  m and 2.5 m). However, for both wave headings, there is a little intense reaction at  $T_p = 5$  s referred to the reasons illustrated in the modal analysis of section 8.1.1. Furthermore, with  $H_s = 2.5$  m, the reaction started acting a little more aggressively than load tugger 1 at wave headings  $135^\circ$  and  $225^\circ$ .

### 8.1.5. Trolley Tugger Power

It is determined to limit the Trolley tuggers' operability by power in order to place a limit on their use. The tuggers will malfunction and finally the operation won't be realized if the power

value is surpassed. The trolley tugger's power limit was specified using the same equation used previously for load tugger, however the tension constant value is (50 kN) and that of power is (204 kW).

#### 8.1.5.1 Trolley tugger 1

The below Figure 8-12, consists of the power limit graphs of trolley tugger 1 for  $H_s = 1.5\text{m}$  in the first graph and  $2.5\text{m}$  for the later one.

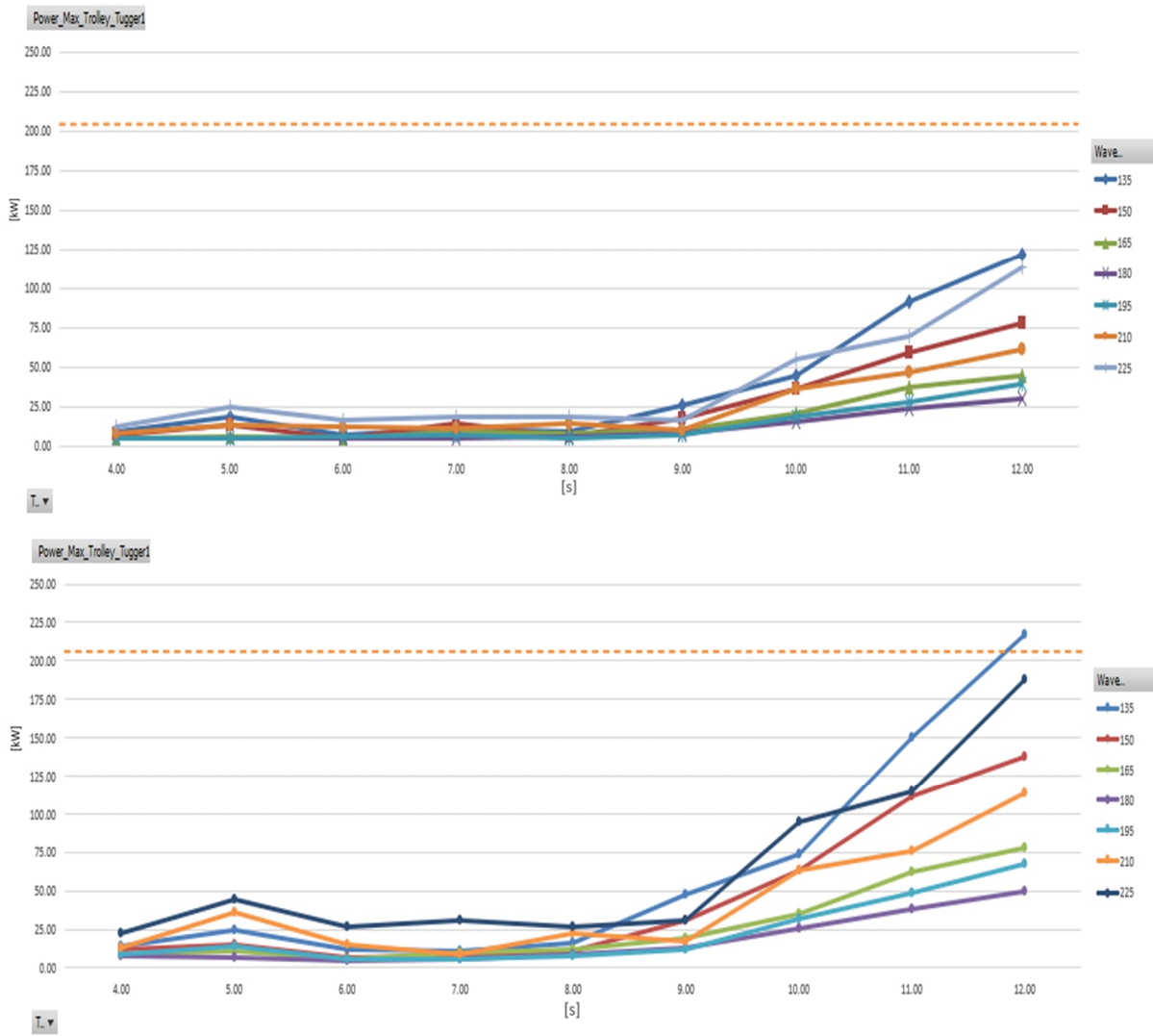


Figure 8-12: Trolley tugger 1 power limit,  $H_s = 1.5\text{ m}$  and  $H_s = 2.5\text{ m}$  above and below respectively

It can be noticed that no exceeding happened to the power limit of all the cases of  $H_s = 1.5\text{m}$ , meanwhile for the cases in  $H_s = 2.5\text{m}$  results, wave heading  $135^\circ$  breached the power limit reaching a value of 217.3 kN. Wave heading  $225^\circ$  was on the brink of breaching the power limit but didn't occur.

### 8.1.5.2 Trolley tugger 2

The trolley tugger 2 power limit graphs for  $H_s = 1.5\text{m}$  in the first graph and  $2.5\text{m}$  in the second are shown in Figure 8-13 below.

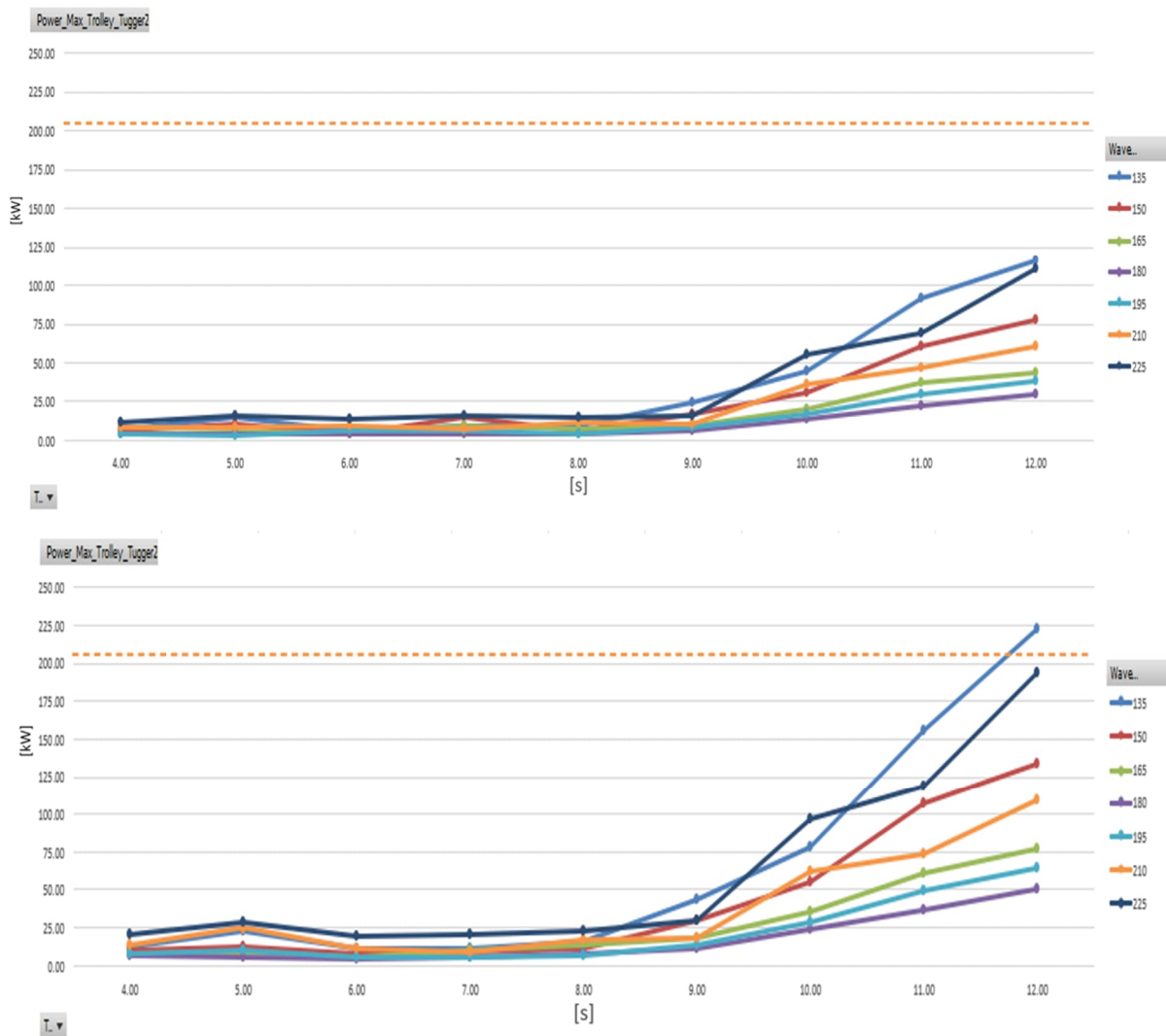


Figure 8-13: Trolley tugger 2 power limit,  $H_s = 1.5\text{ m}$  and  $H_s = 2.5\text{ m}$  above and below respectively

Similar results noticed in the results of trolley tugger 2, It is evident that in all of the  $H_s = 1.5\text{m}$  cases, the power limit was not exceeded. However, in the  $H_s = 2.5\text{m}$  cases, wave heading  $135^\circ$  exceeded the power limit, reaching a value of 222.4 kW. Wave going  $225^\circ$  nearly broke the power limit but was unable to do so.

## 8.2. Slew and Transfer Phase $214^\circ$

The slew and transfer phase of the lifting operation consists of slewing the TMC of Les Alizes with the payload which is the OSS in this case being rigged by the means of the slings to the

main hoist. As well this phase includes the transfer of the OSS to the set down destination which is  $214^\circ$  as a first option.

### 8.2.1. DAF of Main Hoist

Figure 8-14 and Figure 8-15 present the crane wire DAF, with  $H_s = 1.5\text{m}$  and  $H_s = 2.5\text{m}$ , respectively.

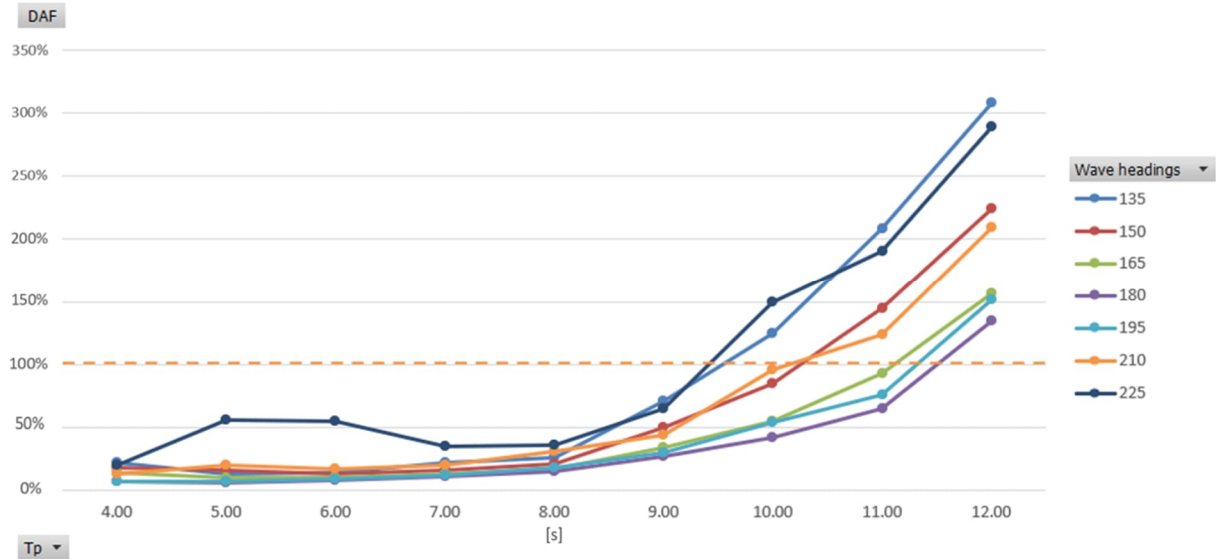


Figure 8-14: Crane wire DAF,  $H_s = 1.5\text{m}$

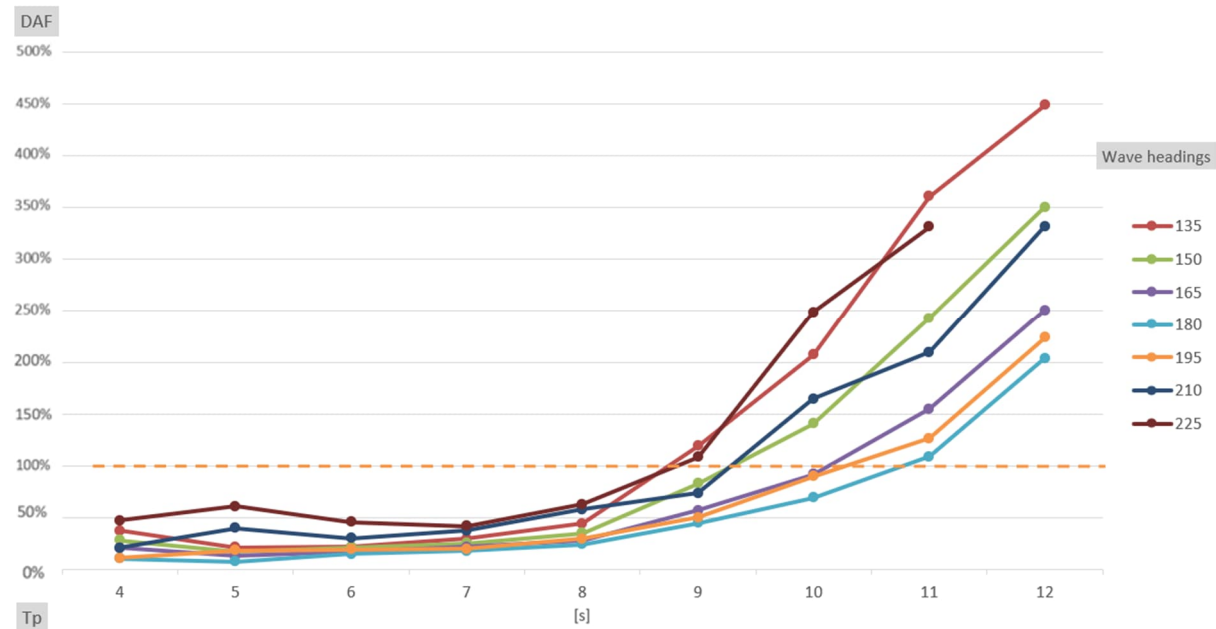


Figure 8-15: Crane wire DAF,  $H_s = 2.5\text{m}$

It is noticed in the above graphs that the DAF values for all wave headings, follow the expected trend from  $T_p = 4\text{s}$  to  $T_p = 12\text{s}$ , where DAF values increase as the  $T_p$  of the encountered wave increases. The failing cases starts to persist from  $T_p = 10\text{s}$  in  $H_s = 1.5\text{m}$  cases, however the

failing in  $H_s = 2.5\text{m}$  cases starts appearing slightly earlier from  $T_p = 9\text{s}$ . The unavailability of the case  $T_p = 12\text{s}$  at wave heading  $225^\circ$  is due to incomplete simulation that didn't converge.

### 8.2.2. Off Lead (OL) of Crane Wires

The mean MPM OL angles for  $H_s = 1.5\text{m}$  and  $H_s = 2.5\text{m}$ , respectively, are displayed in Figure 8-16 and Figure 8-17.

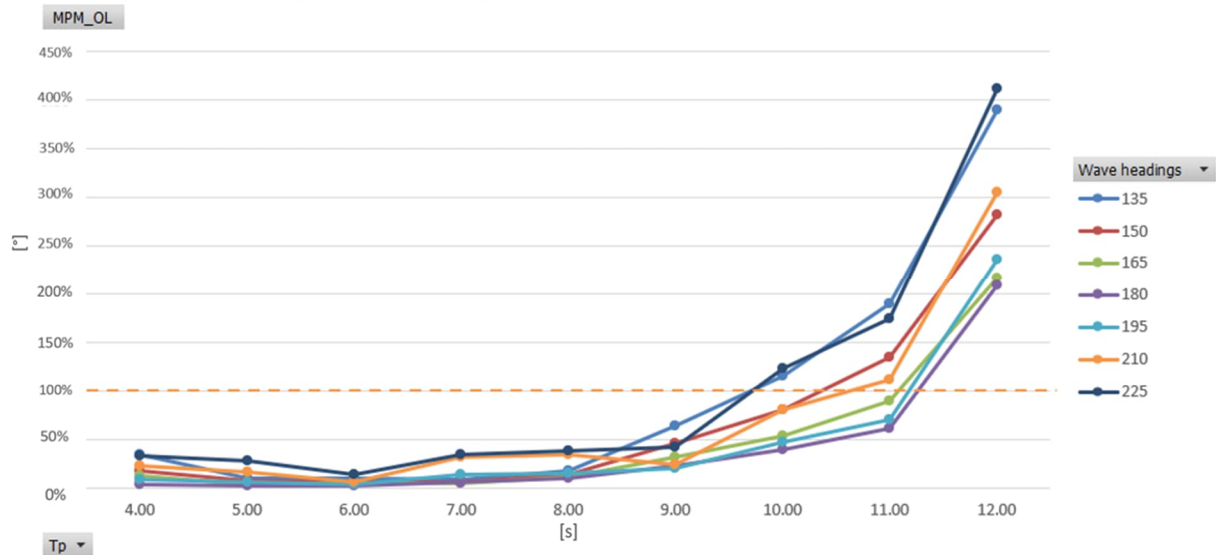


Figure 8-16: Crane wire mean off lead angle,  $H_s = 1.5\text{m}$

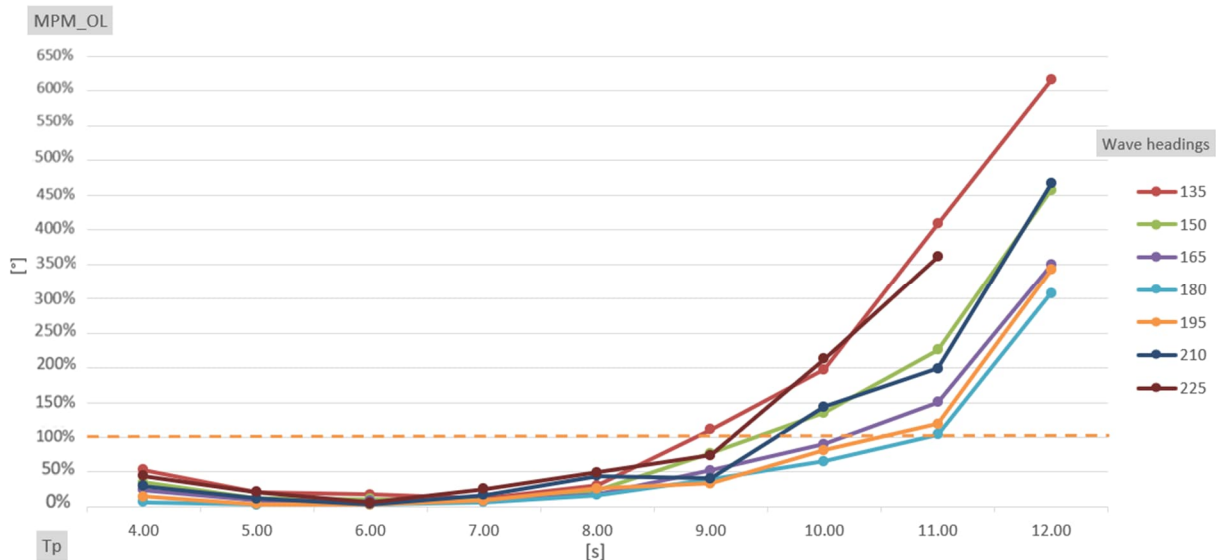


Figure 8-17: Crane wire mean off lead angle,  $H_s = 2.5\text{m}$

The above graphs clearly show that, for all wave headings taken into consideration, the off-lead deviation grows in value as the  $T_p$  value rises, as would be expected. Wave heads  $135^\circ$ , and  $225^\circ$  show some exceedances of the MPM OL limit at  $T_p = 10\text{s}$  for  $H_s = 1.5\text{m}$ . Meanwhile, the exceedance of the MPM OL limit for  $H_s = 2.5\text{m}$  is witnessed at  $T_p = 9\text{s}$  for wave heading  $135^\circ$ . All headings exceed the limit for  $T_p = 12\text{s}$  for both  $H_s$ . It is worth to say that encountered wave

of  $T_p = 4$ s has a little tense response for the monitored parameter for all wave headings being experienced, as it is triggering the natural frequency of the system.

### 8.2.3. Side Lead (SL) of Crane Wires

Figure 8-18 and Figure 8-19 show the mean MPM SL angles for  $H_s = 1.5$ m and  $H_s = 2.5$ m, respectively.

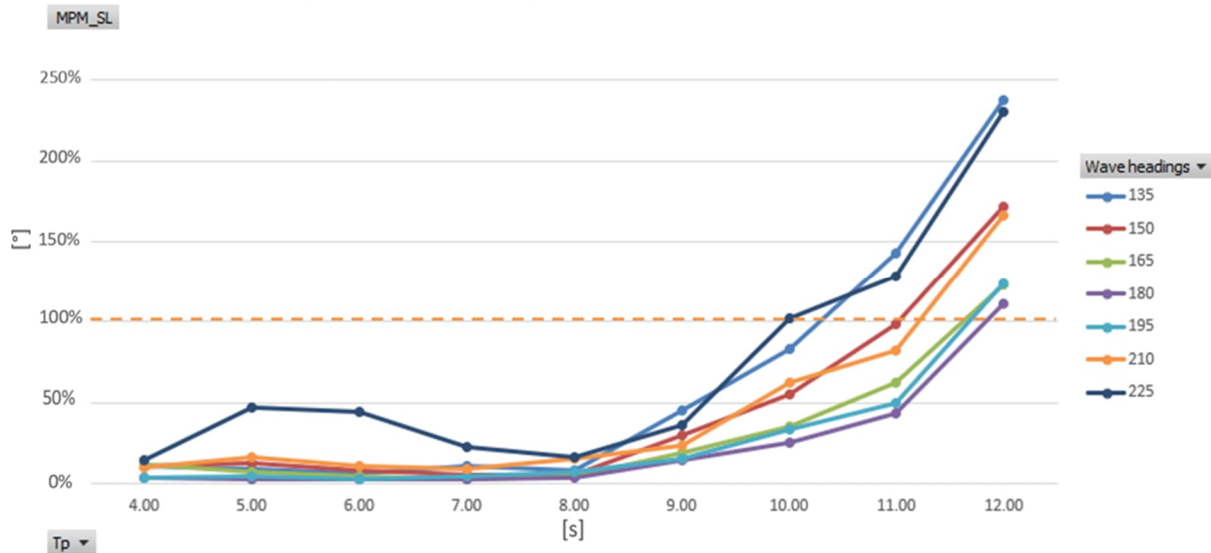


Figure 8-18: Crane wire mean side lead angle,  $H_s = 1.5$ m

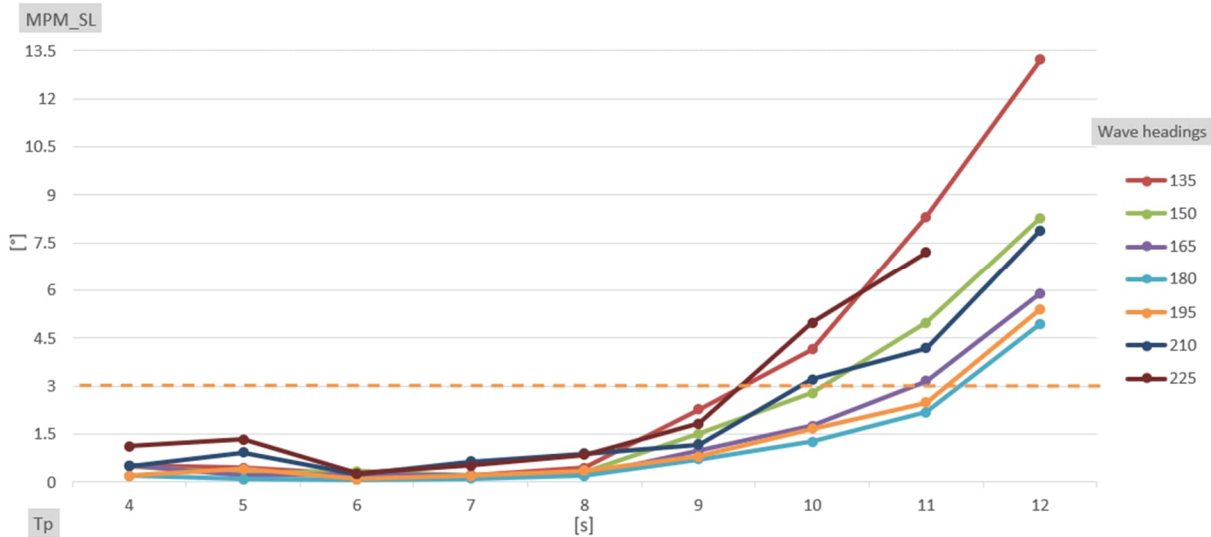


Figure 8-19: Crane wire mean side lead angle,  $H_s = 2.5$ m

The responses for the MPM SL angle for  $H_s = 1.5$ m and  $2.5$ m don't exceed the limit of SL angle until the encountering the wave spectrum of  $T_p = 10$ s.  $H_s = 1.5$ m has slightly above the limit value for wave heading  $225^\circ$  at  $T_p = 10$ s, meanwhile wave headings  $135^\circ$ ,  $210^\circ$  and  $225^\circ$  exceeded the limit of MPM SL for  $H_s = 2.5$ m at the same peak period. After that, it is noticed that all the cases for both significant wave heights pass the limit of MPM SL.

### 8.2.4. Load Tugger Power

#### 8.2.4.1 Load tugger 1

Figure 8-20 displays two graphs that show the power limit being monitored for the duration of the simulation (10800s). Although the load tugger's tension is set at 100 kN, the tugger's payout or haul-in velocity varies with time.

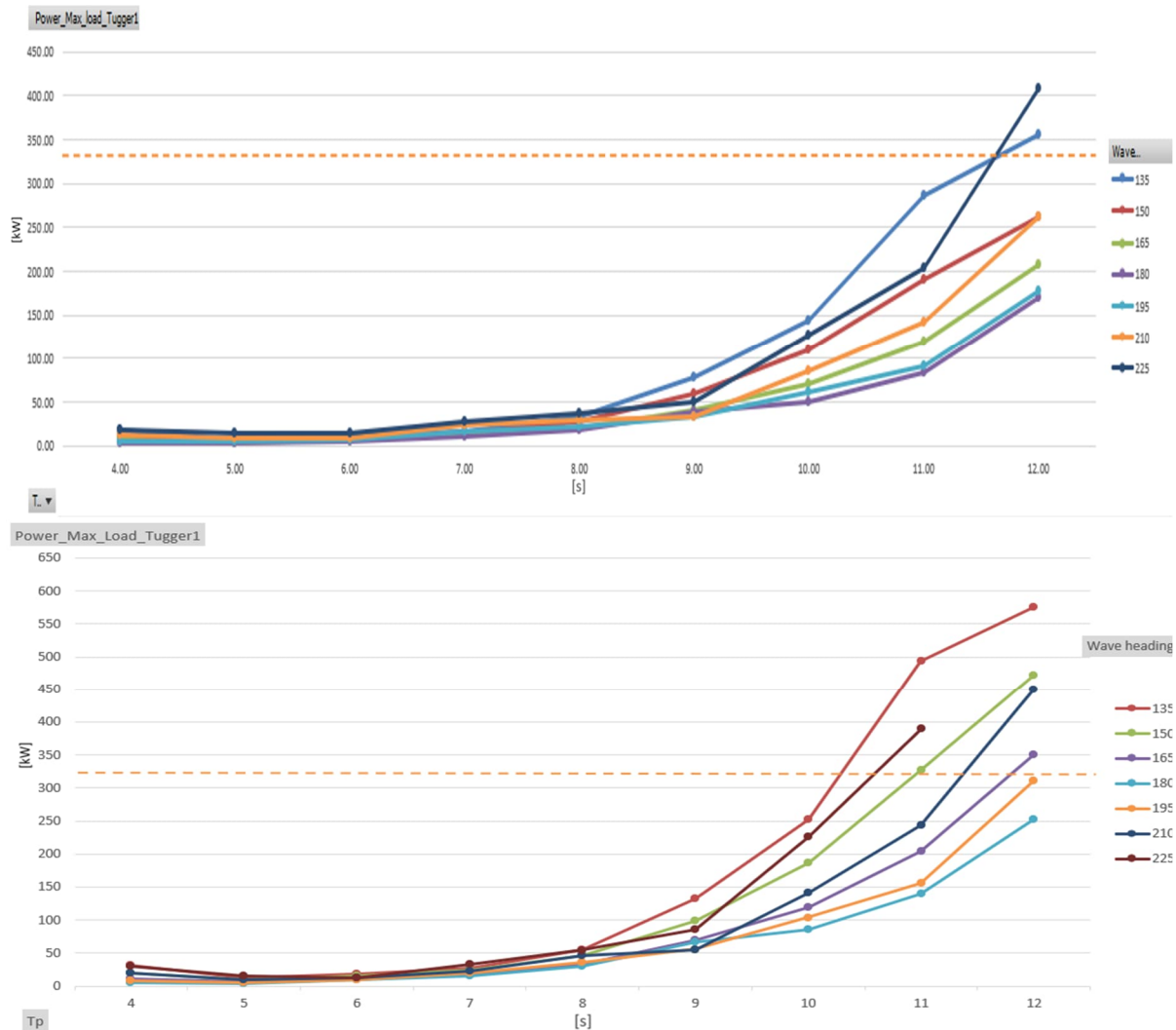


Figure 8-20: Load tugger 1 power limit,  $H_s = 1.5$  m and  $H_s = 2.5$  m above and below respectively

The power data shown in the above figure reflects when the current system used is unable to handle the load in harsh sea-states of the operation is being done at. Following the change in  $T_p$  and  $H_s$ , it is noticed that for  $H_s = 1.5$  m the most deviated wave headings ( $135^\circ$  and  $225^\circ$ ) from the centerline of the Les Alizes, exceed the limit at  $T_p = 12$  s. Meanwhile, the exceedance started at lower wave peak period  $T_p = 11$  s with three wave headings, the earlier mentioned and wave heading  $150^\circ$  for  $H_s = 2.5$  m.



### 8.2.4.2 Load tugger 2

Two graphs that illustrate the power limit being watched during the analysis (10800s) are shown in Figure 8-21. The load tugger's payout, or haul-in velocity fluctuates with time, even if its tension is fixed at 100 kN.

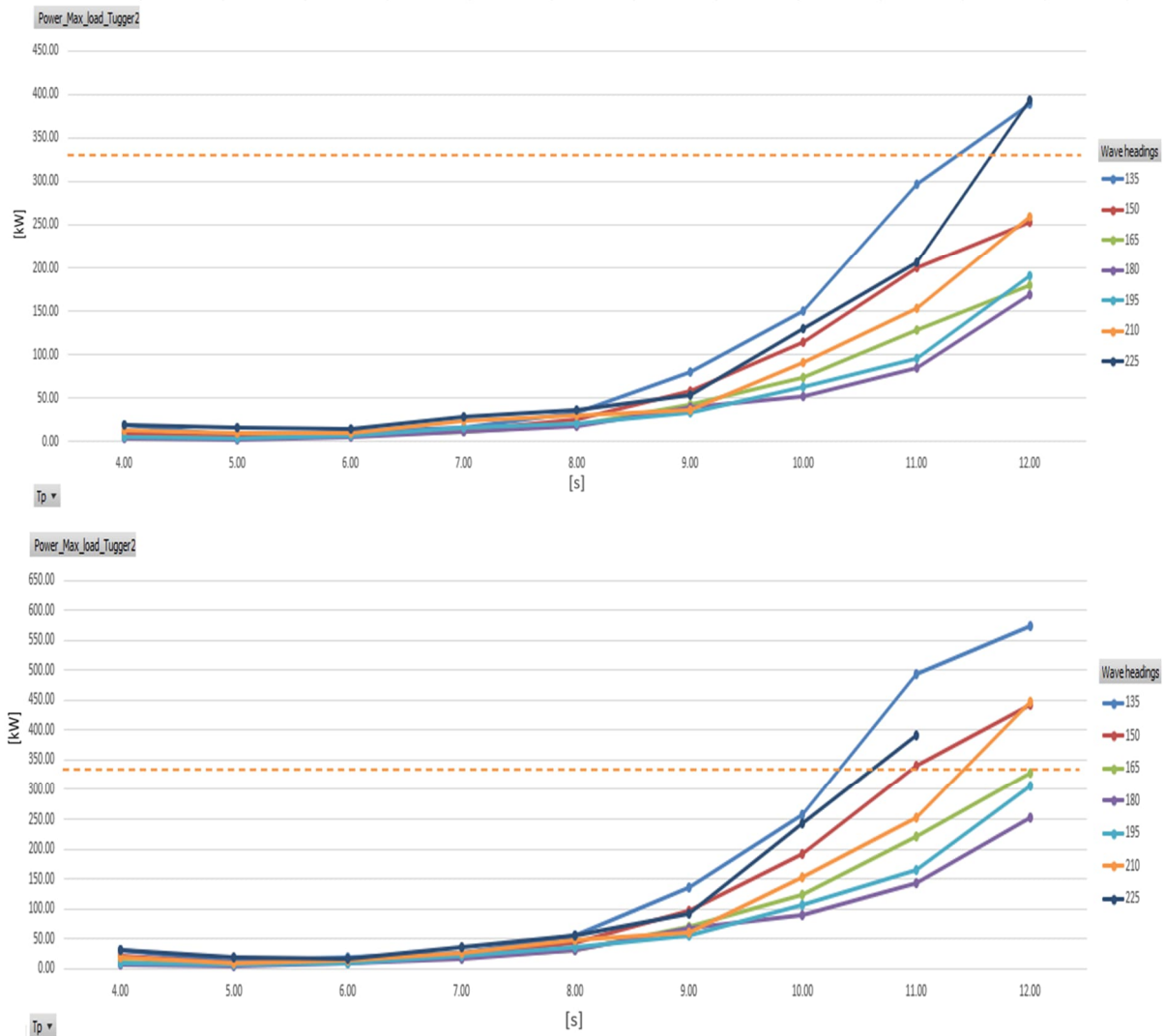


Figure 8-21: Load tugger 2 power limit,  $H_s = 1.5$  m and  $H_s = 2.5$  m above and below respectively

An indication of the degree of feasibility of the procedure is provided by the power data displayed in the above graphs. After the shift in  $T_p$  and  $H_s$ , it is observed that the most distorted wave directions ( $135^\circ$  and  $225^\circ$ ) from the Les Alizes centerline surpass the limit at  $T_p = 12$  s for  $H_s = 1.5$  m. At the same time, the exceedance began at the lower wave peak period  $T_p = 11$  s with three wave headings: the  $150^\circ$  wave heading for  $H_s = 2.5$  m and the previously described wave heading. It can be said that the behavior of both load tuggers follows similar trend during the whole simulation time.



### 8.2.5. Trolley Tugger Power

#### 8.2.5.1 Trolley tugger 1

The trolley tugger 2 power limit graphs for  $H_s = 1.5$  m in the first graph and 2.5 m in the second are shown in Figure 8-22 below.

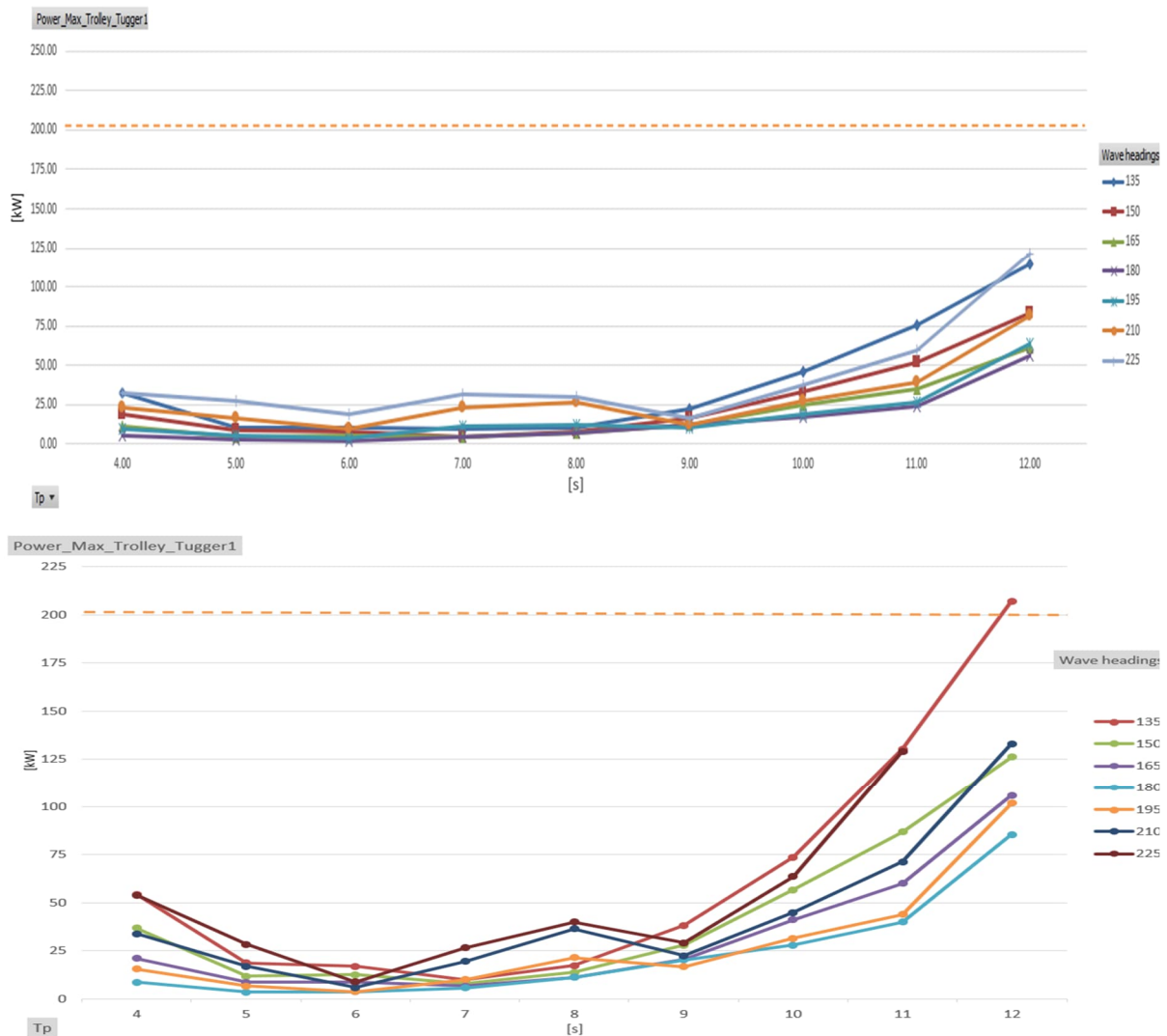


Figure 8-22: Trolley tugger 1 power limit,  $H_s = 1.5$  m and  $H_s = 2.5$  m above and below respectively

From the above figure, it is evident that in all of the  $H_s = 1.5$  m cases, the power limit was not exceeded; however, in the  $H_s = 2.5$  m cases, some transients are noticed through the plots specially for wave headings  $135^\circ$  and  $225^\circ$ . Wave heading  $135^\circ$  exceeded the power limit, reaching a value of 207.1 kW.

The causes of the witnessed transients in the graph above could not be precisely specified. Nonetheless, it could be due to one or more of the following reasons. The trolley tuggers are used to stabilize the spreader of the of the main block, sudden changes in the load position or variation in the tension of the crane wires due to movement of the load may lead to noticeable

transients. The suspended OSS can swing causing a pendulum-like behavior, this eventually requires the tugger to momentarily increase the power to stabilize the load.

### 8.2.5.2 Trolley tugger 2

Figure 8-23 below displays the trolley tugger 2 power limit graphs for  $H_s = 1.5\text{m}$  in the first graph and  $2.5\text{m}$  in the second.

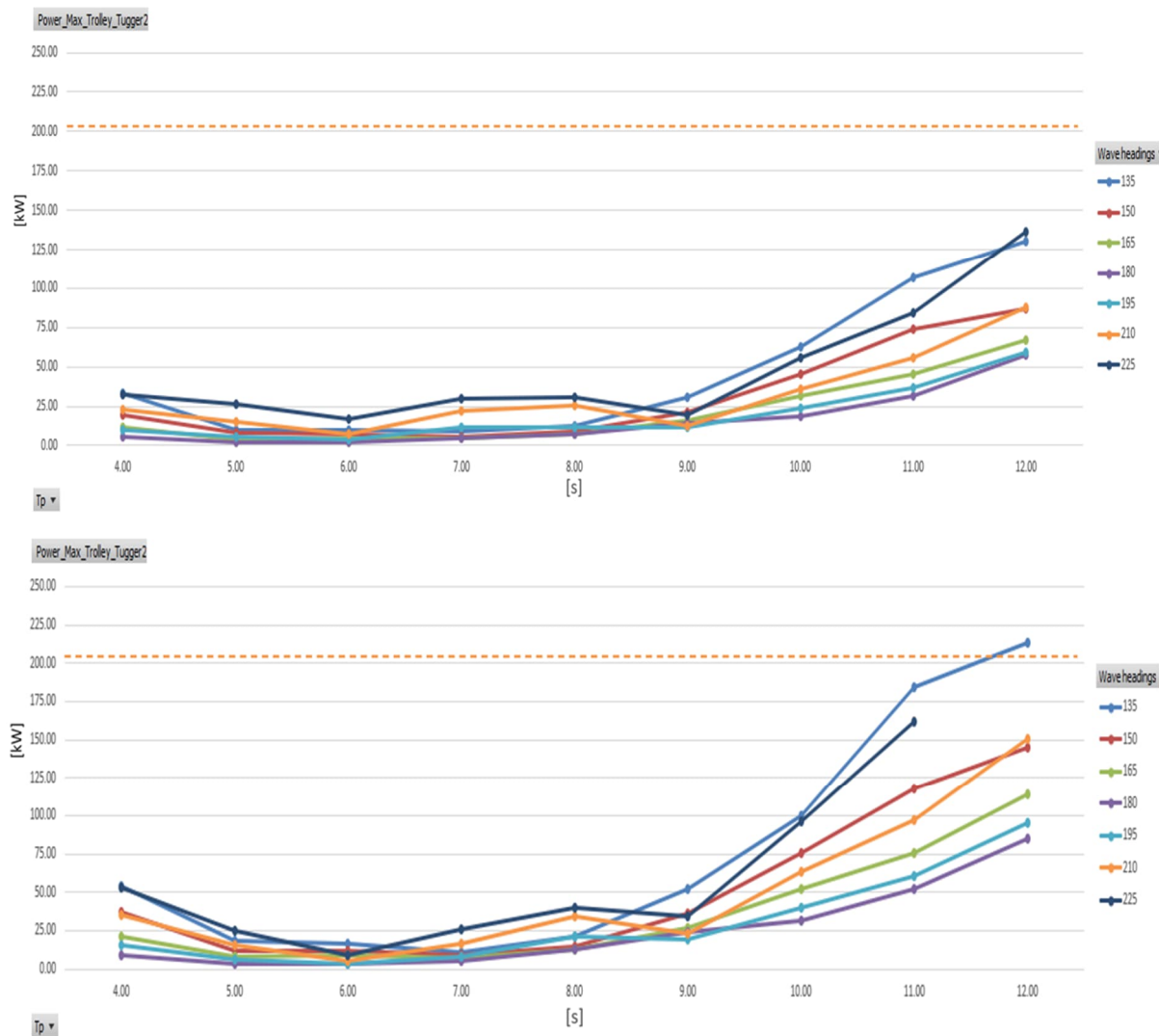


Figure 8-23: Trolley tugger 2 power limit,  $H_s = 1.5\text{ m}$  and  $H_s = 2.5\text{ m}$  above and below respectively

Figure 8-23 shows the power limit was not surpassed in any of the  $H_s = 1.5\text{m}$  cases. Nevertheless, certain transients are visible in the  $H_s = 2.5\text{m}$  cases, particularly for wave headings  $135^\circ$  and  $225^\circ$  but it is relatively less than tugger 1, as seen by the graphs. Wave heading  $135^\circ$  reached a value of 213.2 kW, exceeding the power limit. The reason behind the witnessed transients are elaborated in section 8.1.5.1.

### 8.2.6. Offshore Substation Motion Study

The success of the lifting operation depends largely on the motion exhibited by the payload. For that reason, certain limitations are implemented on the movement and velocity of the OSS.

#### 8.2.6.1 OSS movement in global X and Y

The OSS is limited to move only 1m in the horizontal direction. This limitation is advised to overcome the challenges that might appear during anchoring and stabilizing of the OSS. Movement of OSS might lead to structural problems to the components of OSS and modular support frame, the piles of the OSS will be moving meanwhile the pile sleeves in the MSF will not.

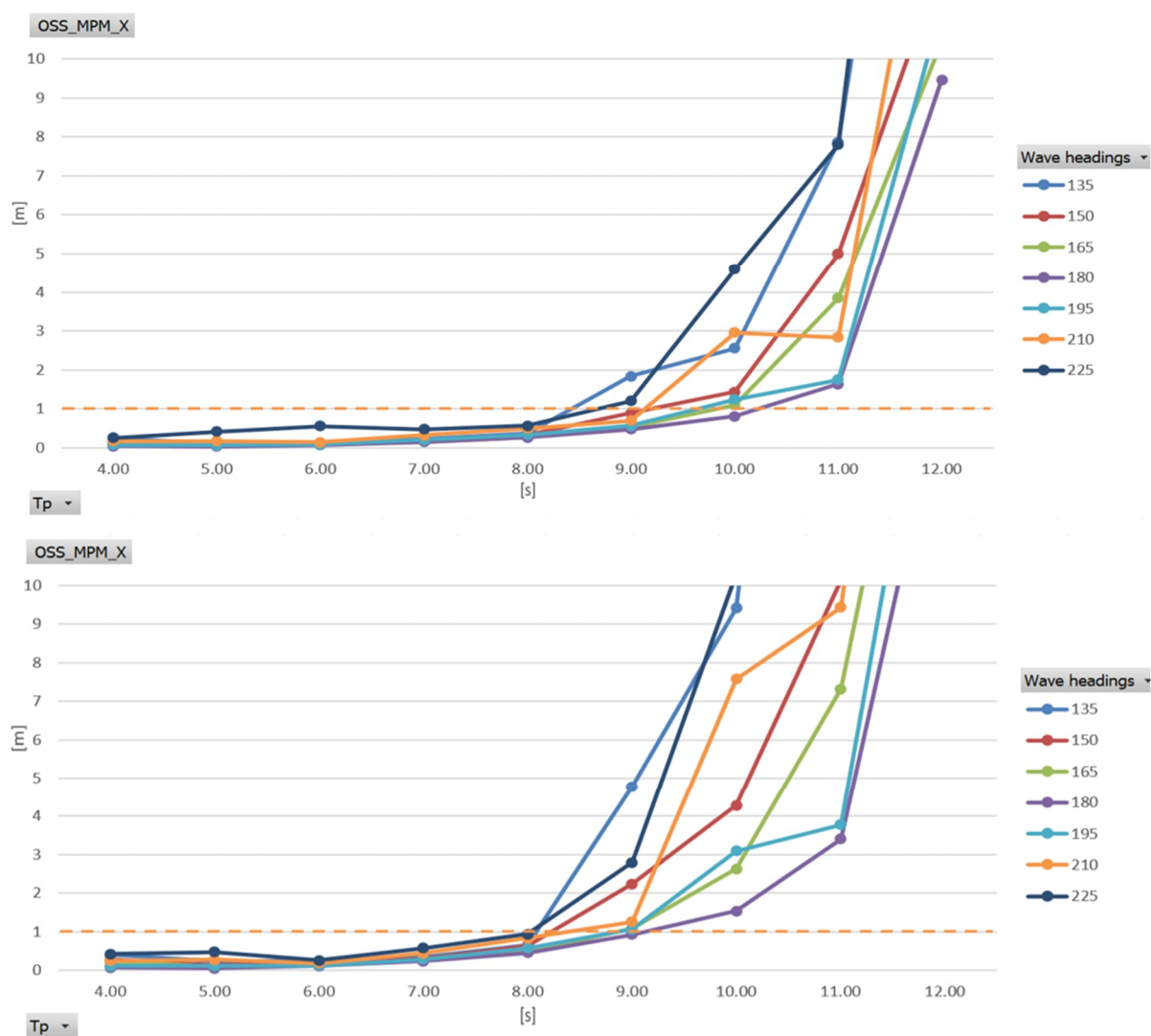


Figure 8-24: OSS movement in global X for  $H_s = 1.5$  m, 2.5 m, above and below respectively

Adding to this, the 1m limitation movement applies for OSS motion in the global Y direction. As the movement as well in this case can increase the potential risk of collision and damage to equipment and structures.

Moving of the payload specially in heavy lift operations can elevate the complexity of the whole operation, decreasing the probability of applying successful deployment. Figure 8-25 shows the obtained motions of the OSS in the global Y direction through the 3 hours simulation period.

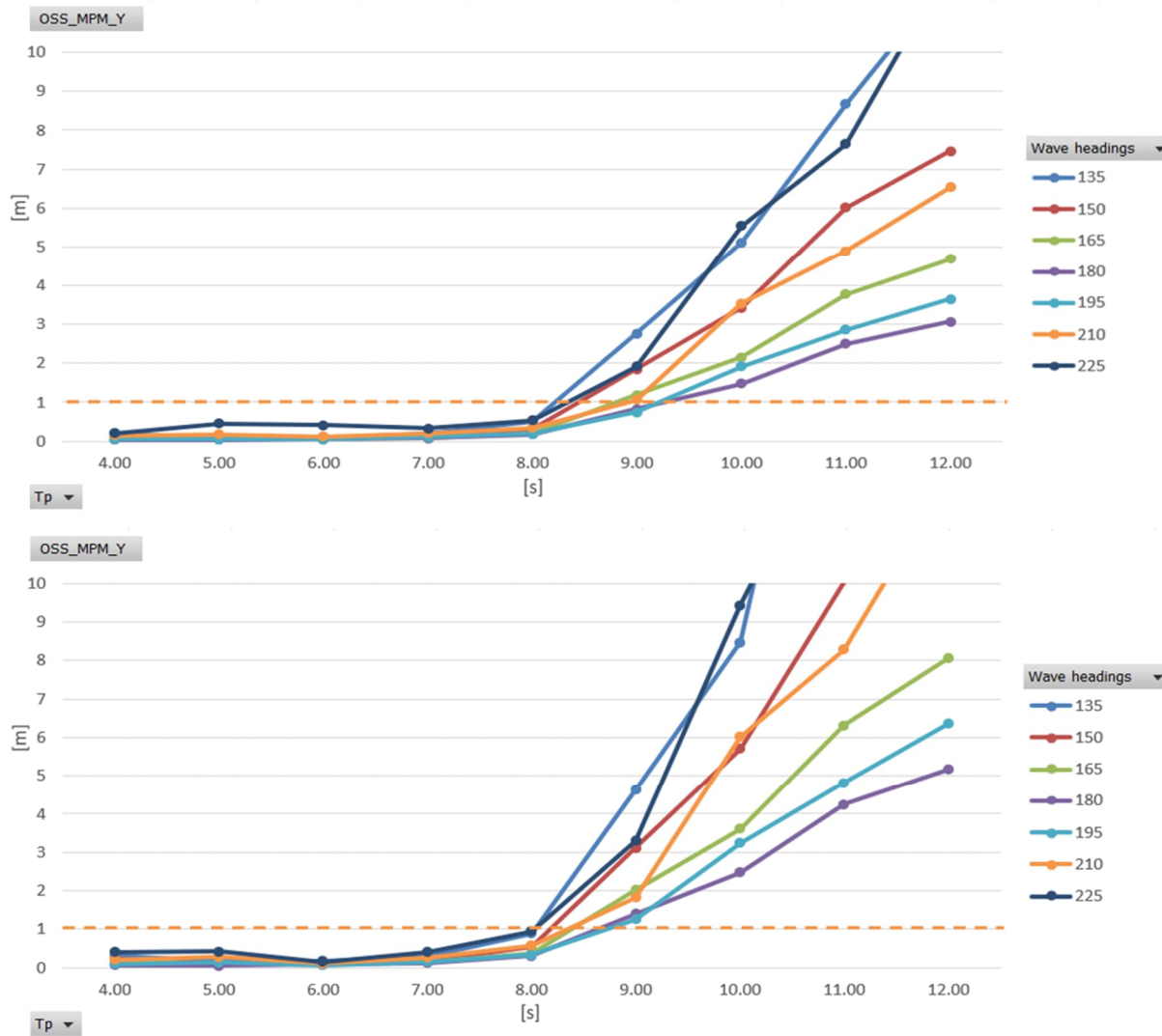


Figure 8-25: OSS movement in global Y for  $H_s = 1.5$  m, 2.5 m, above and below respectively

The figures Figure 8-24 and Figure 8-25 above illustrate the motion limitations for the X and Y global directions that should be respected. The OSS movement witnessed to exceed its limitation set in  $T_p$  higher than 8s. It is worth noting that in all the 4 graphs above, the movement of the OSS starts to ramp up in fast manner from  $T_p = 9$ s though all the cases fail the operation criteria.

### 8.2.6.2 OSS velocity in global X and Y

During installation, the substation's or its parts' moving speed can be crucial. The following factors limits speed. Speed of deployment and lifting; The operation's safety and control may be impacted by the speed at which parts are moved. Reaction time to modifications in the

surroundings; It's critical to have the flexibility to swiftly adapt to shifting weather patterns or sea states.

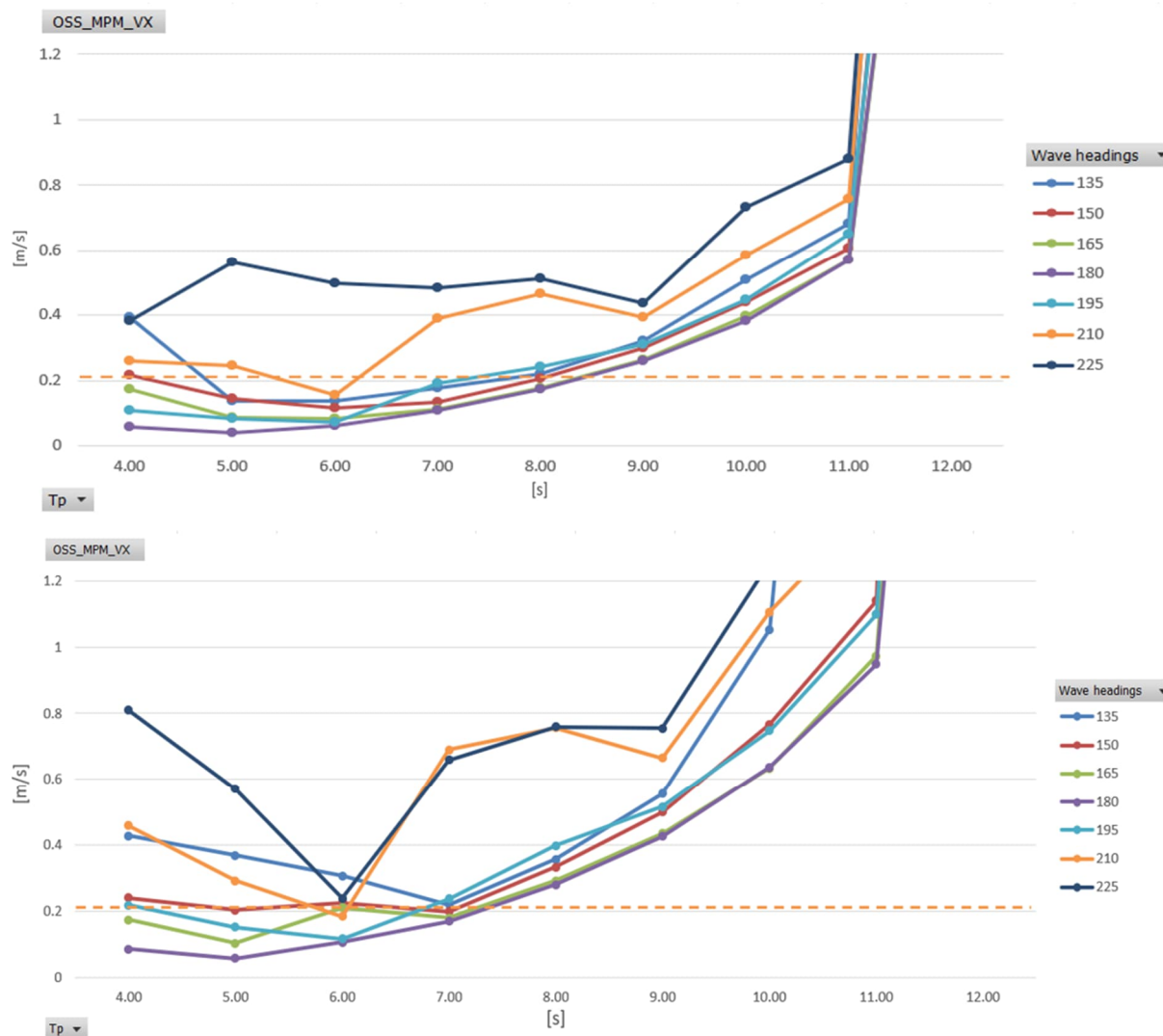


Figure 8-26: OSS velocity in global X for  $H_s = 1.5$  m, 2.5 m, above and below respectively

Also applicable to OSS motion in the global Y direction is the 0.21m/s limiting velocity. In this instance, the movement may also raise the chance of a collision and structural and equipment damage.

Relocating the payload, particularly in high lift operations, can increase the overall operation's complexity and reduce the likelihood of a successful deployment. The acquired OSS velocities in the global Y direction over the three-hour simulation period are displayed in Figure 8-27.

Several reasons could be possible in the formation of such response curves.  $T_p = 4$ s and 5s lead to intense OSS velocity values than the expected, these are shorter wave periods that might concentrate energy in a way that impacts the model more effectively, nonetheless longer period could distribute energy over a longer time. Going up with periods, hydrodynamic damping

could take effect and the system respond less violently to the exhibited wave trains. It is probable that witnessed high velocity could be referred to a combination of resonance effects, reduced damping and system non-linearities.

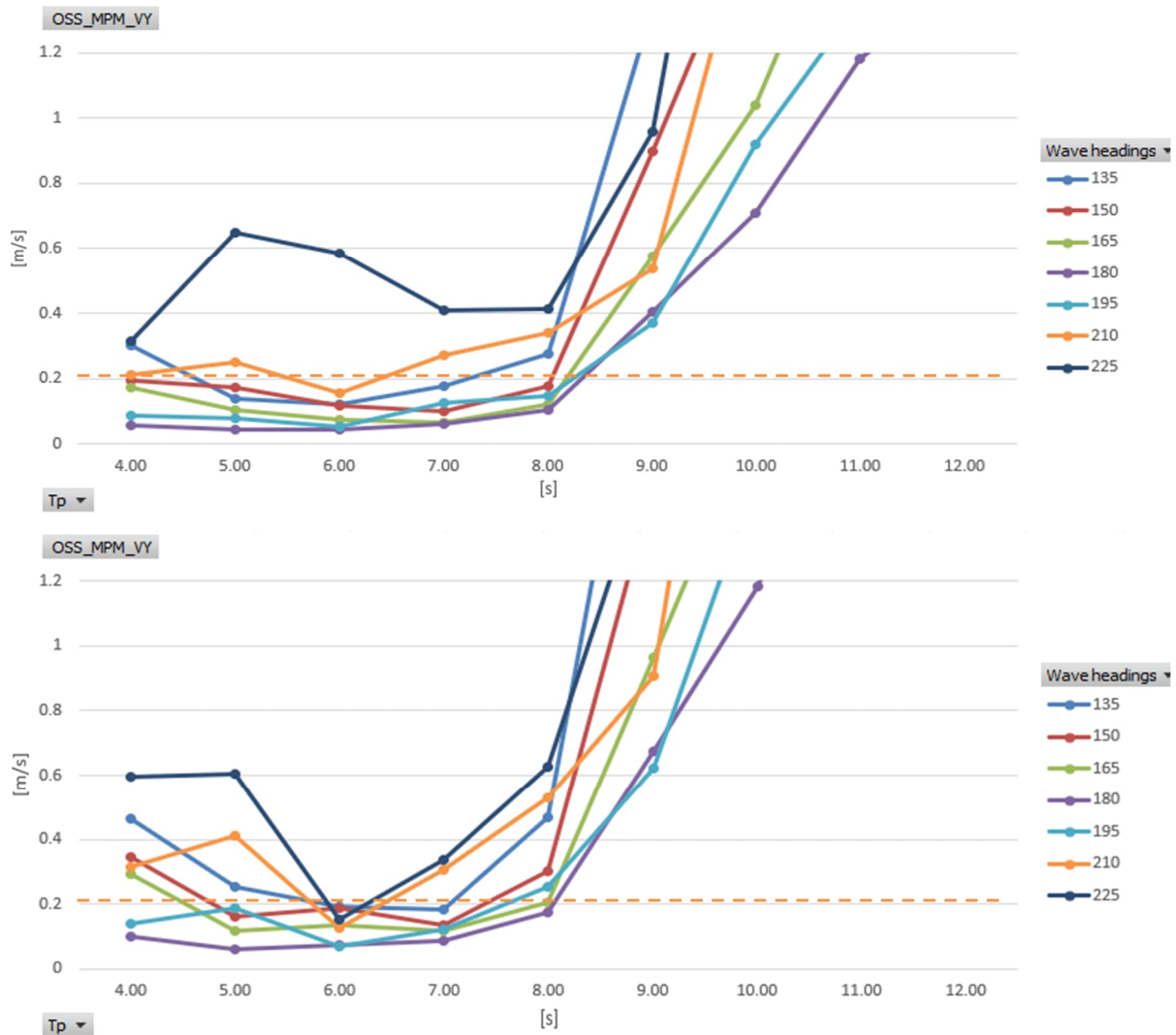


Figure 8-27: OSS velocity in global Y for  $H_s = 1.5$  m, 2.5 m, above and below respectively

The motion constraints for the X and Y global velocities that need to be observed are shown in figures Figure 8-26 and Figure 8-27 above. The OSS velocity was observed to surpass 0.21m/s at several and random wave headings from  $T_p = 4$  s to  $T_p = 8$  s. Meanwhile, Wave headings 210° and 225° were causing the OSS to move faster than the allowed limit for all peak periods except for  $T_p = 6$  s. It is important to note, the OSS graphs corresponding to velocities of the global Y direction in the of the aforementioned graphs begins to ramp up quickly at  $T_p = 8$  s.



### 8.3. Slew and Transfer Phase $224^\circ$

To better decide before executing, an additional phase of slew and transfer was suggested to go under study. The same analysis was done on the system with a choice of slew and transfer angle of  $224^\circ$ .

#### 8.3.1. DAF of Main Hoist

The crane wire DAF is shown in Figure 8-28 and Figure 8-29, with  $H_s = 1.5\text{m}$  and  $2.5\text{m}$ , respectively.

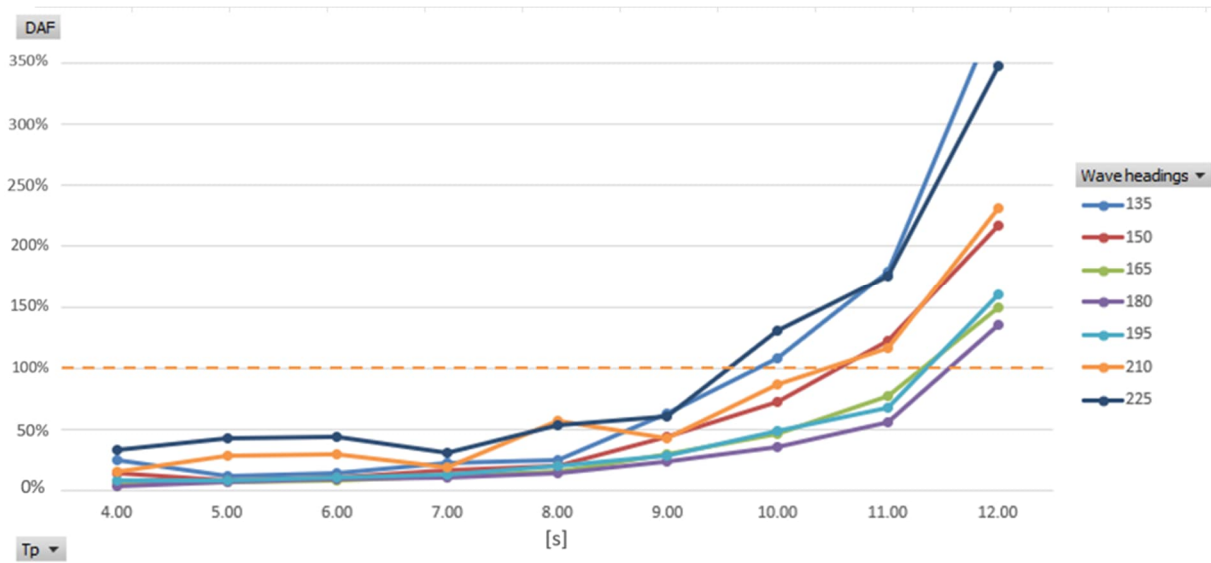


Figure 8-28: Crane wire DAF,  $H_s = 1.5\text{m}$

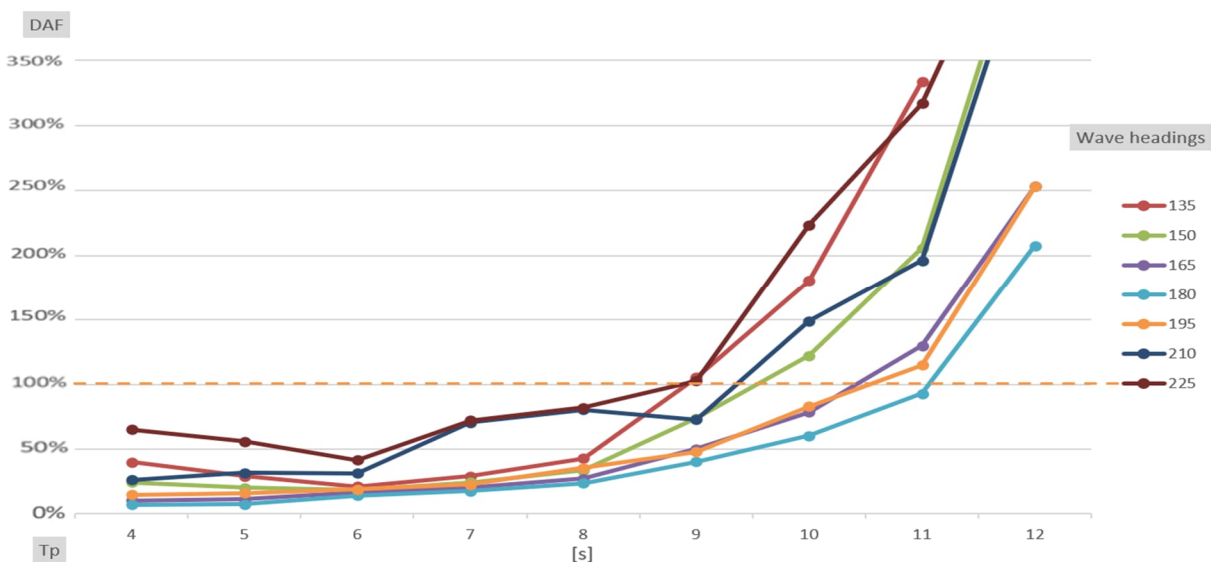


Figure 8-29: Crane wire DAF,  $H_s = 2.5\text{m}$

The DAF values for all wave headings seen in the above graphs, which show that they follow the predicted trend from  $T_p = 4\text{s}$  to  $T_p = 12\text{s}$ , where they rise as the encountered wave's  $T_p$

grows. In  $H_s = 1.5\text{m}$ , the failed cases begin to persist at  $T_p = 10\text{s}$ . In  $H_s = 2.5\text{m}$ , the failing cases begin to manifest somewhat sooner at  $T_p = 9\text{s}$ . The reason for the unavailability of the instance  $T_p = 12\text{s}$  at wave heading  $135^\circ$  is that the simulation was incomplete and failed to converge while attempting to iteratively solve the dynamic equilibrium equations.

### 8.3.2. Off Lead (OL) of Crane Wires

Figure 8-30 and Figure 8-31 show the mean MPM OL angles for  $H_s = 1.5\text{m}$  and  $H_s = 2.5\text{m}$ , respectively.

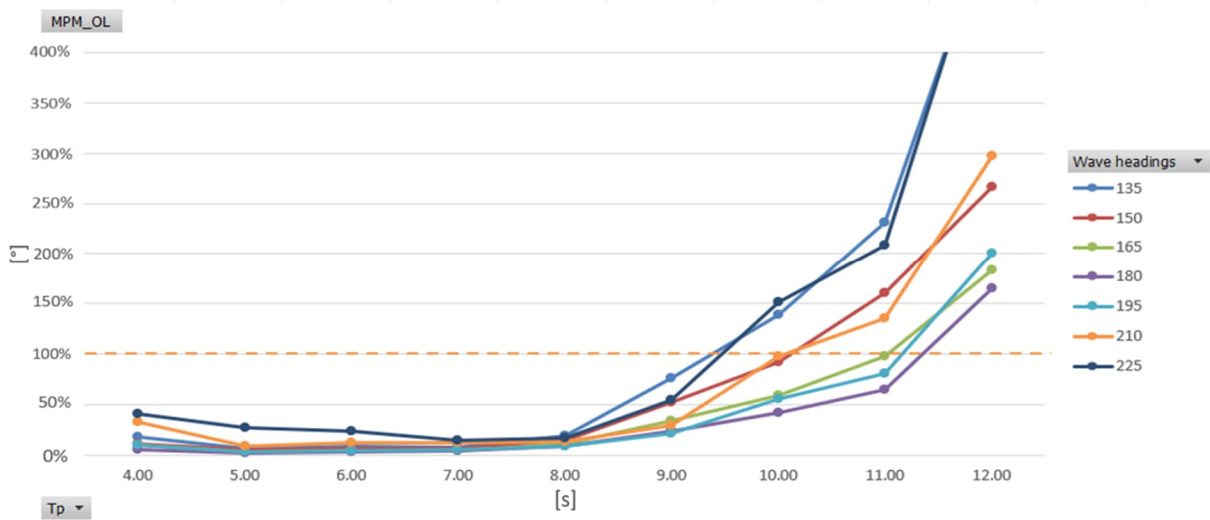


Figure 8-30: Crane wire mean off lead angle,  $H_s = 1.5\text{m}$

It is evident from the above graph that, as would be predicted, the off-lead deviation increases in value as the  $T_p$  value grows for all wave headings taken into consideration. There are some exceedances of the MPM OL limit for wave headings  $135^\circ$  and  $225^\circ$  at  $T_p = 10\text{s}$ . Furthermore, for  $T_p = 12\text{s}$ , headings  $135^\circ$ ,  $165^\circ$  and  $180^\circ$  surpass the limit as well.

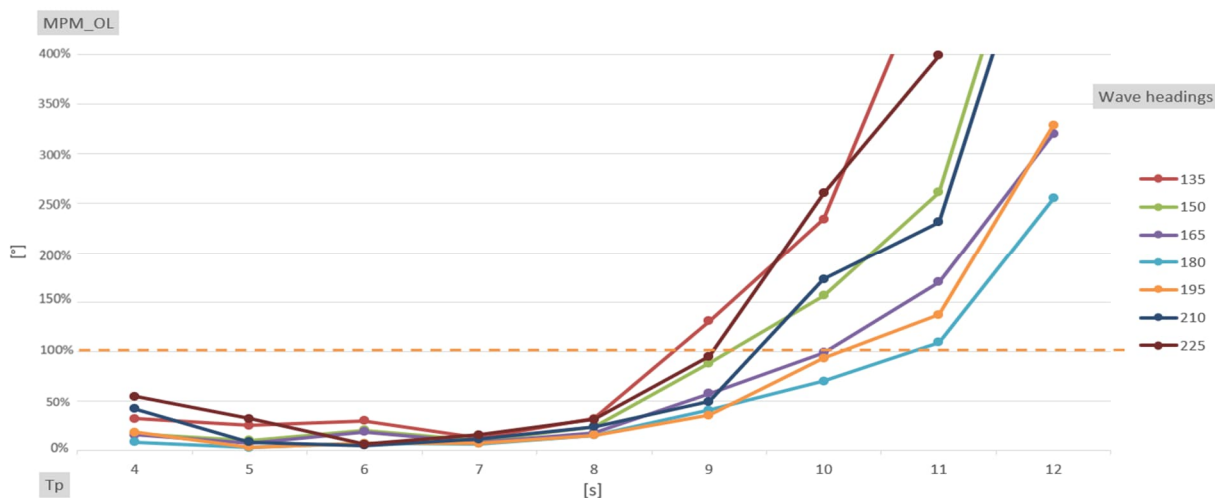


Figure 8-31: Crane wire mean off lead angle,  $H_s = 2.5\text{m}$



The above graph clearly shows that, for all wave headings taken into consideration, the off-lead deviation grows in value as the  $T_p$  value rises, as would be expected. Wave heads  $135^\circ$  and  $225^\circ$  show some exceedances of the MPM OL limit at  $T_p = 10$ s. Additionally, all headings exceed the limit for  $T_p = 12$ s.

### 8.3.3. Side Lead (SL) of Crane Wires

The mean MPM SL angles for  $H_s = 1.5$ m and  $H_s = 2.5$  m are displayed in Figure 8-32 and Figure 8-33, respectively.

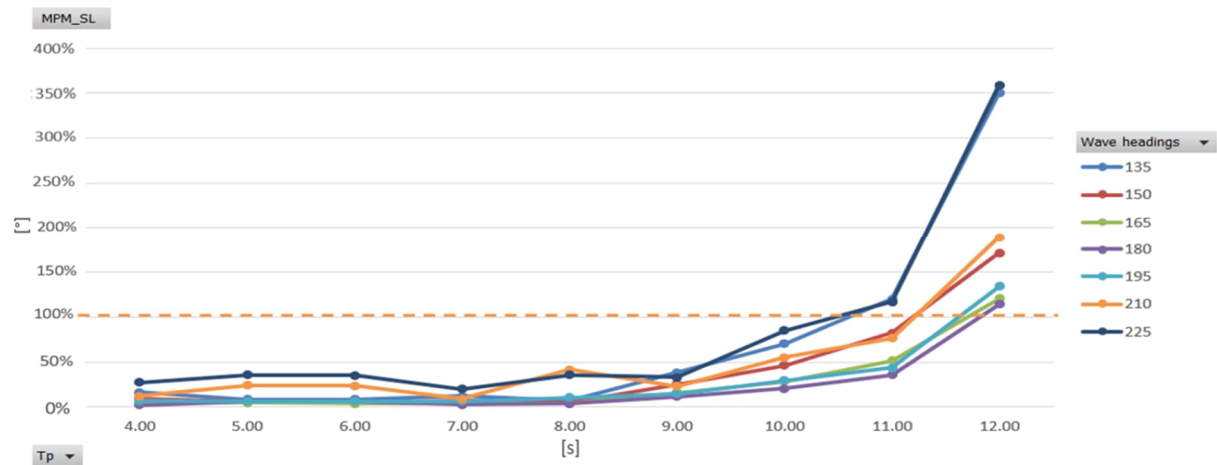


Figure 8-32: Crane wire mean side lead angle,  $H_s = 1.5$ m

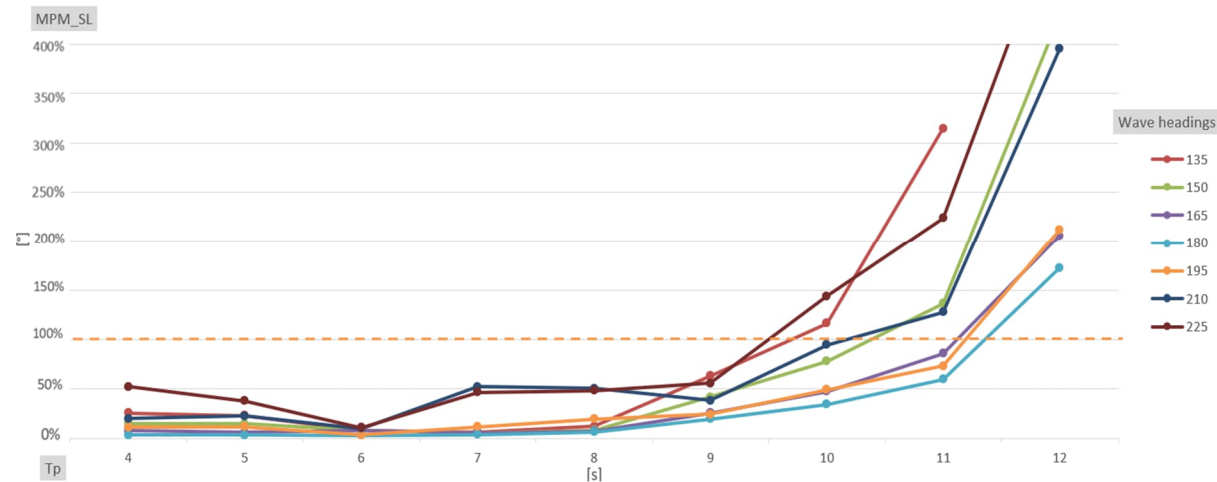


Figure 8-33: Crane wire mean side lead angle,  $H_s = 2.5$ m

The MPM SL angle responses for  $H_s = 1.5$ m and  $2.5$ m do not surpass the SL angle limit until they come into contact with the  $T_p = 10$ s and  $T_p = 11$ s wave spectra. Wave headings  $135^\circ$  and  $225^\circ$  exceeded the MPM SL limit for both  $H_s$ . Following that, it is observed that every instance for both significant wave heights surpass the MPM SL limit.

### 8.3.4. Load Tugger Power

#### 8.3.4.1 Load tugger 1

Two graphs that illustrate the power limit being watched during the simulation (10800s) are shown in Figure 8-34. The load tugger's payout, or haul-in velocity, fluctuates with time even if its tension is fixed at 100 kN.

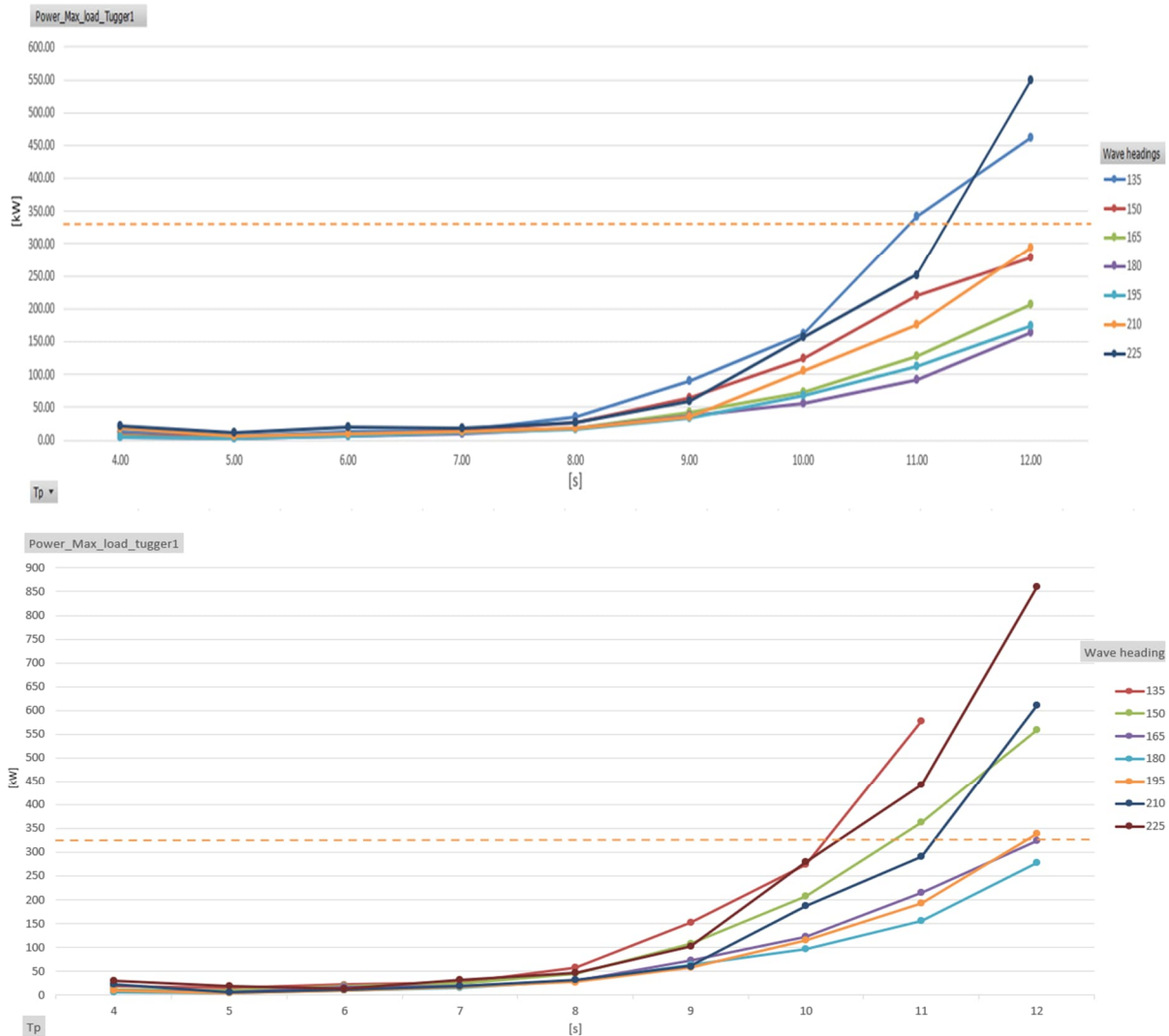


Figure 8-34: Load tugger 1 power limit,  $H_s = 1.5$  m and  $H_s = 2.5$  m above and below respectively

The power data for load tugger 1 is displayed in the above graphs. After the shift in  $T_p$  and  $H_s$ , it is observed that the most distorted wave directions  $135^\circ$  and  $225^\circ$  from the Les Alizes centerline surpass the limit at  $T_p = 12$  s for  $H_s = 1.5$  m. At the same time, the exceedance began at the lower wave peak period  $T_p = 11$  s with three wave headings: the  $135^\circ$ ,  $150^\circ$  and  $225^\circ$  for  $H_s = 2.5$  m. Moreover,  $195^\circ$  and  $210^\circ$  wave headings caused higher values than the limit when they are at  $T_p = 12$  s.

### 8.3.4.2 Load tugger 2

Figure 8-35 shows two graphs that depict the power limit (10800s) that were observed during the analysis. Even if the load tugger's tension is set at 100 kN, its payout, or haul-in velocity, varies over time.

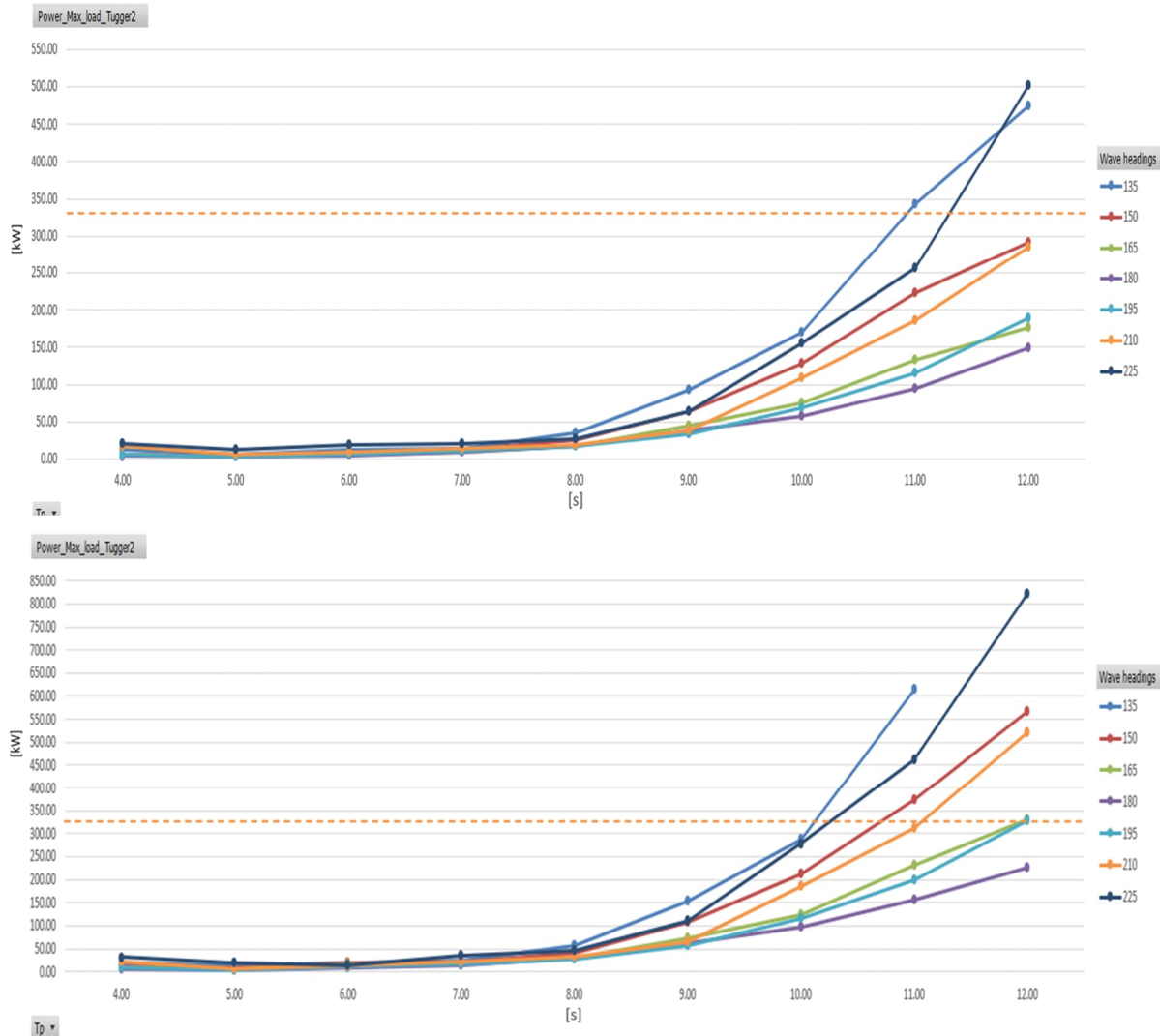


Figure 8-35: Load tugger 2 power limit,  $H_s = 1.5$  m and  $H_s = 2.5$  m above and below respectively

Load tugger 2 power limit graphs shows similar behavior as load tugger 1. As seen before, for  $H_s = 1.5$  m only wave headings  $135^\circ$  and  $225^\circ$  get passed the power limit of the tugger at  $T_p = 12$  s. However, graph 2 shows more headings potentially will be passing the power limit if they are at  $T_p = 12$  s, as seen with wave headings  $150^\circ$  and  $210^\circ$  at  $H_s = 2.5$  m.

### 8.3.5. Trolley tugger power

#### 8.3.5.1 Trolley tugger 1

Figure 8-36 below displays the trolley tugger 2 power limit graphs for  $H_s = 1.5$  m in the first graph and 2.5 m in the second.

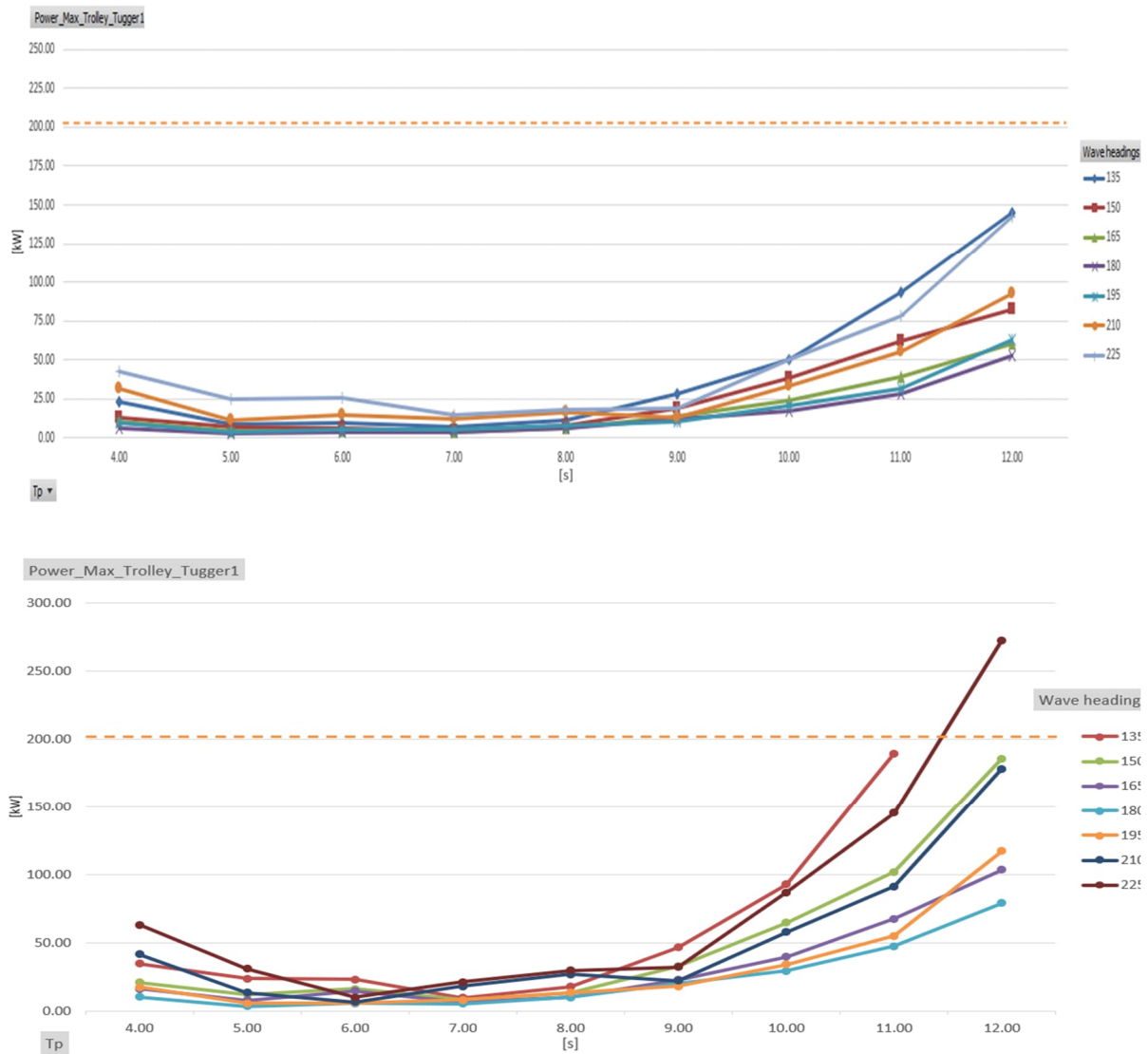


Figure 8-36: Trolley tugger 1 power limit,  $H_s = 1.5$  m and  $H_s = 2.5$  m above and below respectively

The above figure shows that the power limit was not exceeded in any of the  $H_s = 1.5$  m cases. Nevertheless, in the  $H_s = 2.5$  m examples, some transients are visible through the plots, particularly for wave heads of  $135^\circ$  and  $210^\circ$ . Wave heading  $225^\circ$  reached a value of 272.8 kW, exceeding the power limit.

### 8.3.5.2 Trolley tugger 2

Figure 8-37 below displays the trolley tugger 2 power limit graphs for  $H_s = 1.5$  m in the first graph and 2.5 m in the second.

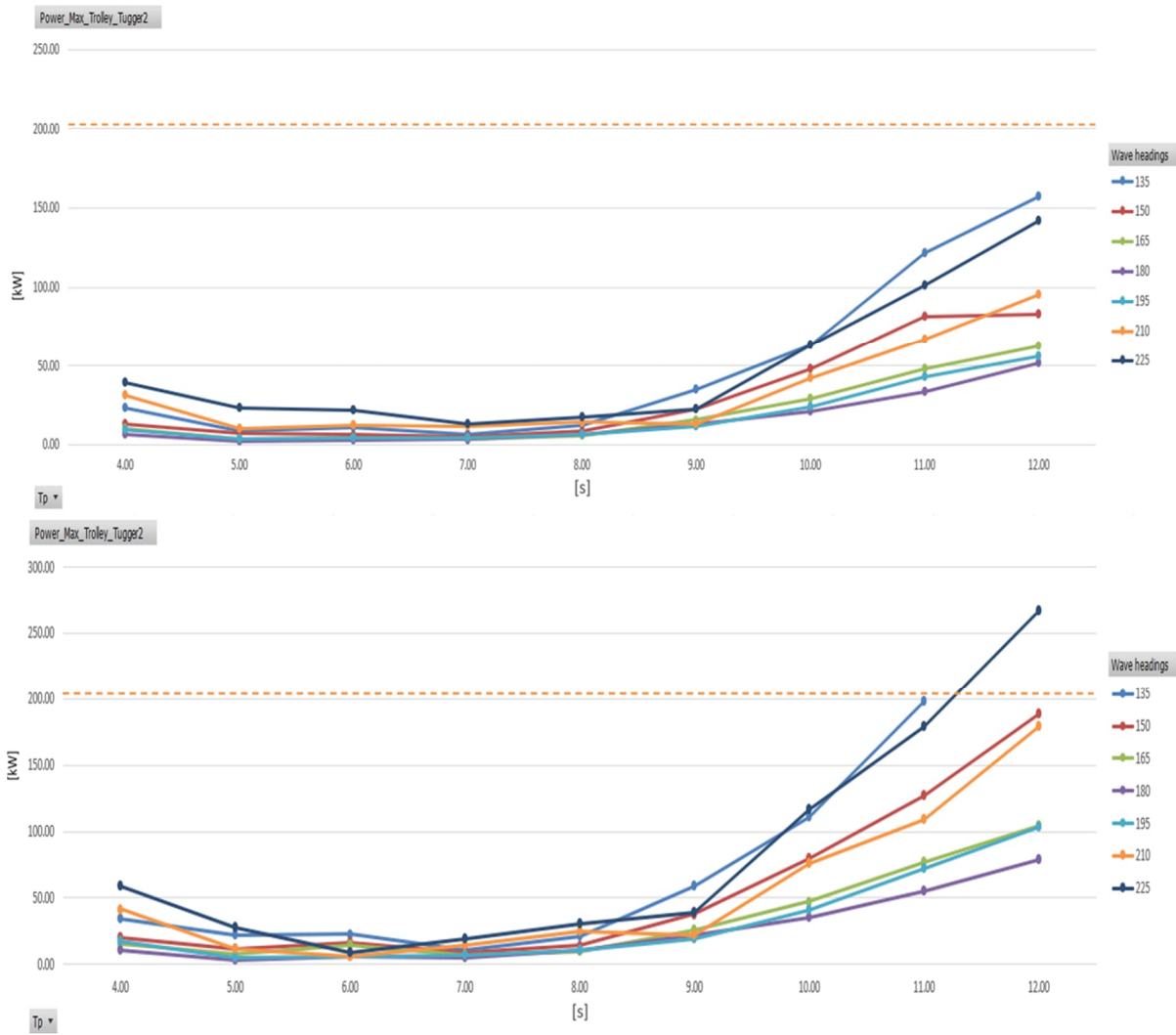


Figure 8-37: Trolley tugger 2 power limit,  $H_s = 1.5$  m and  $H_s = 2.5$  m above and below respectively

Figure 8-37 illustrates that in all of the  $H_s = 1.5$  m scenarios, the power limit was not exceeded as in the case for trolley tugger 1. However, as the graphs show, there are comparatively fewer transients than tugger 1 in the  $H_s = 2.5$  m situations, especially for wave heads of  $135^\circ$  and  $225^\circ$ . The wave heading  $225^\circ$  exceeded the power limit with a value of 267.4 kN.

### 8.3.6. Offshore Substation Motion Study

#### 8.3.6.1 OSS movement in global X and Y

The maximum horizontal movement for the OSS is 1 meter. It is advisable to use this restriction in order to get around any obstacles that may arise when the OSS is being anchored and stabilized.

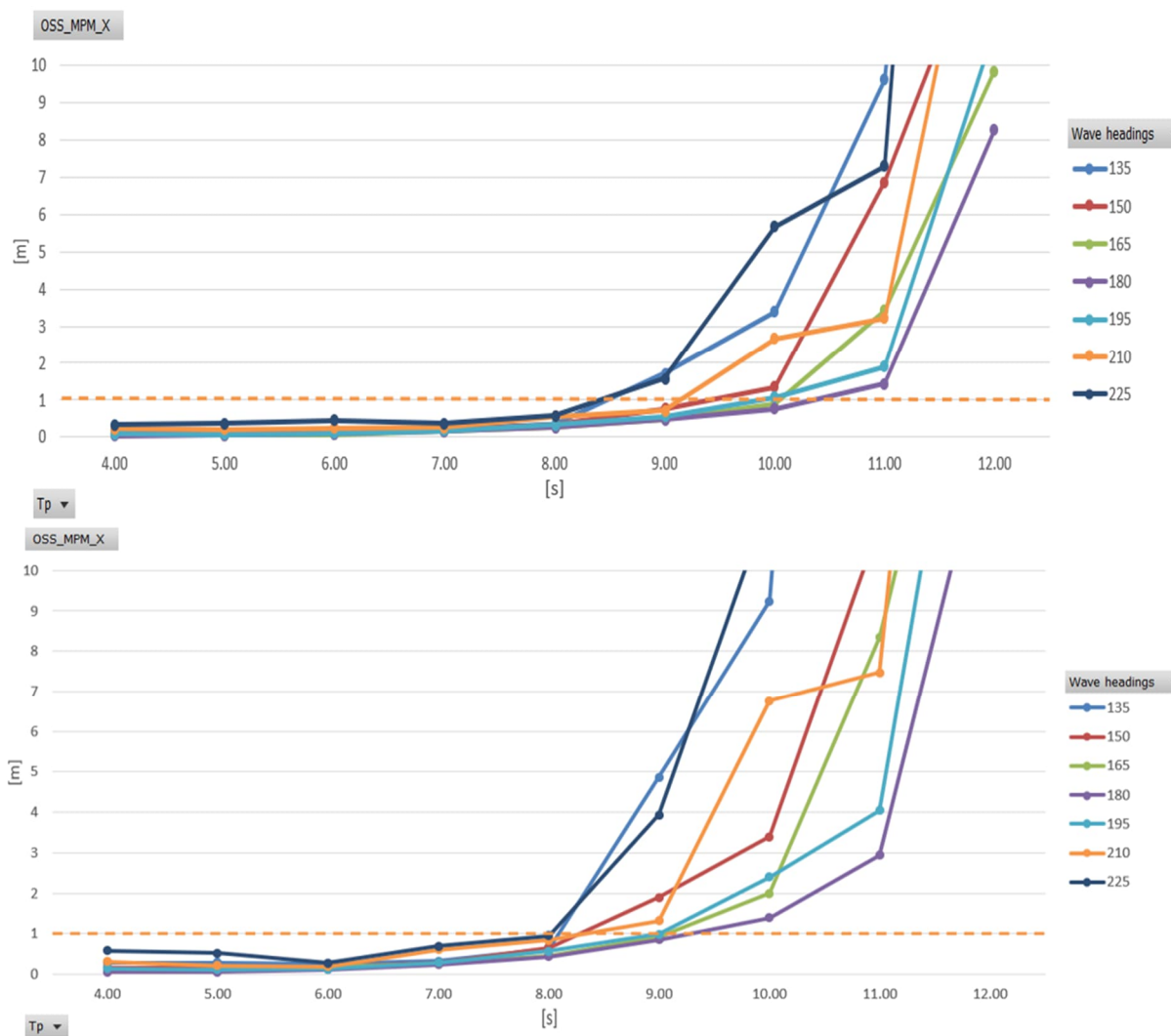
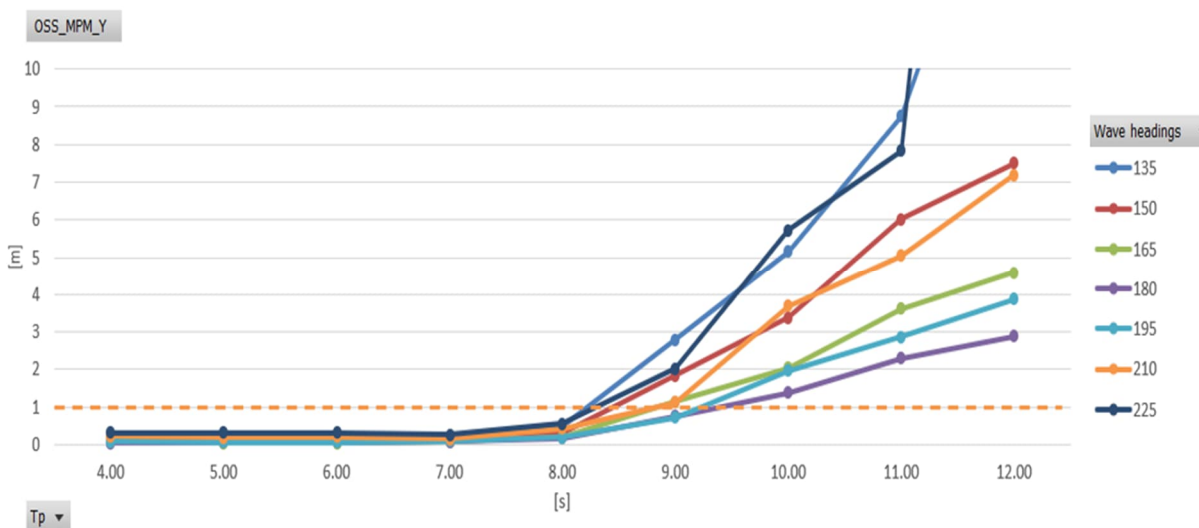


Figure 8-38: OSS movement in global X for  $H_s = 1.5$  m, 2.5 m, above and below respectively



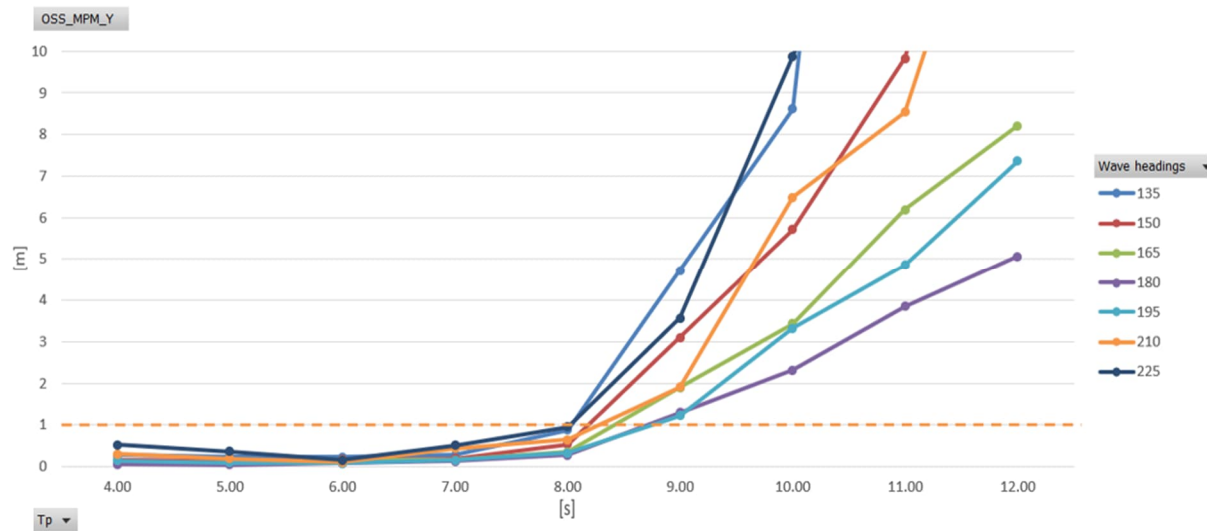
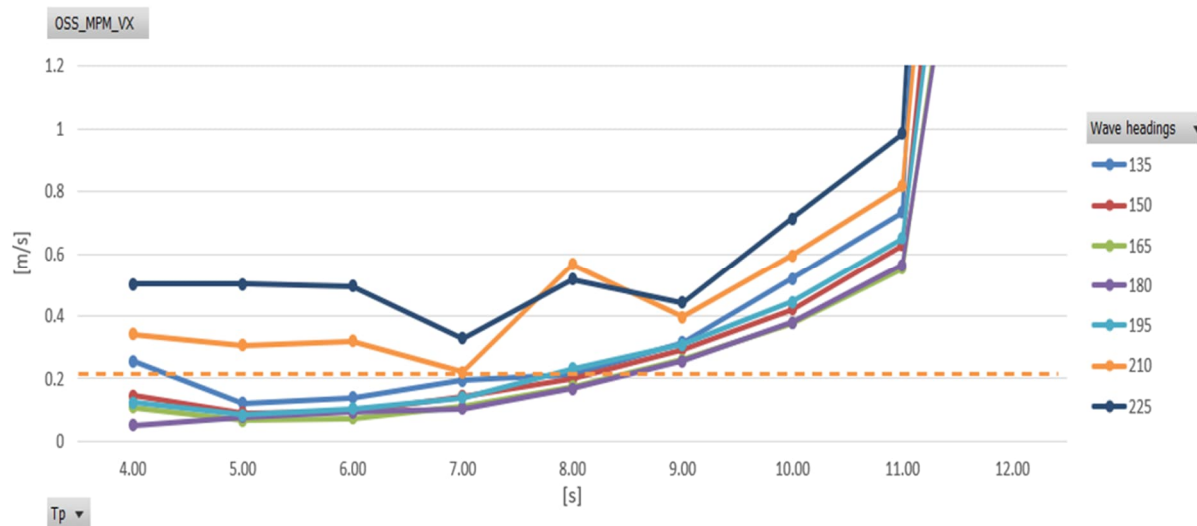


Figure 8-39: OSS movement in global Y for  $H_s = 1.5$  m, 2.5 m, above and below respectively

The motion recordings for the X and Y global directions that need to be observed are shown in Figure 8-38 and Figure 8-39 above. The OSS movement was not observed to surpass its threshold only after  $T_p = 8$ s. It is important to note that the OSS movement in all 4 of the above seen graphs begins to ramp up at  $T_p = 9$ s.

### 8.3.6.2 OSS velocity in global X and Y

The results obtained of velocity in global X direction for  $H_s = 1.5$ m and 2.5m and the wave headings of our interest are shown in Figure 8-40.





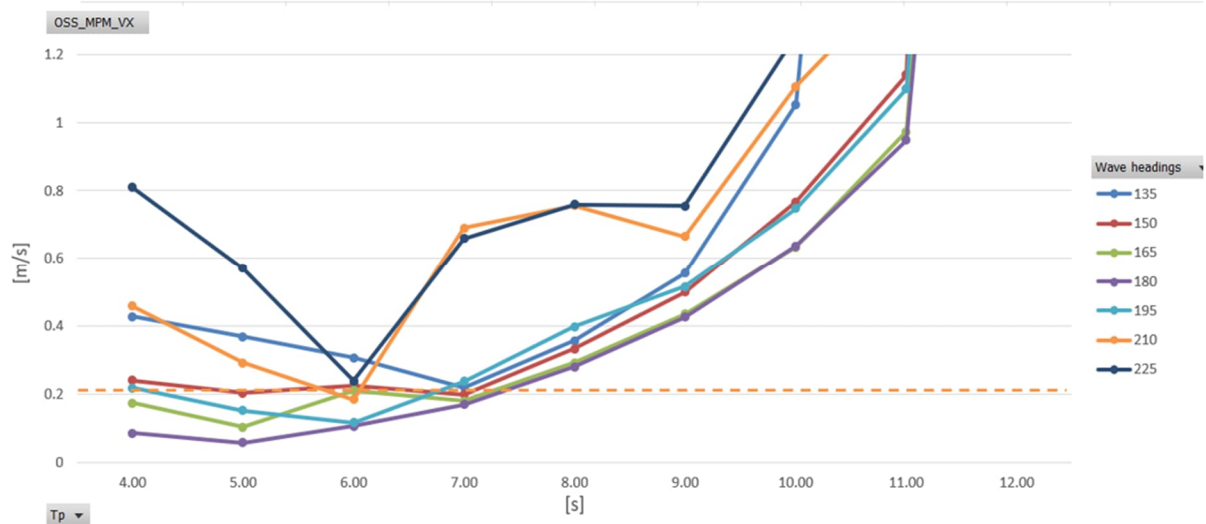


Figure 8-40: OSS velocity in global X for  $H_s = 1.5$  m, 2.5 m, above and below respectively

OSS motion in the global Y direction is also subjected to 0.21 m/s speed limitation. Figure 8-41 provides insights on the values of the velocities obtained from the performed simulations.

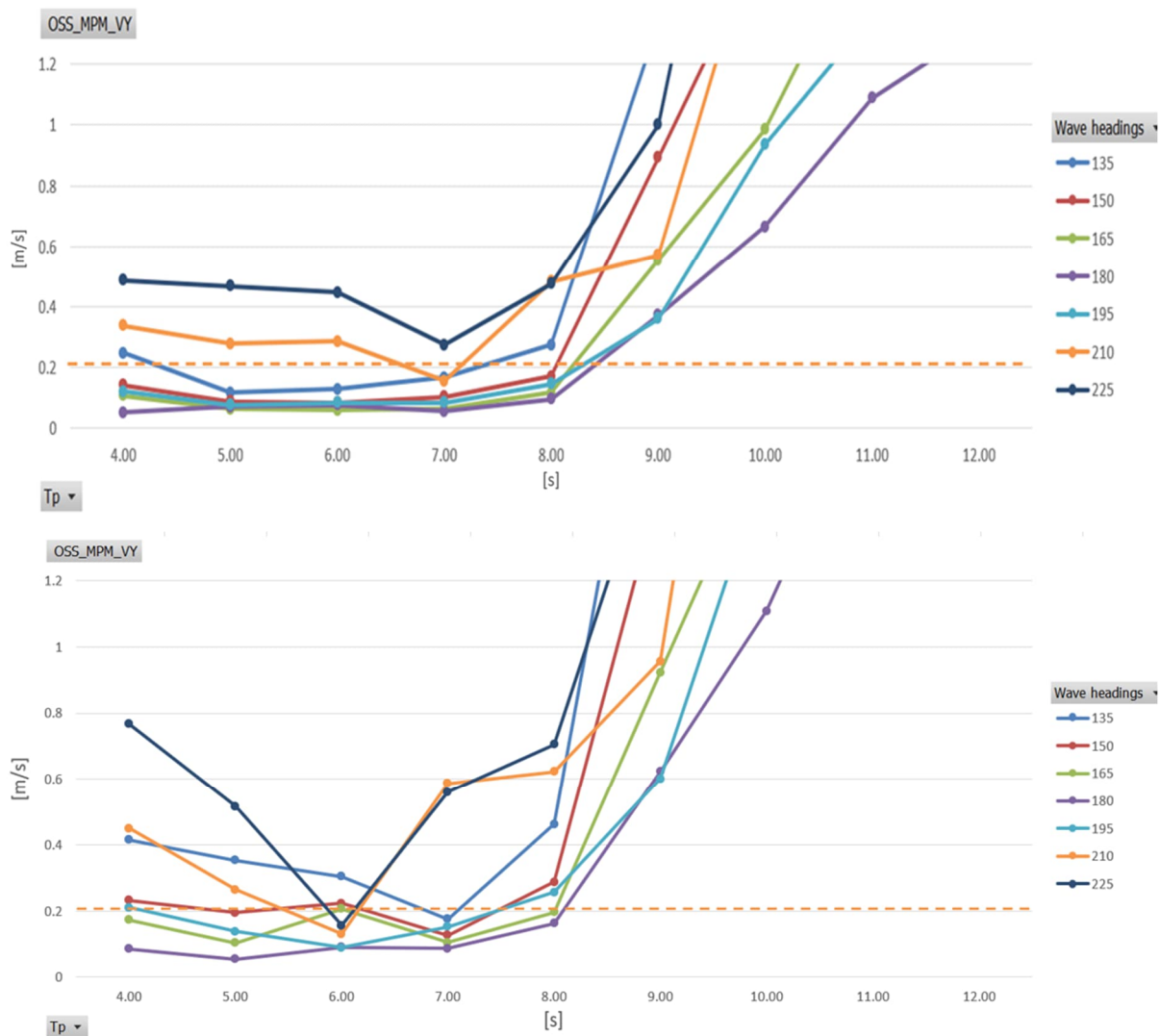


Figure 8-41: OSS velocity in global Y for  $H_s = 1.5$  m, 2.5 m, above and below respectively



It was noted that the OSS velocity exceeded 0.21 m/s at many random wave headings between  $T_p = 4s$  and  $T_p = 8s$  in the graphs corresponding to both directions. At all peak moments, except for  $T_p = 6s$  for  $H_s = 2.5m$  and  $T_p = 7s$  for  $H_s = 1.5m$ , the OSS was moving faster than permitted due to wave headings  $210^\circ$  and  $225^\circ$ . It is significant to observe that at  $T_p = 8s$ , the OSS in the mentioned graphs that correlate to the global Y direction velocities start to ramp up quickly. Also, as we divert from Les Alizes centerline with high value of significant wave height, it is noticed more chaotic and unpredictable behavior will be observed.

From all the considered criteria, velocity constraint was the toughest to pass with the model. As well, this cause to restrict the workability of the slew and transfer phase of the operation leading to allow proceeding only in mild weather conditions.

#### 8.4. Workability

The workability assessment employs the subsequent limiting criteria:

- SWL capacity of main hoist = (Internal confidential)
- Main hoist DAF = (Internal confidential)
- Main hoist off lead = (Internal confidential)
- Main hoist side lead = (Internal confidential)
- OSS movement in X and Y directions = 1 m
- OSS speed in X and Y directions = 0.21 m/s
- Load tugger power = 331 kW
- Trolley tugger power = 204 kW

It is worth noting that tugger restrictions are checked every time step to see whether they are exceeded, therefore they are included immediately in the analysis.

To gain insight into the workability, the permitted significant wave height is calculated for each sea condition (for each combination of  $T_p$  and heading).

The significant wave height for which the time domain analysis is conducted is multiplied by the limiting criterion and divided by the computed MPM result (such as relative motion). The equation then looks like this:

$$H_{s_{allowable}} = \frac{\text{Criterion}}{\text{MPM result}} \cdot H_s \quad (35)$$

Only when the MPM result is fully dynamic (such as a line tension maximum) can the above equation be applied; otherwise, the average should not be scaled linearly. For example, if a mean is included, such that:

$$\text{Line tension MPM} = F_{\text{mean}} + F_{\text{standard\_deviation}} \cdot \text{MPM}_{\text{factor}} \quad (36)$$

Therefore, the allowable Significant wave height will be:

$$Hs_{\text{allowable}} = \frac{\text{Criterion} - \text{mean}}{\text{MPM result} - \text{mean}} \cdot Hs \quad (37)$$

#### 8.4.1. Pick-Up Phase Workability

Following the elaboration of obtaining the allowable significant wave height, workability table for pick up phase is accomplished and the results are presented in Table 8-1.

The table gives an idea on the possible significant wave height that the operation phase can be processed with as a function of a combination of wave heading and peak period. It is evident that operating at significant wave height of 2.5m is possible for a combination of peak period and wave heading values of 4s to 8s and 150° to 195° respectively. Meanwhile operating under the conditions of more divert wave headings and higher periods will require more calm sea states.

Table 8-1: Workability table of pick-up phase

Tp	Wave headings						
	135	150	165	180	195	210	225
4.00	2.50	2.50	2.50	2.50	2.50	2.50	2.50
5.00	2.50	2.50	2.50	2.50	2.50	2.50	1.91
6.00	2.50	2.50	2.50	2.50	2.50	2.50	2.50
7.00	2.50	2.50	2.50	2.50	2.50	2.50	2.12
8.00	2.36	2.50	2.50	2.50	2.50	1.96	1.76
9.00	0.39	0.66	1.14	1.75	1.95	1.56	0.96
10.00	0.26	0.37	0.59	0.90	0.56	0.29	0.18
11.00	0.12	0.17	0.28	0.46	0.39	0.22	0.14
12.00	0.09	0.13	0.22	0.33	0.28	0.17	0.11

#### 8.4.2. Slew and Transfer Phase Workability

During the planning of the analysis, it is decided to consider two options for slew and transfer phase, each with different slewing angle. The purpose of having more than one angle to be studied is to check if the slew and transfer angle will be a possible reason to affect the workability of the lifting operation significantly or not. Below listed the workability tables for both cases (214° and 224°).

The workability tables preview more tight weather conditions to proceed with this phase of the operation, as there were additional limiting criteria imposed on the analysis. The OSS motion analysis was taken into consideration as a limiting criterion while forming the tables, due to

severe consequences that might be the result of OSS behavior, a limit for movement and speed were set for safer proceeding.

Out of the options presented in the tables below and due to the fact that Les Alizes is equipped with DP2 system that can adapt to the alterations of wave headings, the operation will be proceeding with heading's deviation no more than  $15^\circ$ , as well sea-states are to be seen in combination  $H_s$  and  $T_p$ . Operating on  $H_s$  values higher than 2m is not a common practice in offshore heavy lifting operations. Nonetheless, the target of the ongoing analysis is to investigate the feasibility of executing the operation with different sea-states to figure out where the limitations due to environmental window could lay. Based on the two options below corresponding for slewing and transferring phase, it is to be done for angle  $224^\circ$ .

It can be deduced from Table 8-3 that workability of the vessel will be higher, providing same environmental conditions the vessels will be exposed to during the operation. Moreover, the vessel will be operating while the bow wave headings will not be deviating more than  $15^\circ$  from it, due to its technical capabilities, so operating with a slew and transfer angle of  $224^\circ$  seems to be more promising from the shown workability tables below and thus it will be favored during this phase of the operation.

Table 8-2: Workability table of slew and transfer phase of  $214^\circ$

Tp	Wave headings						
	135	150	165	180	195	210	225
4.00	0.88	1.44	1.80	2.50	2.50	1.44	0.86
5.00	2.25	2.50	2.50	2.50	2.50	1.28	0.87
6.00	2.30	2.50	2.50	2.50	2.50	2.50	2.44
7.00	2.28	2.50	2.50	2.50	2.47	1.38	1.18
8.00	1.14	1.54	1.78	1.84	1.30	0.76	0.72
9.00	0.24	0.35	0.55	0.78	0.85	0.58	0.33
10.00	0.13	0.19	0.30	0.44	0.34	0.19	0.12
11.00	0.08	0.11	0.18	0.27	0.23	0.14	0.09
12.00	0.06	0.08	0.10	0.11	0.11	0.09	0.05

Table 8-3: Workability table of slew and transfer phase of 224°

Tp	Wave headings						
	135	150	165	180	195	210	225
4.00	1.23	2.18	2.50	2.50	2.50	1.14	0.65
5.00	2.50	2.50	2.50	2.50	2.50	1.80	0.92
6.00	2.26	2.50	2.50	2.50	2.50	2.50	2.19
7.00	2.38	2.50	2.50	2.50	2.26	1.43	0.96
8.00	1.15	1.59	1.80	1.88	1.36	0.69	0.69
9.00	0.24	0.35	0.57	0.85	0.88	0.55	0.31
10.00	0.13	0.20	0.32	0.47	0.34	0.18	0.12
11.00	0.08	0.12	0.19	0.29	0.23	0.13	0.09
12.00	0.04	0.08	0.11	0.12	0.10	0.07	0.05

## 9. CONCLUSION

### 9.1. Thesis Sum Up

To sum up, transient simulations of offshore substation installation by heavy lift vessel from a moored barge was demonstrated in this thesis. The OSS installation operation mainly consists of three steps: Lifting off the OSS from a moored barge to the Les Alizes and cutting the fastening tools, transfer to installation radius by slewing the tub mounted crane and finally setting down the OSS on the modular support frame. The transient simulations of such installations are investigated using OrcaFlex, a powerful tool for examining the dynamic reactions of marine systems.

The simulations demonstrate the intricate and dynamic interactions that occur during installation between the moored barge, the OSS and the HLV. Wave-induced motions have a substantial impact on the system's stability and can have an impact on the substation's alignment and placement. Certain wave durations and heads exhibit critical resonance effects. Therefore, careful planning is required to prevent circumstances that could elevate vessel and barge motions. The analysis was done for certain conditions, wave headings from  $135^\circ$  to  $225^\circ$  with  $15^\circ$  increment and 5 directions each, due to the versatility of the HLV and its ability to adapt with the incoming waves using the dynamic positioning system the vessel equipped with. Wave peak periods of interest were from  $T_p = 4\text{s}$  to  $12\text{s}$  with  $1\text{s}$  increment.

The study highlights how crucial is to install with windows with the best weather. Unfavourable sea conditions and weather might generate excessive motions, which can create delays or possibly put the operation's safety in danger. A thorough grasp of the ways in which varying wave heights, durations, and orientations affect the viability of the installation procedure can be obtained through transient simulations.

The direction of the waves in relation to the ship is quite important. For example, because of the increased frequency and amplitude of produced motions, it was noticed that a wave heading of  $135^\circ$  during shorter durations ( $T_p = 4\text{s}$ ) greatly reduces workability compared to longer periods ( $T_p = 5$  to  $8\text{s}$ ).

Two options of slew and transfer were considered for the thesis, based on the workability table analysis, slew and transfer at  $224^\circ$  shows more optimistic results than that of the  $214^\circ$ . The workability table summarizes the sea states for which the operation can be planned in a safe

manner, complying with the limiting criteria of the vessel and equipment. When the conditions are met, the marine warranty surveyor will issue a certificate of approval to allow the operations to commence. The limiting criteria were mainly: DAF, OL angle, SL angle, MBL of slings, power exhibited in load and trolley tug lines, OSS movements and velocities in global X and Y directions.

The core objective of this thesis is to achieve a full installation of the OSS with the safest possible conditions. Based on DNV recommendations on heavy lifting operations and some, some environmental and technical limits were implemented, taking in account that the Les Alizes is a HLV equipped with DP2 system and 7 thrusters. The analysis lead to a conclusion that executing this installation operation requires the availability of certain sea conditions. Wave headings should be between  $150^\circ$  and  $195^\circ$ , peak periods should be between 4s and 7s and the significant wave heights preferably not exceeding 2m.

To reduce risks, operational strategies must be effective. The simulations indicate that in order to minimize downtime and guarantee a seamless installation process, accurate timing and coordination are essential. By putting in place adaptive controls and real-time monitoring systems, the operation will be more successful to shifting sea conditions, increasing overall efficiency and safety.

## **9.2. Future Work**

Suggestions for further research on improved simulation models: Subsequent investigations ought to concentrate on enhancing the simulation models by incorporating more complex depictions of the vessel and the offshore substation constructions.

Experimental validation: By carrying out experimental validations on a model of the simulation findings, empirical data can be obtained to enhance the models' accuracy and dependability even more.

Extended-term operational Plans: It will be helpful to create long-term plans for handling unforeseen weather shifts and harsh circumstances. This includes the possibility of using automated decision support systems with predictive analytics to dynamically modify processes along with the system and condition alterations that happen.

In addition to the above mentioned, this thesis offers a foundational analysis and a path forward for further research and technological advancement in this crucial field of offshore engineering.

### 9.3. IMPOSED MOTION ANALYSIS (ADDITIONAL PART)

In OrcaFlex, the term "Imposed Motion Analysis" describes a simulation method where particular motions or displacements are applied to model objects mainly the 6D buoys, usually without accounting for the forces that would otherwise generate such motions. Rather, these movements are predetermined or "Imposed" by the user on the model, which makes it possible to analyze the system's reaction to those movements under control. These are movements (rotations or translations) that are applied to a 6D buoy, like a slew bearing, lumped mass, or crane boom and are defined externally. These motions are not the product of the system's natural dynamic reaction to forces; rather, they are user-defined functions of time.

The type of analysis illustrated in the past 8 chapters was a snapshot analysis, each phase of the operation will be modelled and being used in implicit time domain simulation for continuous three hours, without applying any motion on the available objects. The data extracted for the analysis are based on the three-hour duration signal. Nonetheless, the imposed motion analysis simulates the whole operation in one and half hour, this means all the carried phases and the occurring movements of the crane components will be introduced all in one simulation file, meanwhile only the last thirty minutes will be considered to extract data for our simulation.

This work attributes to an initiative to investigate the results of such type of analysis and compare it with the snapshot analysis. IMA could be beneficiary time wise in the future if it gains enough confidence to be relied on its results. For instance, operations that require significant simulation time due to the need of preparing different configurations of the model, since certain components might change their position while the operation is ongoing.

After adjusting the speed and position of variable elements based on crane manufacturing data sheet, the simulation is executed. The conducted changes concerned hoisting speed, slew bearing speed, booming down speed and adjusting the position of the lumped mass accordingly to compensate as much as possible the induced heel and trim due to crane elements movement.

The Workability table of the IMA is presented in Table 9-1. The results shown provide insights at what conditions we could proceed with the OSS installation. It could be said that these results align with the snapshot results at certain aspects, both types of simulations show the possibility to execute the operation up to  $T_p = 7s$ . However, IMA results show more optimistic allowable significant wave height numbers with regards to deviated wave headings which were not seen in the preceded snapshot analysis.

Table 9-1: Workability table of IMA

Tp	Wave headings						
	135	150	165	180	195	210	225
4.00	2.50	2.50	2.50	2.50	2.50	2.50	2.50
5.00	2.50	2.50	2.50	2.50	2.50	2.50	2.50
6.00	2.50	2.50	2.50	2.50	2.50	2.50	2.50
7.00	2.50	2.50	2.50	2.50	2.50	2.50	2.41
8.00	1.74	2.47	2.50	2.50	2.28	1.78	1.25
9.00	0.28	0.46	0.96	1.40	0.79	0.44	0.31
10.00	0.18	0.32	0.69	0.81	0.40	0.23	0.16
11.00	0.14	0.24	0.49	0.50	0.24	0.13	0.09
12.00	0.04	0.11	0.11	0.10	0.09	0.13	0.05

These results are considered for now as the starting point in this type of analysis. So, no conclusion will be drawn on them. As rules improvise, running this type of simulations with different random seeds and then doing regression analysis are required to gain more confidence on the results we are getting from such a type of analysis.



## REFERENCES

- (n.d.). Retrieved July 2024, from Statistics How To:  
<https://www.statisticshowto.com/continuous-probability-distribution/>
- (n.d.). Retrieved July 2024, from CUEMATH: <https://www.cuemath.com/data/discrete-probability-distribution/>
- (n.d.). Retrieved July 2024, from Statistics How To:  
<https://www.statisticshowto.com/weibull-distribution/>
- (n.d.). Retrieved July 2024, from statistics How To:  
<https://www.statisticshowto.com/rayleigh-distribution/>
- (n.d.). Retrieved July 2024, from Statistics How To:  
<https://www.statisticshowto.com/probability-density-function-definition-examples/>
- Bhandari, P. (2020, October). Retrieved July 2024, from Scribbr:  
<https://www.scribbr.com/statistics/normal-distribution/>
- Bouwer, Q. (2023). *An Overview of Offshore Substation Technologies and Their Applications*. energycentral. Retrieved from <https://energycentral.com/c/ee/overview-offshore-substation-technologies-and-their-applications>
- Brown et Johns. (2024). *European Electricity Review*. Retrieved from Ember: European Electricity Review 2024 | Ember (ember-climate.org)
- Buljan, A. (2020, April 15). *First Triton Knoll Offshore Substation In Place*. Retrieved April 2024, from Offshore Wind: <https://www.offshorewind.biz/2020/04/15/first-triton-knoll-offshore-substation-in-place/>
- C. Vuik et al. (2016). *Numerical Methods for Ordinary Differential*. Delft Academic Press.  
doi:<https://doi.org/10.5074/t.2023.001>
- Cameron et al. (n.d.). *Engineering Mechanics: Statics*. University of Prince Edward Island.  
doi:<https://doi.org/10.32393/EngnMech>
- Climate Watch. (2023). Breakdown of carbon dioxide, methane and nitrous oxide emissions by sector. *Our World in Data*. Retrieved from  
<https://ourworldindata.org/grapher/nitrous-oxide-emissions-by-sector>
- Det Norske Veritas. (2014). *Recommended Practice DNV-RP-C205, Environmental Con*.
- DNV. (2022). *Floating Offshore Wind: The next five years*. Retrieved April 2024, from  
<https://www.dnv.com/focus-areas/floating-offshore-wind/floating-offshore-wind-the-next-five-years>
- DNV. (2023, December). *Marine operations and marine warranty standard*. Retrieved from  
<https://www.dnv.com/oilgas/download/dnv-st-n001-marine-operations-and-marine-warranty/>
- Ember. (2024). *Europe's electricity transition takes crucial strides forward*. Retrieved April 2024, from Ember: <https://ember-climate.org/insights/research/european-electricity-review-2024/>
- European Commission. (2023). *Renewable energy targets*. Retrieved from European Commission: [https://energy.ec.europa.eu/topics/renewable-energy/renewable-energy-directive-targets-and-rules/renewable-energy-targets\\_en](https://energy.ec.europa.eu/topics/renewable-energy/renewable-energy-directive-targets-and-rules/renewable-energy-targets_en)
- Froese, M. (2016). *Making of the modern offshore substation*. Retrieved May 2024, from WindPower Engineering and Development:  
<https://www.windpowerengineering.com/making-modern-offshore-substation/>
- Frost, J. (n.d.). Retrieved from Statistics By Jim: <https://statisticsbyjim.com/basics/unimodal-distribution/>
- Frost, J. (n.d.). Retrieved July 2024, from Statistics By Jim:  
<https://statisticsbyjim.com/probability/weibull-distribution/>
- Huisman. (2019). *Huisman signs contract with Jan de Nul for a 5,000mt Tub Mounted Crane (TMC)*. Retrieved May 2024, from Huisman:

- [https://www.huismanequipment.com/en/media\\_centre/press\\_releases/163-136\\_Huisman-signs-contract-with-Jan-de-Nul-for-a-5-000mt-Tub-Mounted-Crane-TMC](https://www.huismanequipment.com/en/media_centre/press_releases/163-136_Huisman-signs-contract-with-Jan-de-Nul-for-a-5-000mt-Tub-Mounted-Crane-TMC)
- J. Chung et al. (1993). A time integration algorithm for structural dynamics with improved numerical dissipation: the generalized- $\alpha$  method. *Journal of Applied Mechanics*, 371-375.
- Jan de Nul. (2023). *Next-Generation installation vessel Les Alizés kicks off construction works for Ørsted's wind farms Borkum Riffgrund 3 and Gode Wind 3*. Retrieved May 2024, from Jan de Nul: <https://www.jandenul.com/news/next-generation-installation-vessel-les-alizes-kicks-construction-works-orsteds-wind-farms>
- JDN. (2021). *Jan De Nul signs T&I contract for Gode Wind 3 & Borkum Riffgrund 3*. Retrieved May 2024, from Jan de Nul: <https://www.jandenul.com/news/jan-de-nul-signs-ti-contract-gode-wind-3-borkum-riffgrund-3>
- M. W. Toews. (n.d.). *Wikimedia Commons*. Retrieved July 2024, from Creatice commons: <https://creativecommons.org/licenses/by-sa/4.0/>
- Michel K. Ochi. (1988). ON PREDICTION OF EXTREME VALUES. *JOURNAL OF SHIP RESEARCH*, 1-2.
- New York State Official Website. (2024). *Offshore wind 101*. Retrieved April 2024, from NYSERDA: <https://www.nyserda.ny.gov/All-Programs/Offshore-Wind/About-Offshore-Wind/Offshore-Wind-101>
- North Falls. (2024). *North Falls Offshore Wind Farm*. Retrieved April 2024, from North Falls Offshore: <https://www.northfallsoffshore.com/facts-figures/>
- NYSERDA. (2024). *Offshore Wind 101*. Retrieved April 2024, from NYSERDA: <https://www.nyserda.ny.gov/All-Programs/Offshore-Wind/About-Offshore-Wind/Offshore-Wind-101>
- OVERDICK. (2014). *HVDC Sylwin alpha*. Retrieved May 2024, from OVERDICK Offshore: [https://overdick-offshore.com/projects/offshore-wind/hvdc\\_sylwin\\_alpha#:~:text=The%20installation%20was%20conducted%20in%20three%20phases%3A%20following,to%20elevate%20the%20topsides%20to%20the%20required%20height.](https://overdick-offshore.com/projects/offshore-wind/hvdc_sylwin_alpha#:~:text=The%20installation%20was%20conducted%20in%20three%20phases%3A%20following,to%20elevate%20the%20topsides%20to%20the%20required%20height.)
- OVERDICK GmbH. (2012). *Borkum West II - Substation Platform*. Retrieved May 2024, from OVERDICK Offshore: [https://overdick-offshore.com/projects/offshore-wind/borkum\\_west\\_ii\\_-\\_substation\\_platform](https://overdick-offshore.com/projects/offshore-wind/borkum_west_ii_-_substation_platform)
- Ritchie et al. (2020). Sector by sector: where do global greenhouse gas emissions come from? *Our World in Data*. Retrieved from <https://ourworldindata.org/ghg-emissions-by-sector>
- RS Supplier. (n.d.). *Lifting Slings*. Retrieved May 2024, from RS Online: [https://benl.rs-online.com/web/c/access-storage-material-handling/material-lifting-loading-equipment/lifting-slings/?cm\\_mmc=BE-PPC-DS3A-\\_-google-\\_-DSA\\_BENL\\_NL\\_Access+%26+Storage+%26+Material+Handling\\_Index-\\_-Lifting+Slings-\\_-DYNAMIC+SEARCH+ADS&matchtype=b](https://benl.rs-online.com/web/c/access-storage-material-handling/material-lifting-loading-equipment/lifting-slings/?cm_mmc=BE-PPC-DS3A-_-google-_-DSA_BENL_NL_Access+%26+Storage+%26+Material+Handling_Index-_-Lifting+Slings-_-DYNAMIC+SEARCH+ADS&matchtype=b)
- Seiji et al. (2007). Offshore Technology Conference. *State of the Art in Float-Overs*. Houston, Texas, USA. doi:10.4043/19072-MS
- Techet, A. (2005). Design Principles for Ocean Vehicles (13.42). MIT OpenCourseWare. Retrieved from [https://ocw.mit.edu/courses/2-22-design-principles-for-ocean-vehicles-13-42-spring-2005/3fd34b15f4d9ddb167697b3c4e7cca5\\_r8\\_wavespectra.pdf](https://ocw.mit.edu/courses/2-22-design-principles-for-ocean-vehicles-13-42-spring-2005/3fd34b15f4d9ddb167697b3c4e7cca5_r8_wavespectra.pdf)
- The Crown Estate. (2019). *Guide to an offshore wind farm*. Retrieved from <https://www.thecrownestate.co.uk/media/2860/guide-to-offshore-wind-farm-2019.pdf>
- Thomsen, J. W. (2023). *Substations Converting customer requirements to high performance units*. Retrieved April 2024, from CS Wind Offshore: <https://www.cswindoffshore.com/solutions/substations/>

---

Turney, S. (2022, May). Retrieved July 2024, from Scribbr:  
<https://www.scribbr.com/statistics/skewness/>

---

**APPENDICES**

No appendices are attached due to internal confidentiality policy of JDN company.